Synthesis, Analysis and Testing of Photoactive Heterojunction Semiconductors

by

Xiangchao Meng

Thesis submitted to the

Faculty of Graduate and Postdoctoral Studies

in partial fulfillment of the requirements for

the Master of Applied Science degree in Chemical Engineering

uOttawa

Department of Chemical and Biological Engineering

Faculty of Engineering

University of Ottawa

Abstract

Photocatalysis is a growing area of study for a clean and renewable energy source, particularly for the purification of water and air. Researchers have studied the combination of various semiconductors to create photocatalysts with improved activities, but little has been reported in selecting semiconductors based on their extrinsic type – namely n-type or p-type. In this study, a BiOBr (p-type)-Bi_2WO_6 (n-type) heterojunction semiconductor was synthesized by the facile hydrothermal method. The new materials were characterized by X-ray diffraction (XRD), X-ray photoelectron spectroscopy (XPS), scanning electron microscopy (SEM), energy dispersive spectroscopy (EDS), transmission electron microscopy (TEM) and diffuse-reflection spectroscopy (DRS). Degradation of *Rhodamine B* was employed to measure the photocatalytic activity of the as-prepared photocatalysts. On the basis of these techniques, the influence of the synthesis conditions (namely, hydrothermal reaction time and temperature) and the degradation conditions (namely, initial concentration, pH of the initial dye water and amount of catalysts dosage) have been explored and discussed. Furthermore, effect of concentrations of the dopants (the atomic ratio of BiOBr and Bi_2WO_6 were 1:4， 1:1， 4:1) was examined by measuring the degradation rate of *Rhodamine B*. Finally, the mechanism of the degradation process and the enhancement effect of heterojunction were also interpreted by analyzing the quenching effect of the scavengers and the band structure. Conclusively, this study shed light on the benefits of using heterojunction photocatalysts, and also on the importance of considering the semiconductor type when forming composite photocatalysts.

Résumé

L'étude de la photocatalyse en tant que source d'énergie propre et renouvelable, particulièrement pour la dégradation de solvants et la purification de l'eau et de l'air, est en pleine essor. Des études ont été réalisées sur la combinaison de divers semiconducteurs pour créer des photocatalyseurs dont l'activité est améliorée, mais peu de chercheurs se sont penchés sur le choix de semiconducteurs en fonction de leur type extrinsèque – soit type N, soit type P. Dans la présente étude, un semiconducteur à hétérojonction BiOBr-Bi_2WO_6 (type P-type N) a été synthétisé à l'aide de la méthode hydrothermale facile. Les nouvelles matières obtenues ont été caractérisées au moyen des techniques suivantes, entre autres : diffraction des rayons X, spectroscopie de photoélectrons XPS, microscopie électronique à balayage, spectroscopie à dispersion d'énergie, microscopie électronique à transmission et spectroscopie à réflexion diffuse. L'activité photocatalytique des photocatalyseurs préparés a été mesurée par la dégradation de la rhodamine B. À partir des techniques susmentionnées, l'influence des conditions de synthèse (notamment la température et le temps de réaction hydrothermique) et des conditions de dégradation (notamment la concentration initiale, le pH initial de l'eau avec colorant et la proportion des catalyseurs) a été examinée et discutée. En outre, on a évalué l'effet des diverses concentrations des dopants (les rapports atomiques de BiOBr et de Bi_2WO_6 étaient de 1:4, de 1:1 et de 4:1) en mesurant la vitesse de dégradation de la rhodamine B. Enfin, l'analyse de l'effet de désactivation des entraîneurs et de la structure des bandes a permis d'interpréter le mécanisme du processus de dégradation et l'effet d'enrichissement de l'hétérojonction. Pour conclure, la présente étude a clarifié les avantages liés à l'utilisation des photocatalyseurs à hétérojonction, ainsi que l'importance de prendre en considération le type de semiconducteur lors de la création de photocatalyseurs composites.

Acknowledgements

I would like to firstly acknowledge my supervisor, Dr. Zisheng (Jason) Zhang, for his supportive and knowledgeable supervision, and for providing me a research assistant position while I pursued my degree of Master of Applied Science.

I would like to acknowledge the financial support of the Faculty of Graduate and Postdoctoral studies (FGPS) by providing me the Admission Scholarship for international graduate students.

I would also like to acknowledge the technical support by the Centre for Catalysis and Innovation (CCRI) at the University of Ottawa (uOttawa) for the photocatalyst characterization tests including SEM, EDS and TEM tests by Dr. Yun Liu, XPS tests by Dr. Sander Mommers and XRD tests by Dr. Kara Tell. And I would also like to thank the technical officers in the department of Chemical and Biological Engineering, especially Louis Tremblay.

I am indebted to the lab mates working in CBY D510, especially Dr. Joanne Gamage McEvoy for her help at the beginning of this project. I would like to thank the chemical engineering student Fahad Chowdhury for the work on simulation and the proofreading of my papers. I am also grateful to all of my friends for their helpful support during my graduate studies, especially Zhiliang, Zhi, Yuchi, Yuanchen, Yu, Yubo and Yuqian.

Finally, I would like to thank my warm family, the selfless help of my parents, my elder sister and my beloved girlfriend (Zizhen). Without their help, things would have been more difficult in the process of this study.

To my family

Table of contents

List of figures

List of tables

Nomenclature, Abbreviation, and Symbols

- ***Photocatalysts nomenclature***

BiOBr(*x* at%)-Bi_2WO_6: Heterojunction system of bismuth oxybromide and bismuth tungstate, in which atomic ratio of BiOBr accounts for x%.

- ***Abbreviation***

CB: Conduction band

DER: N, N'-Diethyl-rhodamine

DRS: Diffused reflectance spectra

E_{CB}: Potential position of conduction band

E_{VB}: Potential position of valence band

EDS: Energy dispersive X-ray spectrometry

EDTA: Ethylenediaminetetraacetic acid

MER: *N-Ethyl-rhodamine*

RhB: *Rhodamine B*

SEM: Scanning electron microscopy

TEM: Transmission electron microscopy

TER: *N, N, N'-Triethyl-rhodamine*

VB: Valence band

XPS: X-ray photoelectron spectroscopy

XRD: X-ray Diffraction

❖ ***Symbols***

Tauc equation:

E_{photon}= *hv*; *α, K, E_g, n, h* and *v* represent the absorption coefficient, constant for semiconductor (usually equal to 1), bandgap energy, constant for semiconductor depending on the type of the band gap (direct transition: n=1; indirect transition: n=4), Planck constant and irradiation frequency, respectively.

Section Ⅰ:

Introduction

CHAPTER 1:

INTRODUCTION

1.1 Introduction

With the continuous development and advancement of modern civilizations, environmental contamination has spread world-wide. Faced with this issue, mankind has reached a consensus on the importance of environmental treatment and remediation. Photocatalysis, an advanced oxidation process (AOP), indirectly degrades most of the organic pollutants by producing strong oxidants (hydroxyl, •OH). This process has been widely applied in the field of environmental remediation [1-5]. Prominent advantages for photocatalytic processes include non-toxicity, low cost, high efficiency, no secondary-pollution and thorough mineralization. Comparatively, for some physical methods such as adsorption by active carbon and coagulation/flocculation, even though they could lead to approximately 80%-90% reduction of organic compounds in the treatment of dye water [6-8], phase transfer processes alone cannot achieve the final goal of thoroughly decomposing pollutants. Other AOPs that directly use the strong oxidant could cause the complete mineralization of the pollutants, converting them into harmless compounds such as CO_2 and H_2O [9]. It is still noteworthy that some

drawbacks hinder its wide practical application, such as the generation of carcinogenic by-products (chlorite and chlorate) when using chloride in drinking water disinfection [10, 11], and the high cost and harmful by-products (e.g. bromate) of the ozonation process [12].

In 1972, Fujishima and Honda introduced photocatalysis into water splitting and hydrogen and oxygen production in the electrochemical cell [13]. This triggered the intensive concentration on the research and development of photocatalytic science and engineering. Two distinct areas have been studied on heterogeneous photocatalysis: the basic theoretical chemical investigation of mechanisms, reaction kinetics, synthesis and compound modifications, etc. [14-19]; and the industrial scale-up studies associated with the photocatalytic reactor design.

This work focussed on overcoming the low visible-light-driven activity and high recombination rate of electron-hole pairs in photocatalysts implemented in waste water purification. The novel photocatalyst BiOBr-Bi_2WO_6, a heterojunction semiconductor, was synthesized to explore the potential enhancement effect of heterojunction structures on the visible-light-driven photocatalytic performance using some characteristic techniques.

1.2 Objectives

The objectives of this project were as follows:

- Determining the optimum conditions for the synthesis of BiOBr (50 at%)-Bi_2WO_6 composites by facile hydrothermal method, particularly the hydrothermal reaction temperature and holding time;
- Exploring the influence of varying dopant ratios of BiOBr in the composites' photocatalytic properties, especially their photocatalytic degradation efficiency;
- Characterizing the as-prepared BiOBr (50 at%)-Bi_2WO_6 composites under the

optimized synthesis conditions using XRD, XPS, SEM, TEM, EDS, DRS, *etc.*;

- Investigating the photocatalytic activity and reusability of the composites by degrading *Rhodamine B*, as well as the factors that influence the degradation process such as initial concentration, pH and catalyst dosage;
- Proposing and discussing a mechanism for the enhanced photocatalytic activity caused by the heterojunction in the novel photocatalyst.

1.3 Thesis structure

The main body of this thesis includes three sections: introduction, experimental results and conclusions, in which the experimental results have been divided into two chapters. Details about each chapter are as follows:

- **Chapter 1: Introduction**

  The project has been introduced with some background information, the objectives and the thesis structure.

- **Chapter 2: Background and literature review**

  A general paper review of related research and theoretical feasibility of this project has been argued and conclusions have been determined.

- **Chapter 3: Synthesis, analysis and testing of BiOBr-Bi_2WO_6 photocatalytic heterojunction semiconductors**

  The influence of experimental temperature and holding time while synthesizing BiOBr (50 at%)-Bi_2WO_6 heterojunction semi-conductor using the hydrothermal method has been explored, the as-prepared photocatalysts have been characterized and the mechanism of photocatalysis using heterojunction semiconductors has been

interpreted.

- **Chapter 4: Facile synthesis of BiOBr-Bi_2WO_6 heterojunction semiconductors with high visible-light-driven photocatalytic activity**

  The effects of dopant ratios of BiOBr in the composites and the mechanism in the degradation process of *Rhodamine B* have been determined, along with the enhancement effect of a heterojunction structure.

- **Chapter 5: Conclusions**

  General conclusion of this project and suggestions of future work have been listed.

1.4 References

[1] R. Portela, M.D. Hernández-Alonso, Environmental Applications of Photocatalysis, Design of Advanced Photocatalytic Materials for Energy and Environmental Applications, Springer2013, pp. 35-66.

[2] M. Pelaez, N.T. Nolan, S.C. Pillai, M.K. Seery, P. Falaras, A.G. Kontos, P.S. Dunlop, J.W. Hamilton, J.A. Byrne, K. O'Shea, A review on the visible light active titanium dioxide photocatalysts for environmental applications, Applied Catalysis B: Environmental, 125 (2012) 331-349.

[3] M.R. Hoffmann, S.T. Martin, W. Choi, D.W. Bahnemann, Environmental applications of semiconductor photocatalysis, Chem Rev, 95 (1995) 69-96.

[4] K. Yogo, M. Ishikawa, Recent progress in environmental catalytic technology, Catal Surv Jpn, 4 (2000) 83-90.

[5] R. Andreozzi, V. Caprio, A. Insola, R. Marotta, Advanced oxidation processes (AOP) for water purification and recovery, Catalysis Today, 53 (1999) 51-59.

[6] P.K. Malik, Dye removal from wastewater using activated carbon developed from sawdust: adsorption equilibrium and kinetics, J Hazard Mater, 113 (2004) 81-88.

[7] I. Khouni, B. Marrot, P. Moulin, R. Ben Amar, Decolourization of the reconstituted textile effluent by different process treatments: Enzymatic catalysis, coagulation/flocculation and nanofiltration processes, Desalination, 268 (2011) 27-37.

[8] C.S.D. Rodrigues, R.A.R. Boaventura, L.M. Madeira, Technical and economic feasibility of polyester dyeing wastewater treatment by coagulation/flocculation and Fenton's oxidation, Environ Technol, 35 (2014) 1307-1319.

[9] A. Matilainen, M. Sillanpää, Removal of natural organic matter from drinking water by advanced oxidation processes, Chemosphere, 80 (2010) 351-365.

[10] S. Sorlini, F. Gialdini, M. Biasibetti, C. Collivignarelli, Influence of drinking water treatments on chlorine dioxide consumption and chlorite/chlorate formation, Water Res, 54 (2014) 44-52.

[11] M. Khairy, M. Kolb, A. Mostafa, A. El-Fiky, M. Bahadir, Risk posed by chlorinated organic compounds in Abu Qir Bay, East Alexandria, Egypt, Environ Sci Pollut R, 19 (2012) 794-811.

[12] S. Sharma, J. Buddhdev, M. Patel, J.P. Ruparelia, Studies on Degradation of Reactive Red 135 Dye in Wastewater using Ozone, Procedia Engineering, 51 (2013) 451-455.

[13] A. Fujishima, K. Honda, Electrochemical photolysis of water at a semiconductor electrode, nature, 238 (1972) 37-38.

[14] H. Tong, S. Ouyang, Y. Bi, N. Umezawa, M. Oshikiri, J. Ye, Nano‐photocatalytic

Materials: Possibilities and Challenges, Adv Mater, 24 (2012) 229-251.

[15] N. Serpone, E. Pelizzetti, Photocatalysis: fundamentals and applications, Wiley New York1989.

[16] C. Fu, T. Li, J. Qi, J. Pan, S. Chen, C. Cheng, Theoretical study on the electronic and optical properties of Ce^{3+}-doped TiO_2 photocatalysts, Chem Phys Lett, 494 (2010) 117-122.

[17] H. Yu, K. Zhang, C. Rossi, Theoretical study on photocatalytic oxidation of VOCs using nano-TiO_2 photocatalyst, Journal of Photochemistry and Photobiology A: Chemistry, 188 (2007) 65-73.

[18] H. Gao, J. Zhou, D. Dai, Y. Qu, Photocatalytic Activity and Electronic Structure Analysis of N‐doped Anatase TiO_2: A Combined Experimental and Theoretical Study, Chem Eng Technol, 32 (2009) 867-872.

[19] C. Hung, K. Wu, C. Yeh, J. Sun, C. Hsu, Photoelectrocatalytic property of microporous Pt-TiO_2/Ti electrodes, Thin Solid Films, 529 (2013) 19-24.

CHAPTER 2:

BACKGROUND AND LITERATURE REVIEW

2.1 Introduction

Approximately 3×10^{24} J of solar energy irradiates on the earth's surface annually, which is over 10^4 times the global consumption of energy based on the data from the U.S. Energy Information Administration (EIA). Effective storage or transfer of solar energy drives extensive research and tremendous results continue to be obtained. The photocatalytic process, one of the most promising techniques in utilizing solar energy, attracted growing interest in the past 4 decades. On one hand, photocatalysis could use solar energy to produce hydrogen, which has high chemical potential, and release oxygen via water splitting, analogous to natural photosynthesis [1, 2]. On the other hand, photocatalysis shows potential in the field of environmental remediation including waste water treatment and purification of polluted air [2-5]. As has been widely introduced, TiO_2 was regarded as one of the most promising photocatalysts due to its high chemical stability, low cost and environmental-friendly properties [6, 7]. However, some drawbacks emerged from the extensive research on TiO_2

such as low visible-light-driven activity and high recombination rate of the photo-generated electron-hole pairs; solutions were explored and introduced for these issues such as the surface modification of TiO_2 [8]. Meanwhile, synthesizing novel photocatalysts has become a popular topic for improving the photocatalytic activity under visible light by attaining suitable band gaps for stimulation. Bismuth composites attribute greatly to this category with relatively high photocatalytic performance in degrading organics in waste water or polluted air. At the same time, establishing a heterojunction was regarded as an effective measure to prevent the recombination of electron-hole pairs. In this chapter, the various heterojunctions established on the basis of Bismuth composite semiconductors will be reviewed and introduced.

2.2 Photocatalysis

The use of semiconductors as photocatalysts is ascribed to its special electrical configuration. Band theory is usually explained by the top two energy bands. Each box in the diagram in Fig. 2-1 represents a band of energy levels. Comparing the band configurations of the metal, semiconductor and insulator, the high conductivity of metals is ascribed to the partly filled conduction band which results in electron conduction with a small potential gradient. Comparatively, the fully filled valence band and completely empty conductive band in insulator and semiconductor electrical configurations form a band gap which is a significant concept in photocatalysis. The magnitude of the gap distinguishes these two categories; insulators generally have band gaps larger than 3 eV while semiconductors have less than 3 eV band gaps. The narrow band gap leads to electrons in the highest energy band (valence band, VB) of a semiconductor to require very little energy to jump to the adjacent band (conduction band, CB). Every leap of the electron to the conductive band leaves a positive hole in the valence band. Since there is a discontinuity between the conduction band and the

valence band, the longevity of electron-hole pairs are extended. The band gaps of frequently-used semiconductors have been illustrated in [9, 10].

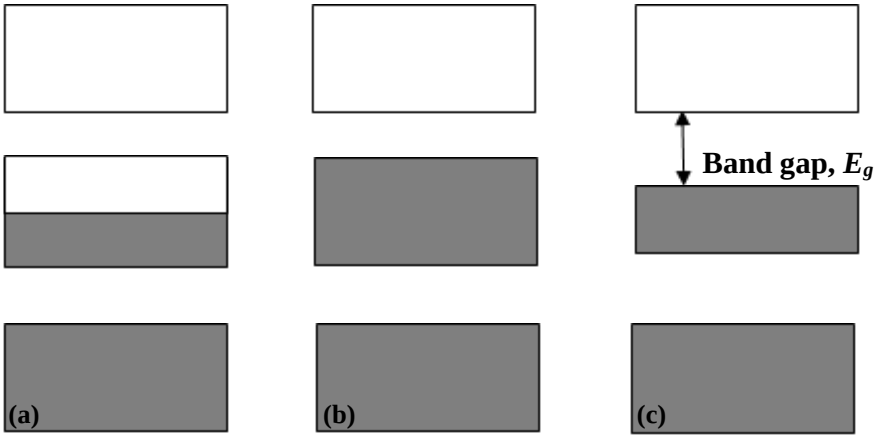

Fig. 2-1. Band diagrams of (a) Metal (b) Semiconductor and (c) Insulator.

The energy of the incident light is sufficient to activate the electron leap from the valence band to the conduction band when $hv > E_g$ (where h is Planck constant and v is the frequency). For instance, the band gap of the widely used photocatalyst TiO_2 is 3.2 eV. Only irradiation with wavelengths lower than 387.5 nm could stimulate the electrons in the valence band. As a result, most of the research using TiO_2 as the photocatalyst use UV lamps as their incidence source, which would increase the operating cost and therefore hinder the photocatalytic industrial scale-up [11]. Upon irradiation, the photo-generated electrons and holes could separately participate in various chemical reactions (*Equation 1-5*) [12]. The formation of the very strong oxidant hydroxyl could trigger the complete degradation of pollutants. The standard electrode potentials of some oxidants can be seen in Table 2-1.

$$TiO_2 + h\nu \longrightarrow h^+_{VB} + e^-_{CB} \quad \textit{(Eq. 1)}$$

$$H_2O + h^+_{VB} \longrightarrow \bullet OH + H^+ \quad \textit{(Eq. 2)}$$

$$h^+ + \text{Pollutant} \longrightarrow \text{Pollutant}^+ \quad \textit{(Eq. 3)}$$

$$\bullet OH + \text{Pollutant} \longrightarrow CO_2 + H_2O \quad \textit{(Eq. 4)}$$

$$O_2 + e^-_{CB} \longrightarrow \bullet O_2^- \quad \textit{(Eq. 5)}$$

Table 2-1. Standard electrode potential of general oxidants (at 25 °C).

Oxidant	Standard electrode potential (V)	Oxidant	Standard electrode potential (V)
F_2	2.87	$HClO_4$	1.63
•OH	2.80	ClO_2	1.50
O_3	2.07	Cl_2	1.36
H_2O_2	1.77	$Cl_2O_7^{2-}$	1.33
MnO_2	1.68	O_2	1.23

2.3 Properties of Bi_2WO_6 and BiOBr

2.3.1 Bi_2WO_6

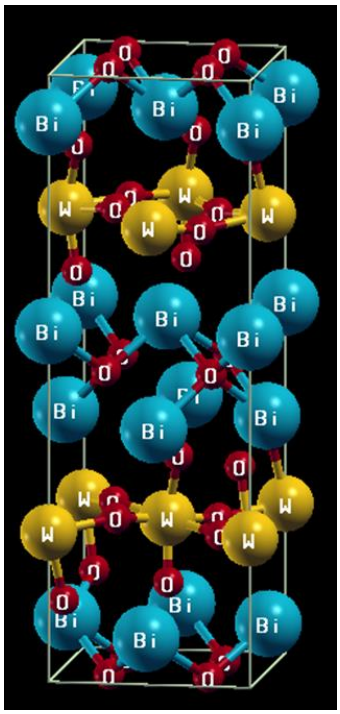

Fig. 2- 2. Structure of Bi_2WO_6. (Simulated by Quantum Espresso [13])

Bi_2WO_6 is the simplest member in the Aurivillius family which has the general formula of $Bi_2A_{n-1}B_nO_{3n+3}$ (where A= Ca, Sr, Ba, Pb, Bi, Na, K; B= Ti, Nb, Ta, Mo, W, Fe). It has recently received great interest in the field of environmental remediation, to be used as a photocatalyst[14]. The crystal structure of Bi_2WO_6 consists of alternating layers of $(Bi_2O_2)^{2+}$ and $(WO_4)^{2-}$, shown in Fig. 2-2. It has been reported that Bi_2WO_6 possesses some special physical properties such as ferroelectric piezoelectricity, pyroelectricity, catalytic behavior and a non-linear dielectric susceptibility, which resulted in the promising implementation of this material [15].

In 1999, Kudo and Hijii synthesized the Bi_2WO_6 with the solid state reaction and used it for splitting water to produce H_2 and O_2 under visible-light irradiation [16]. Since then, Bi_2WO_6 has increasingly gained the attention of researchers and has undergone extensive chemical investigation. The current synthesis methods can be summarized as follows:

- ***Solid state reaction*** [16]

  Solid state reaction was the first synthesis method used for preparing Bi_2WO_6. Bi_2O_3 and WO_3 were mixed in the ethanol solution and the mixture was dried for 5 h under 353 K and then sintered at 1173 K for 12 h [17]. The as-prepared Bi_2WO_6 with a band gap of 2.69 eV was employed as a photocatalyst to decompose the organic contaminants ($CHCl_3$ and CH_3CHO) under visible light. Results suggested that the Bi_2WO_6 could completely mineralize these organic pollutants. However, the big particle size, low surface area (0.64 m^2/g, less than 2% of P-25 which is 49.41 m^2/g) and relatively low visible-light-driven photocatalytic activity restricted the wide application of this synthesis method, leading to further research for alternative methods.

- ***Hydrothermal method***

  Typically, synthesis of Bi_2WO_6 by hydrothermal method used $Bi(NO_3)_3 \cdot 5H_2O$ and $Na_2WO_4 \cdot 2H_2O$ with the ratio of Bi : W = 2:1 as precursors. The hydrothermal reaction occurred in Teflon-lined stainless steel autoclaves in an oven at a specific temperature for some time. This formed a well-crystalline structure as illustrated in [18]. The formation process could be divided into three steps: self-aggregation, Ostwald ripening and self-organization [19, 20]. The hierarchical microsphere was the general structure of Bi_2WO_6 synthesized by this method. It should be mentioned that the crystal structure was greatly influenced by the synthesis conditions, especially the pH value of the

precursors. In other words, the structure of Bi_2WO_6 could be controlled by adjusting the synthesis conditions [21, 22]. The 3-D dimensional hierarchical (layer-by-layer) microspheres were transformed into 2-D nano-plates due to the curved architecture disappearing at each step of pH increase. Correspondingly, some physical and chemical properties of the photocatalysts changed such as their optical properties, BET surface areas and even the photocatalytic degradation efficiencies. Another significant factor in the hydrothermal method is the addition of a surfactant, which usually plays the template role during the synthesis process. For example, when adding P123 in the precursor, which is a tri-block copolymer typically used as a surfactant ($EO_{20}PO_{70}EO_{20}$, Plur-onic P123), the synthesized structure of Bi_2WO_6 was a tyre- and helix-like structure. Comparatively, without a surfactant in the precursor, it would be more like the hierarchical microspheres. Conclusively, the structure of Bi_2WO_6 synthesized by the facile hydrothermal method could be controlled by adjusting the experimental conditions.

- ***Microwave-assisted solvothermal method*** [23]

  Microwaves have been widely used in the synthesis of nanomaterials recently, as they can change the kinetics and selectivity of chemical reactions [24, 25]. The microwave-assisted technique is considered superior since it is rapid, environmentally friendly, simple and efficient. According to the research performed on the microwave-assisted solvothermal method in the synthesis of Bi_2WO_6, it only took about 5 minutes to synthesize the flower-like Bi_2WO_6 particles [23, 26]. The photocatalytic activities of the photocatalysts synthesized by the microwave-assisted solvothermal method were similar to the activities of those synthesized by the hydrothermal method, but in

reduced reaction time.

- ***Ultrasonic-assisted method*** [27]

  It has been confirmed that the photocatalytic activity of the Bi_2WO_6 synthesized by the ultrasonic-assisted method was 4-6 times higher than that of the photocatalysts synthesized by solid-state reaction [27]. In this method, a $Bi(NO_3)_3 \cdot 5H_2O$ and $Na_2WO_4 \cdot 2H_2O$ mixture was exposed to high-intensity ultrasound for 1 hour so as to produce the visible-light-induced Bi_2WO_6 nanoplate-like photocatalysts.

- ***Low-temperature combustion method*** [28]

  The low-temperature combustion synthesis (LCS) method has been reported in the preparation of other photocatalysts such as TiO_2 [29], ZnO [30] and WO_3 [31]. Zhang *et al.* introduced the synthesis of Bi_2WO_6 by the LCS method in 2010 [28]. The precursor consisting of $Bi(NO_3)_3 \cdot 5H_2O$ and $Na_2WO_4 \cdot 2H_2O$ was reacted on a hot plate which was preheated to a specific temperature (200 °C in [28]) until a yellow fluffy product was produced(Bi_2WO_6). As-prepared Bi_2WO_6 with high surface area owing for its small size in nanomaterial levels evidently enhanced the photocatalytic activity in degrading *Rhodamine B* (RhB) and Phenol.

Among all these synthesis methods of preparing Bi_2WO_6, hydrothermal method has gradually become the mainstream method owing to its simple operation and apparatus, facile experimental conditions, high productivity and also its environmentally friendly process. Furthermore, the pH and other synthesis conditions could be adjusted to control the chemical and physical properties as required in various conditions. Experimental results also proved that Bi_2WO_6 synthesized by the hydrothermal method possessed high visible-light-induced photocatalytic activity.

2.3.2 BiOBr

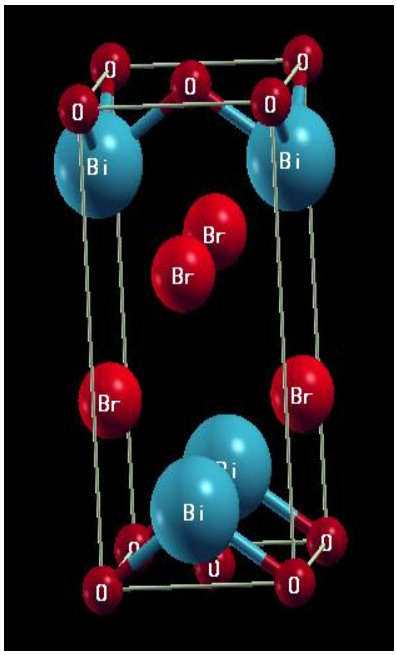

Fig. 2- 3. Structure of BiOBr. (Simulated by Quantum Espresso [13])

BiOBr, one of the bismuth oxyhalides, is a layer-structured semiconductor, $[Bi_2O_2]$ layer and Br atoms layer are interleaved to form the tetragonal structure (Fig. 2-3). Huang *et al*. theoretically calculated the electronic structure of BiOBr based on the density functional theory (DFT) [32]. The band gap of BiOBr was 2.92 eV which means it could be activated by irradiation with wavelengths lower than 420 nm, which is within the visible-light range [33]. It further calculated that the valence band of BiOBr consists of O 2p and Br 4p orbitals while Bi 6p orbitals contribute mostly to the conduction band.

Various synthesis methods have been tried and reported to prepare BiOBr. The general synthesis methods recently employed are as follows:

- ***Hydrolysis*** [34]

  As the simplest synthesis method, hydrolysis has been once employed in preparation

of BiOBr. $BiBr_3$ was hydrolyzed by adding Na_2CO_3 (*Eq. 6*) to adjust the pH of the solution between 6 and 10. The precipitates were separated by filtration and washed by distilled water several times until BiOBr was obtained. SEM images of BiOBr synthesized by the hydrolysis method shown suggested that it possessed the hierarchical structure with relatively poor crystallinity.

$$BiBr_3 + H_2O \xrightarrow{hydrolysis} BiOBr\downarrow + 2HBr \qquad \textbf{(Eq. 6)}$$

❖ ***Hydrothermal method***

Similar to the synthesis of Bi_2WO_6, the hydrothermal method was also applied in the synthesis of BiOBr. Bi $(NO_3)_3 \cdot 5H_2O$ was dissolved in acetic acid and dropwise added into the KBr solution, resulting in yellow precipitates forming immediately. The suspended solution was transferred into the Teflon-lined stainless steel autoclaves which were moved into the oven. The possible formation process of BiOBr could be illustrated as:

$$Bi^{3+} + CH_3CH_2COOH \longrightarrow BiO^+ + CH_3CHO + 2H^+ \qquad \textbf{(Eq. 7)}$$

$$Bi^{3+} + H_2O \longrightarrow BiO^+ + 2H^+ \qquad \textbf{(Eq. 8)}$$

$$BiO^+ + Br^- \longrightarrow BiOBr \qquad \textbf{(Eq. 9)}$$

Above is the typical process for the synthesis of BiOBr without surfactant, where flake-like structures could be obtained [33]. Meanwhile, by using a surfactant, some special and interesting structures could be formed. For example, using polyvinyl pyrrolidone (PVP) to modify the hydrothermal method, the structure of the prepared BiOBr was the hierarchical microflowers [35, 36]. Not only was the size and shape controlled, the optical properties and the final photocatalytic activities were greatly influenced, and it confirmed that the hierarchical microspheres were beneficial for the separation of the

electron-hole pairs, improving the photocatalytic performance. In other words, the photocatalytic activity in the degradation of organics could be controlled by adjusting the synthesis conditions resulting in structural differences.

- ***Solvothermal method***

The only difference between the hydrothermal and solvothermal method is the solvent in the precursor solution. Instead of aqueous, the solute was dissolved in diethylene glycol (DEG) or ethylene glycol (EG) [37]. These solvents played the template role to induce the assembly of hierarchical microspheres, which is beneficial for the improvement of photocatalytic performance [38]. The proposed formation processes included three steps: the formation of nanoplates in the early stage similar to the hydrothermal method, the EG-induced assembly of the nanoplates to form loose microspheres and the formation of hierarchical microspheres via the recrystallization process [39]. Furthermore, Zhang et al. utilized microwaves to assist the solvothermal method and optimize the synthesis route [40].

By employing the organic solvent, synthesis of 3D hierarchical microspheres by the solvothermal method resulted in some beneficial properties in photocatalysis, such as high visible-light-driven activity in the degradation of organic pollutants, and improved control of the structure. However, drawbacks of this method include the presence of impurities in the product and the inevitable secondary environmental pollution for using the organic solvent [41].

- ***Microemulsion method***

To overcome the problems with the synthesis of nanomaterials (*e.g.* complex operation

of controlling the particle structure and size), microemulsion has been used as the medium for the preparation of nanoparticles. Henle *et al.* introduced the synthesis of nano-sized particles of BiOBr using the microemulsion method [42]. The microemulsions consist of nonionic surfactants Marlophen NP5 ($RO(CH_2CH_2O)_xH$, x=5, R=nonylphenyl, M=440 g/mol, SASOL), heptane and aqueous salt solutions, in which the micelles act as the template and dictate the size of the target products. $Bi(NO_3)_3 \bullet 5H_2O$ and KBr were dissolved in the microemulsions to obtain BiO^+ and Br^- as separate microemulsions. The mixture of these separate microemulsions was stirred for 24 h, and then the precipitation was separated by centrifugation to get the BiOBr samples. Results exhibited that 3-22 nm BiOBr particles were synthesized. A large amount of surfactant was consumed during the process, which contributed to the method's complexity and high cost.

In conclusion, BiOBr could be synthesized by various methods and each of them has its benefits and drawbacks. After comprehensive consideration, hydrothermal and solvothermal methods would still be the preferred method due to its facile experimental conditions, and its simple and inexpensive operation process.

2.4 Introduction of heterojunction

Combining photocatalysts to establish a heterojunction, an interface between two or more semiconductors, results in a composite with reduced recombination rate of electron-hole pairs [43]. Such composites have generated increasing attention in photocatalysis, leading to publications of promising results. The mechanism involved is the interfacial transfer of electrons and holes as in [43], in which electrons jump from the conduction band of one

semiconductor to that of another semiconductor and holes move oppositely so as to achieve an efficient charge separation [44-46].

On the basis of commercially used TiO_2, numerous heterojunction composites have been synthesized with relatively high photocatalytic performance in the degradation of organics [47-51]. However, the low visible-light-driven photocatalytic activity and high recombination rate of carriers prevent its wide application. In this context, bismuth composites with high photocatalytic activity induced by visible-light irradiation were synthesized at specific run-time and conditions, while the high recombination rate of charges inhibit the further improvement of the photocatalytic performance. Many of approaches to modify the bismuth semiconductors have been tried [20], and it has been confirmed that the establishment of a heterojunction structure was the most promising and effective method. Correspondingly, numerous results related to bismuth heterojunction were reported, such as $ZnWO_4/Bi_2WO_6$ [52, 53], Graphene/BiOBr [54], $Bi_2O_2CO_3/Bi_2WO_6$ [55], BiOI/BiOBr [56], BiOCl/BiOBr [57], $Bi_2WO_6/BiVO_4$ [58, 59], WO_3/Bi_2WO_6 [60, 61], Bi_2O_3/Bi_2WO_6 [62-64] and g-C_3N_4/Bi_2WO_6 [65] *etc.* Before this paper, $BiOBr/Bi_2WO_6$ has rarely been reported except for one paper that synthesized $BiOBr/Bi_2WO_6$ composites using the solvothermal method in the presence of ionic liquid [C_{16}mim]Br in [66]. The complex, costly and environmental-unfriendly operation process impelled this work, hence the BiOBr-Bi_2WO_6 composites will be synthesized by the facile hydrothermal method.

2.5 Conclusions

The mechanism of photocatalysis has been introduced, which utilizes the energy of light to produce high oxidative species and experiences a secondary reaction to degrade the organic

pollutants. Bi_2WO_6 and BiOBr, two kinds of semiconductors with promising application in photocatalysis, have suitable band gaps to be stimulated by visible-light irradiation. By establishing a heterojunction, the recombination rate of photon-electron carriers could be reduced so as to improve the photocatalytic performance in decomposition of organics. Finally, the drawbacks of BiOBr-Bi_2WO_6 composites that are currently prepared by the solvothermal method impel this work, hence the BiOBr-Bi_2WO_6 heterojunction semiconductors will be synthesized by facile hydrothermal method.

2.6 References:

[1] A. Fujishima, K. Honda, Electrochemical photolysis of water at a semiconductor electrode, nature, 238 (1972) 37-38.

[2] K. Zhang, C. Liu, F. Huang, C. Zheng, W. Wang, Study of the electronic structure and photocatalytic activity of the BiOCl photocatalyst, Applied Catalysis B: Environmental, 68 (2006) 125-129.

[3] R. Daghrir, P. Drogui, D. Robert, Photoelectrocatalytic technologies for environmental applications, Journal of Photochemistry and Photobiology A: Chemistry, 238 (2012) 41-52.

[4] K. Yogo, M. Ishikawa, Recent progress in environmental catalytic technology, Catal Surv Jpn, 4 (2000) 83-90.

[5] Y. Xu, Y. He, X. Cao, D. Zhong, J. Jia, TiO2/Ti rotating disk photoelectrocatalytic (PEC) reactor: a combination of highly effective thin-film PEC and conventional PEC processes on a single electrode, Environmental science & technology, 42 (2008) 2612-2617.

[6] R. Thiruvenkatachari, S. Vigneswaran, I. Moon, A review on UV/TiO_2 photocatalytic oxidation process (Journal Review), Korean J Chem Eng, 25 (2008) 64-72.

[7] A.L. Linsebigler, G. Lu, J.T. Yates, Photocatalysis on TiO_2 Surfaces: Principles, Mechanisms, and Selected Results, Chem Rev, 95 (1995) 735-758.

[8] S.G. Kumar, L.G. Devi, Review on Modified TiO_2 Photocatalysis under UV/Visible Light: Selected Results and Related Mechanisms on Interfacial Charge Carrier Transfer Dynamics, The Journal of Physical Chemistry A, 115 (2011) 13211-13241.

[9] M. Kaneko, I. Okura, Photocatalysis science and technology, Kodansha Springer, (2002).

[10] Y. Xu, M.A. Schoonen, The absolute energy positions of conduction and valence bands of selected semiconducting minerals, Am Mineral, 85 (2000) 543-556.

[11] S. Malato, J. Blanco, A. Vidal, C. Richter, Photocatalysis with solar energy at a pilot-plant scale: an overview, Applied Catalysis B: Environmental, 37 (2002) 1-15.

[12] S. Kwon, M. Fan, A.T. Cooper, H. Yang, Photocatalytic applications of micro-and nano-TiO_2 in environmental engineering, Crit Rev Env Sci Tec, 38 (2008) 197-226.

[13] G. Paolo, B. Stefano, B. Nicola, C. Matteo, C. Roberto, C. Carlo, C. Davide, L.C. Guido, C. Matteo, D. Ismaila, C. Andrea Dal, G. Stefano de, F. Stefano, F. Guido, G. Ralph, G. Uwe, G. Christos, K. Anton, L. Michele, M.-S. Layla, M. Nicola, M. Francesco, M. Riccardo, P. Stefano, P. Alfredo, P. Lorenzo, S. Carlo, S. Sandro, S. Gabriele, P.S. Ari, S. Alexander, U. Paolo, M.W. Renata, QUANTUM ESPRESSO: a modular and open-source software project for quantum simulations of materials, Journal of Physics: Condensed Matter, 21 (2009) 395502.

[14] M. Shang, W. Wang, S. Sun, L. Zhou, L. Zhang, Bi_2WO_6 Nanocrystals with High Photocatalytic Activities under Visible Light, The Journal of Physical Chemistry C, 112 (2008) 10407-10411.

[15] Y. Shi, S. Feng, C. Cao, Hydrothermal synthesis and characterization of Bi_2MoO_6 and Bi_2WO_6, Mater Lett, 44 (2000) 215-218.

[16] A. Kudo, S. Hijii, H_2 or O_2 Evolution from Aqueous Solutions on Layered Oxide Photocatalysts Consisting of Bi^{3+} with $6s_2$ Configuration and d_0 Transition Metal Ions, Chem Lett, 1999 (1999) 1103-1104.

[17] J. Tang, Z. Zou, J. Ye, Photocatalytic Decomposition of Organic Contaminants by Bi_2WO_6

Under Visible Light Irradiation, Catal Lett, 92 (2004) 53-56.

[18] Y. Li, J. Liu, X. Huang, G. Li, Hydrothermal Synthesis of Bi_2WO_6 Uniform Hierarchical Microspheres, Cryst Growth Des, 7 (2007) 1350-1355.

[19] L. Zhang, W. Wang, Z. Chen, L. Zhou, H. Xu, W. Zhu, Fabrication of flower-like Bi_2WO_6 superstructures as high performance visible-light driven photocatalysts, J Mater Chem, 17 (2007) 2526-2532.

[20] L. Zhang, Y. Zhu, A review of controllable synthesis and enhancement of performances of bismuth tungstate visible-light-driven photocatalysts, Catalysis Science & Technology, 2 (2012) 694-706.

[21] C. Zhang, Y. Zhu, Synthesis of Square Bi_2WO_6 Nanoplates as High-Activity Visible-Light-Driven Photocatalysts, Chem Mater, 17 (2005) 3537-3545.

[22] L. Zhang, W. Wang, L. Zhou, H. Xu, Bi_2WO_6 Nano- and Microstructures: Shape Control and Associated Visible-Light-Driven Photocatalytic Activities, Small, 3 (2007) 1618-1625.

[23] L. Wu, J. Bi, Z. Li, X. Wang, X. Fu, Rapid preparation of Bi_2WO_6 photocatalyst with nanosheet morphology via microwave-assisted solvothermal synthesis, Catalysis Today, 131 (2008) 15-20.

[24] Z. Ni, R.I. Masel, Rapid Production of Metal−Organic Frameworks via Microwave-Assisted Solvothermal Synthesis, J Am Chem Soc, 128 (2006) 12394-12395.

[25] A.V. Murugan, T. Muraliganth, A. Manthiram, Comparison of Microwave Assisted Solvothermal and Hydrothermal Syntheses of $LiFePO_4$/C Nanocomposite Cathodes for Lithium Ion Batteries, The Journal of Physical Chemistry C, 112 (2008) 14665-14671.

[26] X.-F. Cao, L. Zhang, X.-T. Chen, Z.-L. Xue, Microwave-assisted solution-phase preparation of flower-like Bi_2WO_6 and its visible-light-driven photocatalytic properties, Crystengcomm, 13 (2011) 306-311.

[27] L. Zhou, W. Wang, L. Zhang, Ultrasonic-assisted synthesis of visible-light-induced Bi_2MO_6 (M=W, Mo) photocatalysts, Journal of Molecular Catalysis A: Chemical, 268 (2007) 195-200.

[28] Z. Zhang, W. Wang, M. Shang, W. Yin, Low-temperature combustion synthesis of Bi_2WO_6 nanoparticles as a visible-light-driven photocatalyst, J Hazard Mater, 177 (2010) 1013-1018.

[29] T. Aarthi, G. Madras, Photocatalytic reduction of metals in presence of combustion synthesized nano-TiO_2, Catal Commun, 9 630-634.

[30] J. Lee, S. Park, H.-J. Park, J.-H. Lee, H.-S. Kim, Y.-J. Chung, Photocatalytic degradation of TOC from aqueous phenol solution using solution combusted ZnO nanopowders, J Electroceram, 22 (2009) 110-113.

[31] W. Morales, M. Cason, O. Aina, N.R. de Tacconi, K. Rajeshwar, Combustion Synthesis and Characterization of Nanocrystalline WO_3, J Am Chem Soc, 130 (2008) 6318-6319.

[32] W.L. Huang, Q. Zhu, Electronic structures of relaxed BiOX (X=F, Cl, Br, I) photocatalysts, Comp Mater Sci, 43 (2008) 1101-1108.

[33] Z. Jiang, F. Yang, G. Yang, L. Kong, M.O. Jones, T. Xiao, P.P. Edwards, The hydrothermal synthesis of BiOBr flakes for visible-light-responsive photocatalytic degradation of methyl orange, Journal of Photochemistry and Photobiology A: Chemistry, 212 (2010) 8-13.

[34] Y. Wang, Z. Shi, C. Fan, X. Wang, X. Hao, Y. Chi, Synthesis, characterization, and

photocatalytic properties of BiOBr catalyst, J Solid State Chem, 199 (2013) 224-229.

[35] X. Shi, X. Chen, X. Chen, S. Zhou, S. Lou, Y. Wang, L. Yuan, PVP assisted hydrothermal synthesis of BiOBr hierarchical nanostructures and high photocatalytic capacity, Chemical Engineering Journal, 222 (2013) 120-127.

[36] Y.M. Cao, F.M. Wang, Z.F. Jia, N. Liu, Surfactant-assisted hydrothermal synthesis of multilayered flower-like BiOBr with enhanced visible light photocatalytic activity, Adv Mat Res, 476 (2012) 1541-1546.

[37] L. Ye, Y. Su, X. Jin, H. Xie, C. Zhang, Recent advances in BiOX (X = Cl, Br and I) photocatalysts: synthesis, modification, facet effects and mechanisms, Environmental Science: Nano, 1 (2014) 90-112.

[38] Y. Huo, J. Zhang, M. Miao, Y. Jin, Solvothermal synthesis of flower-like BiOBr microspheres with highly visible-light photocatalytic performances, Applied Catalysis B: Environmental, 111–112 (2012) 334-341.

[39] X. Zhang, Z. Ai, F. Jia, L. Zhang, Generalized One-Pot Synthesis, Characterization, and Photocatalytic Activity of Hierarchical BiOX (X = Cl, Br, I) Nanoplate Microspheres, The Journal of Physical Chemistry C, 112 (2008) 747-753.

[40] L. Zhang, X.-F. Cao, X.-T. Chen, Z.-L. Xue, BiOBr hierarchical microspheres: Microwave-assisted solvothermal synthesis, strong adsorption and excellent photocatalytic properties, J Colloid Interf Sci, 354 (2011) 630-636.

[41] H. Cheng, B. Huang, Z. Wang, X. Qin, X. Zhang, Y. Dai, One-Pot Miniemulsion-Mediated Route to BiOBr Hollow Microspheres with Highly Efficient Photocatalytic Activity, Chemistry – A European Journal, 17 (2011) 8039-8043.

[42] J. Henle, P. Simon, A. Frenzel, S. Scholz, S. Kaskel, Nanosized BiOX (X = Cl, Br, I) Particles Synthesized in Reverse Microemulsions, Chem Mater, 19 (2007) 366-373.

[43] N. Serpone, P. Maruthamuthu, P. Pichat, E. Pelizzetti, H. Hidaka, Exploiting the interparticle electron transfer process in the photocatalysed oxidation of phenol, 2-chlorophenol and pentachlorophenol: chemical evidence for electron and hole transfer between coupled semiconductors, Journal of Photochemistry and Photobiology A: Chemistry, 85 (1995) 247-255.

[44] M. Fujii, T. Kawai, S. Kawai, Photocatalytic activity and the energy levels of electrons in a semiconductor particle under irradiation, Chem Phys Lett, 106 517-522.

[45] M.F. Finlayson, B.L. Wheeler, N. Kakuta, K.H. Park, A.J. Bard, A. Campion, M.A. Fox, S.E. Webber, J.M. White, Determination of flat-band position of cadmium sulfide crystals, films, and powders by photocurrent and impedance techniques, photoredox reaction mediated by intragap states, The Journal of Physical Chemistry, 89 (1985) 5676-5681.

[46] J.R. White, A.J. Bard, Electrochemical investigation of photocatalysis at cadmium sulfide suspensions in the presence of methylviologen, The Journal of Physical Chemistry, 89 (1985) 1947-1954.

[47] Q.C. Xu, D.V. Wellia, Y.H. Ng, R. Amal, T.T.Y. Tan, Synthesis of Porous and Visible-Light Absorbing Bi_2WO_6/TiO_2 Heterojunction Films with Improved Photoelectrochemical and Photocatalytic Performances, The Journal of Physical Chemistry C, 115 (2011) 7419-7428.

[48] L. Yang, S. Luo, Y. Li, Y. Xiao, Q. Kang, Q. Cai, High Efficient Photocatalytic Degradation of p-Nitrophenol on a Unique Cu_2O/TiO_2 p-n Heterojunction Network Catalyst, Environmental Science & Technology, 44 (2010) 7641-7646.

[49] H. Huang, D. Li, Q. Lin, Y. Shao, W. Chen, Y. Hu, Y. Chen, X. Fu, Efficient Photocatalytic Activity of PZT/TiO_2 Heterojunction under Visible Light Irradiation, The Journal of Physical Chemistry C, 113 (2009) 14264-14269.

[50] H. Huang, D. Li, Q. Lin, W. Zhang, Y. Shao, Y. Chen, M. Sun, X. Fu, Efficient Degradation of Benzene over $LaVO_4$/TiO_2 Nanocrystalline Heterojunction Photocatalyst under Visible Light Irradiation, Environmental Science & Technology, 43 (2009) 4164-4168.

[51] H. Yu, S. Chen, X. Quan, H. Zhao, Y. Zhang, Fabrication of a TiO_2−BDD Heterojunction and its Application As a Photocatalyst for the Simultaneous Oxidation of an Azo Dye and Reduction of Cr(VI), Environmental Science & Technology, 42 (2008) 3791-3796.

[52] M. Hojamberdiev, K.-i. Katsumata, K. Morita, S.A. Bilmes, N. Matsushita, K. Okada, One-step hydrothermal synthesis and photocatalytic performance of $ZnWO_4$/Bi_2WO_6 composite photocatalysts for efficient degradation of acetaldehyde under UV light irradiation, Applied Catalysis A: General, 457 (2013) 12-20.

[53] D. He, L. Wang, D. Xu, J. Zhai, D. Wang, T. Xie, Investigation of Photocatalytic Activities over Bi_2WO_6/$ZnWO_4$ Composite under UV Light and Its Photoinduced Charge Transfer Properties, ACS Applied Materials & Interfaces, 3 (2011) 3167-3171.

[54] X. Zhang, X. Chang, M.A. Gondal, B. Zhang, Y. Liu, G. Ji, Synthesis and photocatalytic activity of graphene/BiOBr composites under visible light, Appl Surf Sci, 258 (2012) 7826-7832.

[55] X. Huang, H. Chen, One-pot hydrothermal synthesis of $Bi_2O_2CO_3$/Bi_2WO_6 visible light photocatalyst with enhanced photocatalytic activity, Appl Surf Sci, 284 (2013) 843-848.

[56] H. Lin, H. Ye, X. Li, J. Cao, S. Chen, Facile anion-exchange synthesis of BiOI/BiOBr

composite with enhanced photoelectrochemical and photocatalytic properties, Ceram Int, 40 (2014) 9743-9750.

[57] J. Zhang, J. Xia, S. Yin, H. Li, H. Xu, M. He, L. Huang, Q. Zhang, Improvement of visible light photocatalytic activity over flower-like BiOCl/BiOBr microspheres synthesized by reactable ionic liquids, Colloids and Surfaces A: Physicochemical and Engineering Aspects, 420 (2013) 89-95.

[58] P. Ju, P. Wang, B. Li, H. Fan, S. Ai, D. Zhang, Y. Wang, A novel calcined Bi_2WO_6/$BiVO_4$ heterojunction photocatalyst with highly enhanced photocatalytic activity, Chemical Engineering Journal, 236 (2014) 430-437.

[59] S. Chaiwichian, B. Inceesungvorn, K. Wetchakun, S. Phanichphant, W. Kangwansupamonkon, N. Wetchakun, Highly efficient visible-light-induced photocatalytic activity of Bi_2WO_6/$BiVO_4$ heterojunction photocatalysts, Mater Res Bull, 54 (2014) 28-33.

[60] M. Gui, W. Zhang, Y. Chang, Y. Yu, One-step hydrothermal preparation strategy for nanostructured WO_3/Bi_2WO_6 heterojunction with high visible light photocatalytic activity, Chemical Engineering Journal, 197 (2012) 283-288.

[61] G. He, G. He, A. Li, X. Li, X. Wang, Y. Fang, Y. Xu, Synthesis and visible light photocatalytic behavior of WO_3 (core)/Bi_2WO_6 (shell), Journal of Molecular Catalysis A: Chemical, 385 (2014) 106-111.

[62] Y. Hao, F. Li, F. Chen, M. Chai, R. Liu, X. Wang, In situ one-step combustion synthesis of Bi_2O_3/Bi_2WO_6 heterojunctions with notable visible light photocatalytic activities, Mater Lett, 124 (2014) 1-3.

[63] Y. Peng, M. Yan, Q. Chen, C. Fan, H. Zhou, A. Xu, Novel one-dimensional Bi_2O_3-Bi_2WO_6

p-n hierarchical heterojunction with enhanced photocatalytic activity, Journal of Materials Chemistry A, 2 (2014) 8517-8524.

[64] M. Gui, W. Zhang, Q. Su, C. Chen, Preparation and visible light photocatalytic activity of Bi_2O_3/Bi_2WO_6 heterojunction photocatalysts, J Solid State Chem, 184 (2011) 1977-1982.

[65] S.C. Yan, Z.S. Li, Z.G. Zou, Photodegradation Performance of g-C_3N_4 Fabricated by Directly Heating Melamine, Langmuir, 25 (2009) 10397-10401.

[66] J. Xia, J. Di, S. Yin, H. Xu, J. Zhang, Y. Xu, L. Xu, H. Li, M. Ji, Facile fabrication of the visible-light-driven Bi_2WO_6/BiOBr composite with enhanced photocatalytic activity, RSC Advances, 4 (2014) 82-90.

Section Ⅱ:

Synthesis of BiOBr-Bi_2WO_6 heterojunction semiconductors

CHAPTER 3:

SYNTHESIS, ANALYSIS AND TESTING OF BiOBr-Bi_2WO_6 PHOTOCATALYTIC HETEROJUNCTION SEMICONDUCTORS*

Xiangchao Meng, Jason (Zisheng) Zhang

*Submitted to ***International journal of photoenergy***

Abstract:

In photocatalysis, the recombination of electron-hole pairs is generally regarded as one of its most serious drawbacks. The synthesis of various composite photocatalysts with heterojunction structures has increasingly shed light on preventing this recombination. In this work, a BiOBr-Bi_2WO_6 photocatalytic heterojunction semiconductor was synthesized by the facile hydrothermal method and applied in the photocatalytic degradation process. It was determined that both reaction time and temperature significantly affected the crystal structure

and morphologies of the photocatalysts. BiOBr (50 at%)-Bi_2WO_6 composites were prepared under optimum synthesis conditions (120 ℃ for 6 h) and by theoretically analyzing the DRS results, it was determined that it possessed the suitable band gap (2.61 eV) to be stimulated by visible-light irradiation. The photocatalytic activities of the as-prepared photocatalysts were evaluated by the degradation of *Rhodamine B (RhB)* under visible-light irradiation. The experimental conditions, including initial concentration, pH and catalyst dosage, were explored and the photocatalysts in this system were proven stable enough to be reused for several runs. Moreover, the interpreted mechanism of the heterojunction enhancement effect proved that the synthesis of a heterojunction structure provided an effective method to decrease the recombination rate of the electron-hole pairs, thereby improving the photocatalytic activity.

Keywords: photocatalysis; hydrothermal; BiOBr-Bi_2WO_6; heterojunction; Rhodamine B (RhB)

3.1 Introduction

Photocatalysts are growing more prominent due to their essential role in most of today's environmental and energy-source problems. Since 1972, photocatalysis has been heavily researched and an increasing number of results have been published [1]. The involved fields mainly include hydrogen generation by water-splitting [2, 3] and the remediation of environmental problems related to industrial wastewater treatment [4], ground water purification [5, 6], disinfection [7, 8] and removal of air pollutants [9, 10]. Simultaneously, the defects of using photocatalysts were highlighted throughout their prosperous development, specifically the low visible-light driven photocatalytic activities (commercially used photocatalysts-TiO_2 could only be activated by UV light) and the high recombination rates of the photo-generated electron-hole pairs.

Based on recent works, remediation trials aimed at overcoming the drawbacks mentioned above include modification of existing photocatalysts (*e.g.* metal deposition, doping, *etc.*) [11] and synthesis of novel photocatalysts with high-visible light driven photocatalytic activities such as C_3N_4 [12], Graphene [13], and Bismuth composites (*e.g.* BiOX, X=F, Cl, Br and I, Bi_2WO_6 *etc.*) [14, 15]. Bismuth composites have high visible-light photocatalytic activity due to their well-dispersed valence bands consisting of not only O 2p orbitals like in metal oxide semiconductors, but also Bi 6s orbitals. As a result, the composites have better separation of electron-hole pairs despite their narrow band gaps [16]. By adjusting the synthesizing conditions, a variety of morphologies of bismuth composites were prepared, such as nanoplate-like structures, micro-porous spheres, and hierarchical structures. This is because the structure of the photocatalyst, to some extent, influences their properties. For example,

semiconductors with a 3D structure could have slightly narrower band gaps than plate-like semiconductors [15].

Heterojunction semiconductors are gradually emerging recently due to the enhancement effect on the photocatalytic activity. Due to the high visible-light driven photocatalytic activity of bismuth composites and comparatively high recombination rate of the photo-generated electron-hole pairs, researchers focused on recombining two different bismuth composites to establish the heterojunction structure, in which the self-formed electric field could push the electrons and holes to opposite sides of the heterojunction, effectively separating the charge carriers. Many heterojunction semiconductors with high photocatalytic degradation of pollutants have been reported that use either Bi_2WO_6 or BiOBr in the composite [17-22]. However, to the knowledge of the author, a BiOBr-Bi_2WO_6 heterojunction photocatalyst synthesized by the facile hydrothermal method has still not been reported. Theoretically, a BiOBr-Bi_2WO_6 composite has a suitable band gap for stimulation by visible-light irradiation and can be applied in the degradation of pollutants in dye water via generation of oxidative species such as hydroxyl radicals, superoxide radicals and hydrogen peroxide.

This report presents the preparation of BiOBr-Bi_2WO_6 heterojunction semiconductors using the facile hydrothermal method. The crystal structures and morphologies of the as-prepared photocatalysts were observed by XRD and SEM techniques. DRS and classical Tauc formulation were applied to evaluate and calculate the band gaps. The photo-degradation of *Rhodamine B (RhB)* was used to measure the photocatalytic activity of the composites under visible-light irradiation (wavelength λ>410 nm) in a slurry reactor. The influence of experimental conditions in synthesizing the samples and photocatalytic degradation process

was explored and introduced. Finally, the mechanism of the heterojunction enhancement effect was illustrated with the band structure.

3.2 Experimental

3.2.1 Synthesis of BiOBr-Bi_2WO_6 composites

The facile hydrothermal method was used as the synthesis method to prepare the BiOBr-Bi_2WO_6 composites. All of the reagents were purchased from Sigma-Aldrich in their pure form. 2 g $Bi(NO_3)_3$•$5H_2O$ was dissolved in 80 mL acetic acid and then dropwise added into the solution containing 0.45 g Na_2WO_4•$2H_2O$ and 0.16 g KBr. Herein, the atomic ratio of BiOBr/Bi_2WO_6 was 1:1. The turbid liquid was then moved into 45 mL Teflon-lined stainless steel autoclaves (purchased from Parr Instrument Company) and magnetically stirred for 30 minutes under room temperature. Next, the autoclaves were heated in the oven at a designated temperature for a designated amount of time. In this work, the temperatures that were chosen are 90 ℃, 120 ℃, 150 ℃, 180 ℃ and 210 ℃, respectively. Meanwhile, the time of the heat preservation were 3 h, 6 h, 9 h, 12 h and 15 h, respectively. After the autoclaves naturally cooled down to room temperature, the precipitate was separated by centrifugation (1500 rpm for 5 minutes) and finally dried in the oven (80 ℃ for 12 h).

3.2.2 Characterization

The crystal structures were characterized by X-ray powder diffraction (XRD) with a Cu-Kα radiation Diffractometer at 40 kV and 44mA recorded with 2θ scope ranging from 5-80 °. As for the morphologies, field-emission scanning electron microscopy (FE-SEM) was used. The UV-vis diffusion reflectance spectra of the photocatalysts were performed by a UV-vis spectrophotometer (Thermo Evolution 300) equipped with an accessory to analyze powder samples.

3.2.3 Photocatalytic reactor and photocatalytic activity measurement

The photocatalytic reactor was a slurry batch photoreactor (Fig. 3-1). The light source was a 300 W tungsten halide bulb (purchased from USHIO) with a cut-off filter (purchased from Kenko Zeta, transmittance>90%) to filter out the irradiation with wavelengths below 410 nm so that the irradiation in this system attributed only to visible light. The intensity of the irradiation was found to be approximately 4.7×10^{-3} Einstein$\bullet m^{-2} \bullet s^{-1}$ measured by a quantum meter (Biospherical QSL-2100; 400 nm<λ<700 nm). The sufficiently high irradiation intensity aimed to prevent the dependence of the reaction rate on the generation of the electron-hole pairs, and the controlled factor of the photocatalytic activity was the mass transfer. A cooling jacket was applied outside the reactor, and the temperature of the degradation process was kept around (20±2) ℃. Meanwhile, the solid-liquid solution was stirred magnetically under 180 rpm to enhance the mass transfer.

Fig. 3-1. Photo of the photocatalytic reactor used in this system.

Rhodamine B (RhB) was regarded as the polluting organic in the dye water. In each experiment, 200 mL of waste water (aqueous RhB solution) with a specific concentration was added into the 500 mL beaker, and a certain amount of the specific photocatalyst was mixed with the waste water under magnetic stirring for 30 min in the dark to attain the adsorption-desorption balance. The photocatalytic degradation was then performed for 2 hours in the presence of visible light irradiation. About 1 mL of the suspension was taken out from the reactor every 10 min, and the supernatant solution was separated using the centrifuge and measured by UV-Vis spectrophotometer (Puxi, UV 1901). The peak absorbance for RhB was λ=554nm. The degradation efficiency of RhB was calculated using the following equation:

$$\omega_{\mathrm{degradation}\,efficiency} = \frac{c_o - c_t}{c_o} \times 100\%$$

Where c_o is the initial concentration of RhB and c_t is the concentration of RhB at the specific testing time during the degradation.

To study the influencing factors of the degradation process, the initial concentration of RhB, pH of the dye water and the dosage amount of the photocatalysts in the slurry system would be explored.

3.3. Results and Discussion

3.3.1 XRD analysis

Two factors, the time of the heat preservation and the temperature in the synthesis process, were explored, and the crystal structures of the BiOBr-Bi_2WO_6 composites synthesized under different experimental conditions were measured by X-ray diffraction techniques.

Firstly, the effect of holding time of the autoclaves in the oven was studied and shown in Fig. 3-2. All of the XRD patterns synthesized under various holding time at 120 ℃ showed that characteristic peaks were in good agreement with the tetragonal structure for BiOBr in the standard JCPDS card (09-0393) and the orthorhombic structure for Bi_2WO_6 in the standard JCPDS card (39-0256). With the holding time rising up to 6 h, the characteristic peaks became much sharper which signifies an increase in crystallinity. When the holding time was exceeded 6 h, the outline and the intensity of the characteristic peaks were similar, which suggested that 6 h was enough for the synthesis of the BiOBr-Bi_2WO_6 composites just from the point of the crystal structure.

Secondly, the effect of the synthesis temperature of the autoclaves in the oven was studied, and the XRD pattern of the BiOBr-Bi_2WO_6 composites synthesized under various temperature and holding 6 h were shown in Fig. 3-3. It could be concluded that the composites before hydrothermal treatment singly consisted of tetragonal BiOBr, and with increasing temperature, the characteristic peaks of orthorhombic Bi_2WO_6 became more prominent such as the typical peak at 2θ=28.30 °. When the temperature was over 120 ℃, the characteristic peaks of BiOBr became weaker and the characteristic peaks of Bi_2WO_6 became stronger. At 210 ℃, only some stunted characteristic peaks of Bi_2WO_6 were found. This phenomena might be because

temperatures higher than 120 ℃ was in favor of the growth of Bi_2WO_6 and probably went against the growth of BiOBr [23]. The XRD results indicate that the crystal structures of BiOBr-Bi_2WO_6 composites could be selectively synthesized by adjusting the hydrothermal reaction holding time and temperature, and the well-crystallized BiOBr-Bi_2WO_6 composites could be synthesized with facile experimental conditions at 120 ℃ for 6 h.

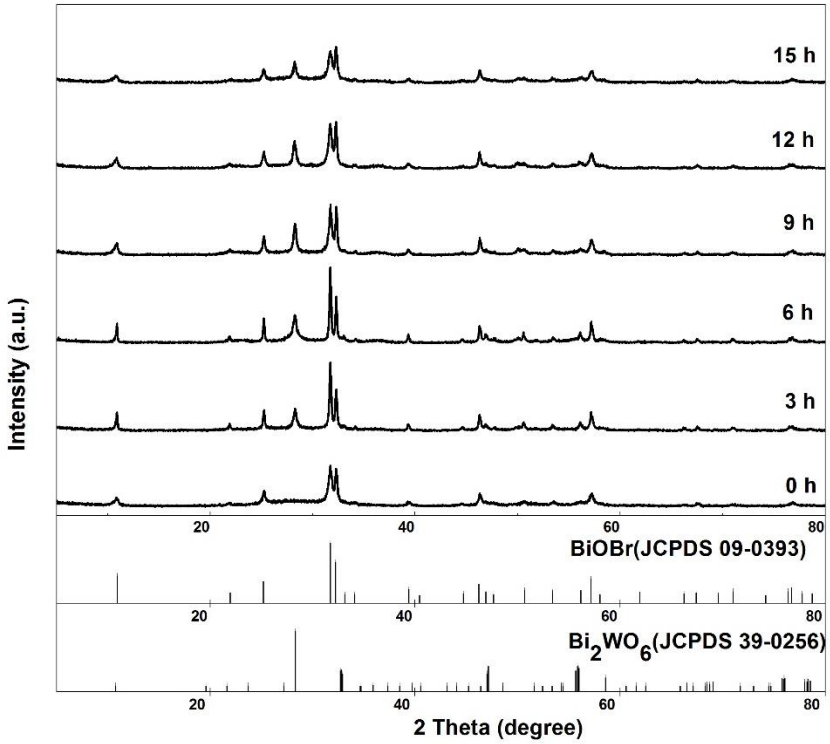

Fig. 3-2. XRD pattern of the BiOBr-Bi_2WO_6 composites synthesized for various time at 120 °C.

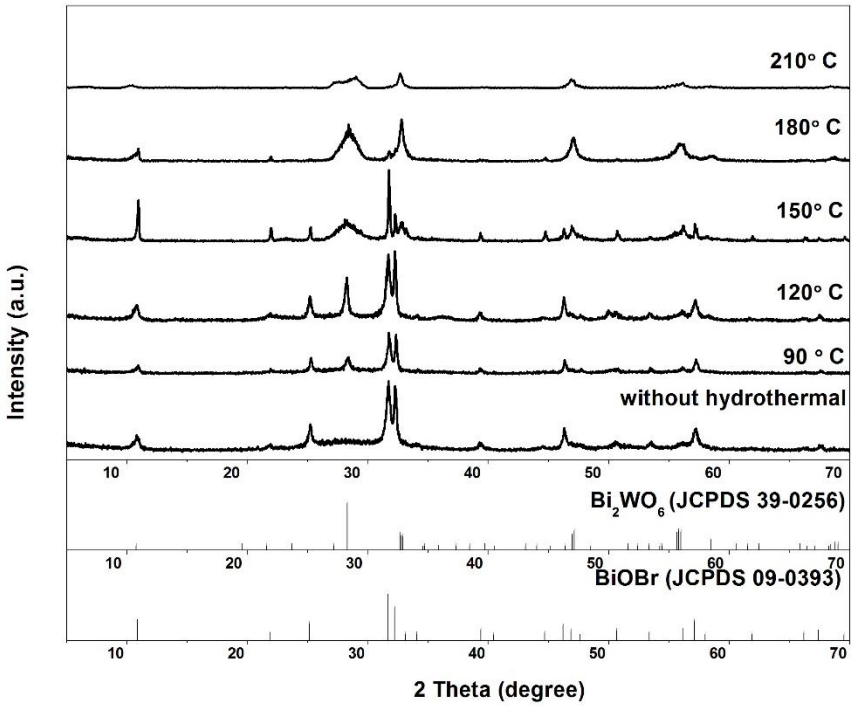

Fig. 3-3. XRD pattern of BiOBr-Bi_2WO_6 composites synthesized for 6 h under various temperature.

3.3.2 SEM analysis

Field-emission scanning electron microscopy (FE-SEM) has been performed to analyze the morphologies of the as-prepared BiOBr-Bi_2WO_6 composites. The formation process of BiOBr-Bi2WO6 composites involved hydrothermal ripening, which is a common phenomenon in crystal growth process. Based on the images in Fig. 3-4, it suggested that by increasing the reaction time from 3 h to 15 h (while keeping the temperature at 120 ℃), the structure changed from thin and irregularly shaped agglomerate nanoplates to flawless bigger microspheres. Specifically, when the reaction time was 6 h, the composites could be described as nanoplate-like BiOBr covered with flake-like Bi_2WO_6. When the reaction time exceeded 6 h, the size increase from about 1 μm (at 6 h) to about 8 μm (at 15 h) could be interpreted as the intrinsic anisotropic growth habit which could happen when the energy was high enough to overcome the reaction barriers (heated over 120 ℃ in our system) [24]. The surface became

much smoother due to the recrystallization process, which frequently took place during the hydrothermal synthesis of nanomaterials [25, 26]. The tighter the structure was, the lower the total energy of the system would be via minimal surface energy. SEM images of the photocatalysts synthesized under various temperatures for 6 h were shown in Fig. 3-5. They were hierarchical microspheres with increasingly better-crystallized flake-like Bi_2WO_6 grown on the surface when the temperature increased from 90 ℃ to 210 ℃. Combined with the results of XRD, it indicated that high temperatures selectively accelerated the formation of flake-like Bi_2WO_6. These results are highly consistent with the XRD results analyzed in the previous section and further prove that adjusting the experimental conditions could control the structure of the BiOBr-Bi_2WO_6 composites.

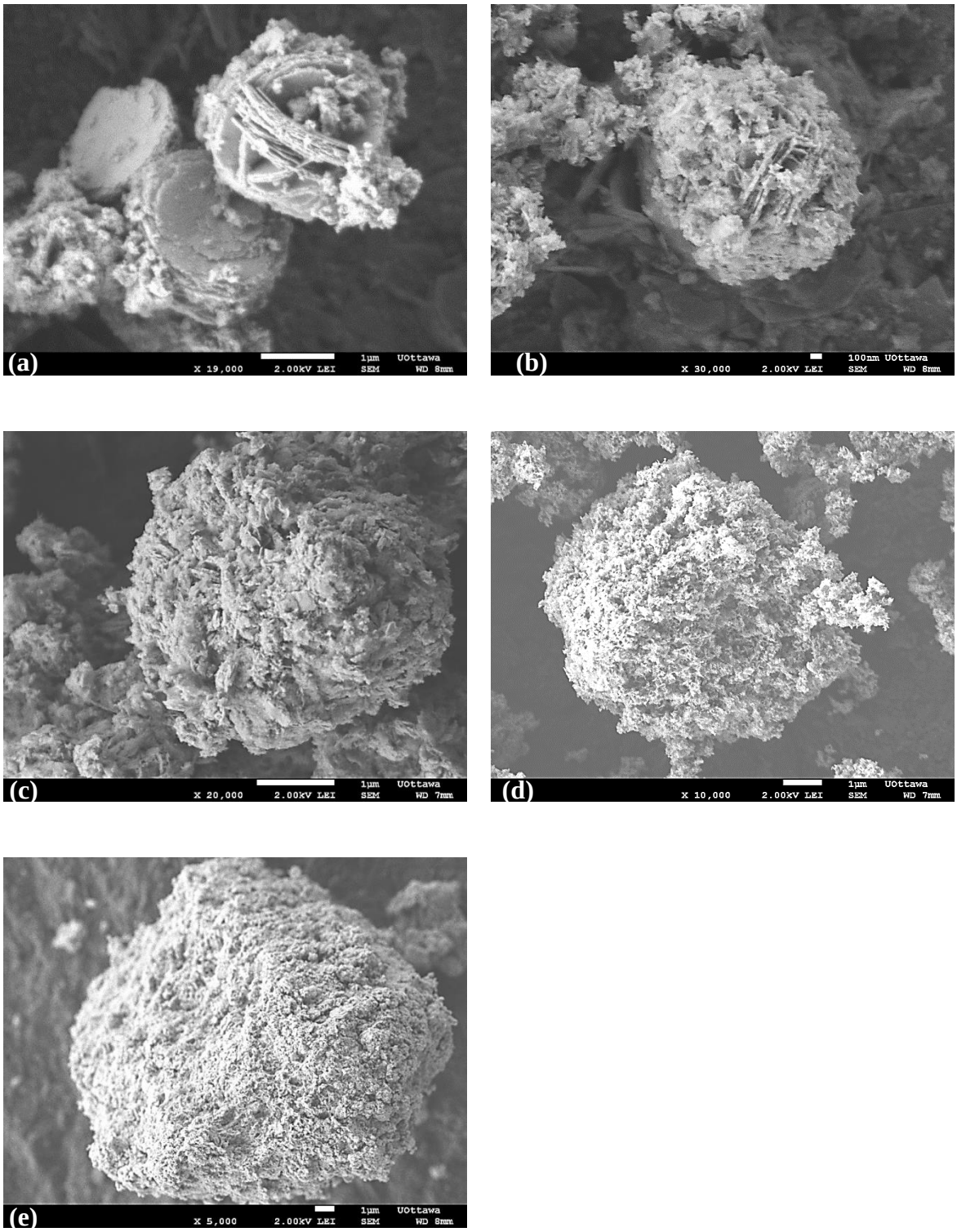

Fig. 3-4. FESEM images of BiOBr-Bi_2WO_6 composites synthesized for (a) 3 h, (b) 6 h, (c) 9 h, (d) 12 h and (e) 15 h under 120 °C.

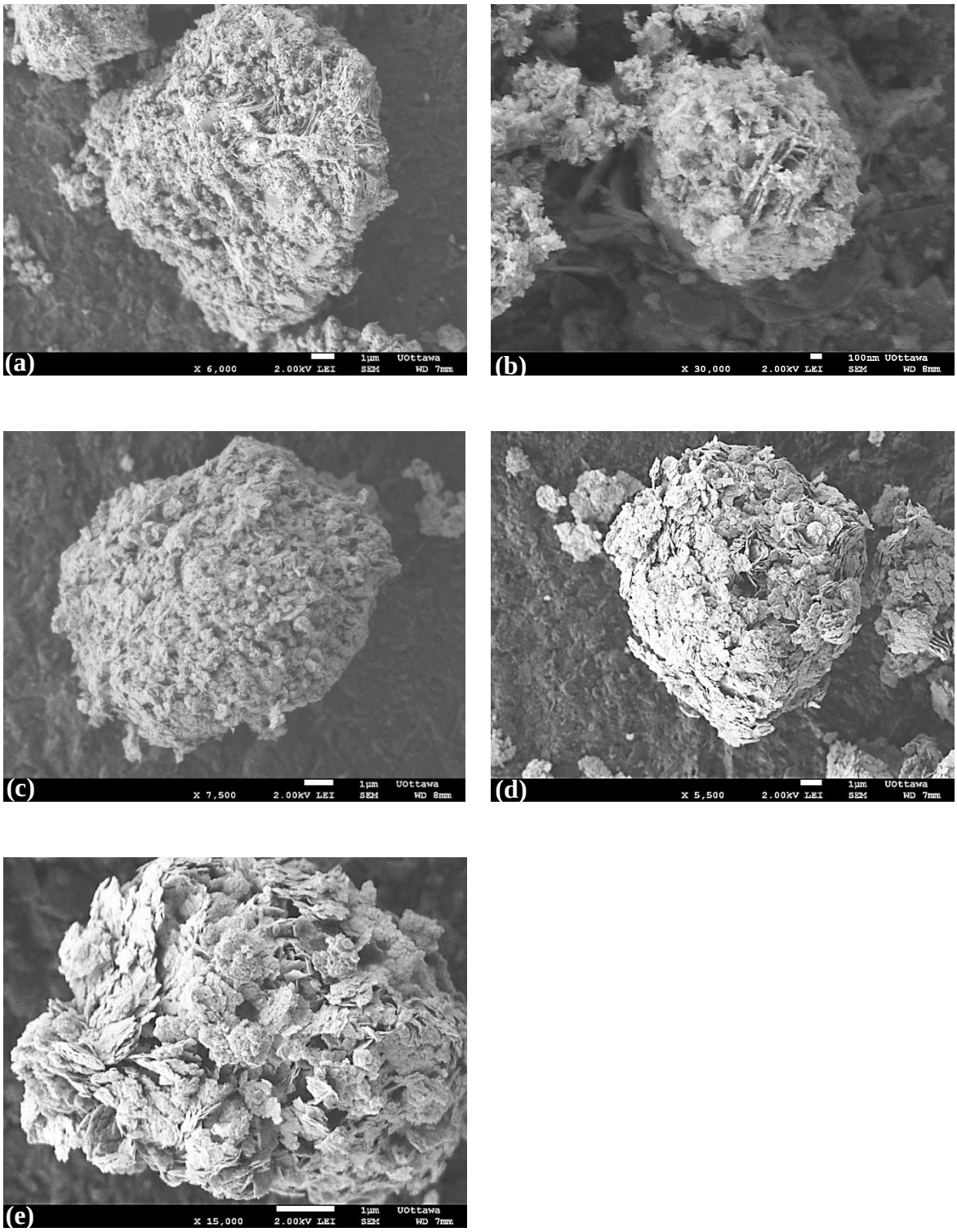

Fig. 3-5. FESEM images of BiOBr-Bi_2WO_6 composites synthesized for 6 h under (a) 90 °C, (b) 120 °C, (c) 150 °C, (d) 180 °C and (e) 210 °C.

3.3.3 UV-vis Diffuse Reflectance Spectrum (DRS) analysis

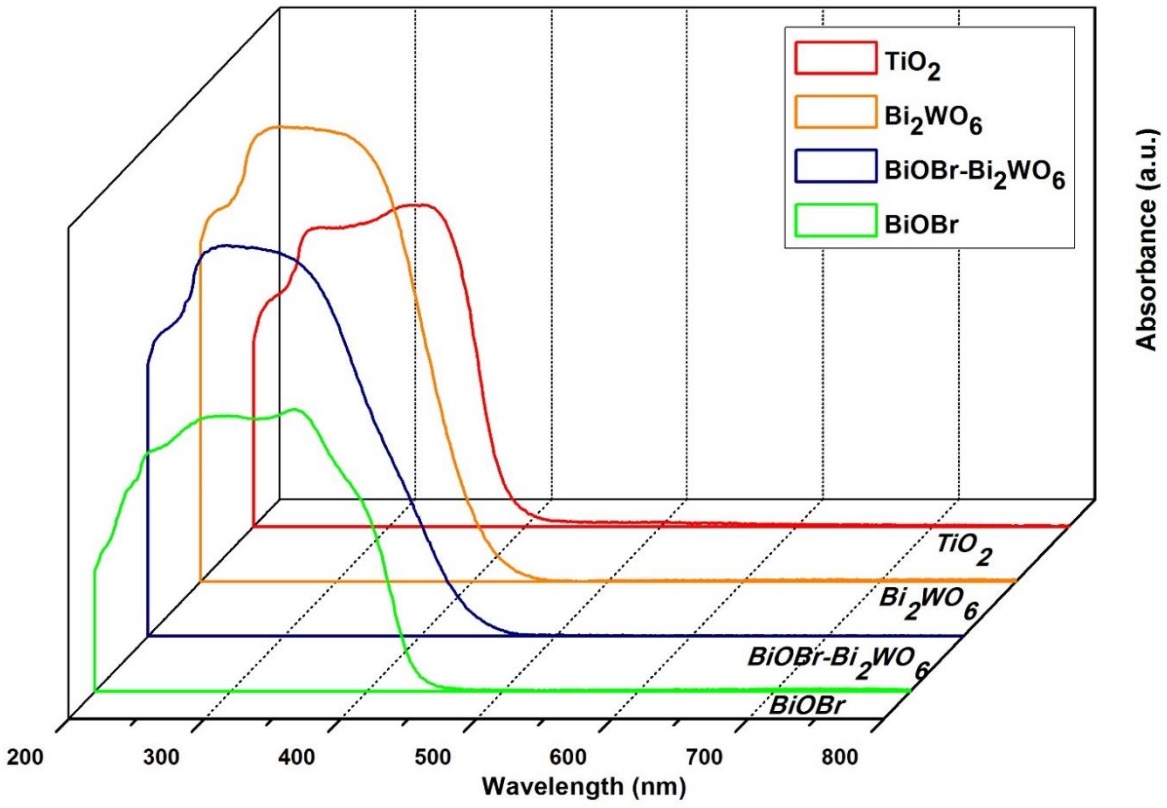

Fig. 3-6. UV-vis diffuse reflectance spectra (DRS) of TiO_2 (anatase), pure Bi_2WO_6, BiOBr-Bi_2WO_6 composites and pure BiOBr. (pure Bi_2WO_6 and BiOBr were synthesized by the hydrothermal method).

Optical properties of the as-prepared photocatalysts were measured by their UV-vis reflectance spectra. Fig. 3-6 shows the reflectance spectra of samples including pure Bi_2WO_6, BiOBr (50 at%)-Bi_2WO_6 composite, pure BiOBr and TiO_2 (P25, anatase). All of these results exhibit a significant increase in absorbance at the wavelength of irradiation lower than some specific value. For the band-gap transition, for example, the value for the BiOBr (50 at%)-Bi_2WO_6 composite was about 470 nm. Calculation of the band gap used the following classical Tauc equation (*Eq.1*) for indirect semiconductors.

$$\alpha E_{photon} = K(E_{photon} - E_g)^{\frac{n}{2}} \quad \textbf{(Eq.1)}$$

where $E_{photon} = h\nu$; α, K, E_g, n, h and ν represent the absorption coefficient, constant for semiconductor (usually equal to 1), bandgap energy, constant for semiconductor depending on the type of the band gap (for indirect transition: n=4) [27-29], Planck constant and irradiation frequency, respectively [30]. The band-gap value (E_g) were extrapolated by plotting $(\alpha \times E_{photon})^{1/2}$ versus E_{photon} shown in Fig. 3-7, and the band-gaps were 3.10 eV, 2.80 eV, 2.61 eV and 2.72 eV for TiO_2, pure Bi_2WO_6, BiOBr(50 at%)-Bi_2WO_6 composites and pure BiOBr, respectively. It suggested that the bismuth composites are suitable for being activated by visible light and that TiO_2 could only be stimulated by irradiation with wavelengths lower than 400 nm, i.e. the ultraviolet region. Furthermore, a red-shift from 2.61 eV to 2.72 eV was observed when the BiOBr formed a heterojunction with Bi_2WO_6, which could be due to the notable effects of the shape and structure. SEM images of pure BiOBr, Bi_2WO_6 and the BiOBr (50 at%)-Bi_2WO_6 composites were shown in Fig. 3-8. The 3D superstructure of the BiOBr-Bi_2WO_6 heterojunction could decrease the band-gap compared to the plate-like BiOBr; similar results appeared in [15]. Conclusively, synthesizing the novel photocatalysts (bismuth composites in this work) with suitable band-gaps could theoretically widen the wavelength of the irradiation into the visible light range.

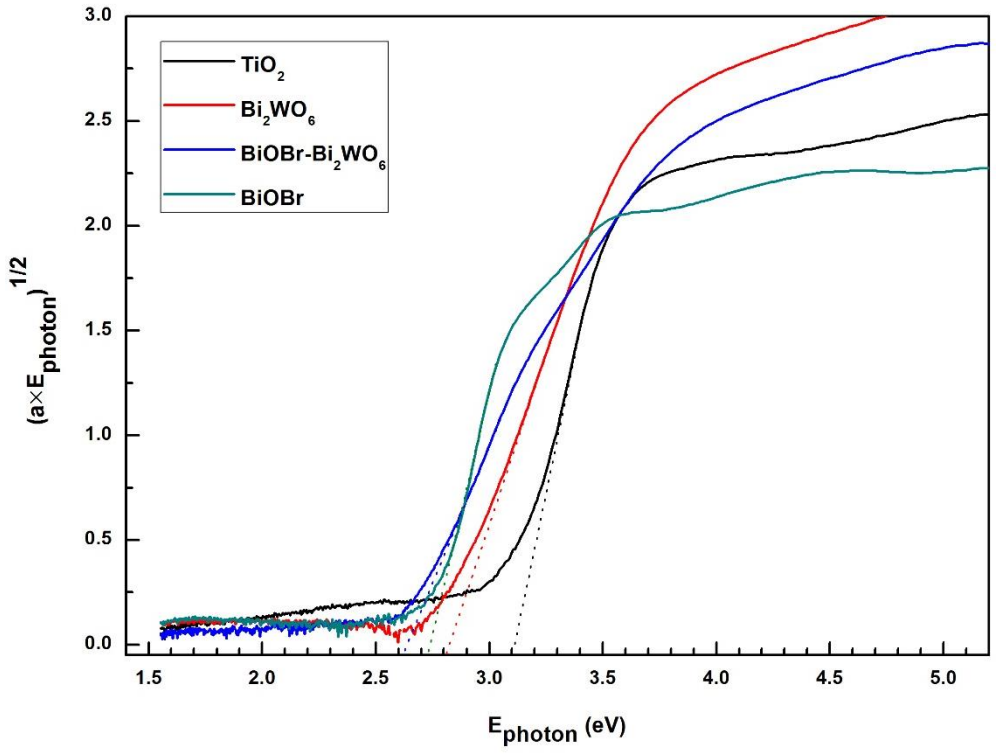

Fig. 3-7. $(\alpha*E_{photon})^{1/2}$-$E_{photon}$ curves of TiO_2 (anatase), pure Bi_2WO_6, BiOBr-Bi_2WO_6 composite and pure BiOBr. (pure Bi_2WO_6 and BiOBr were synthesized by the hydrothermal method).

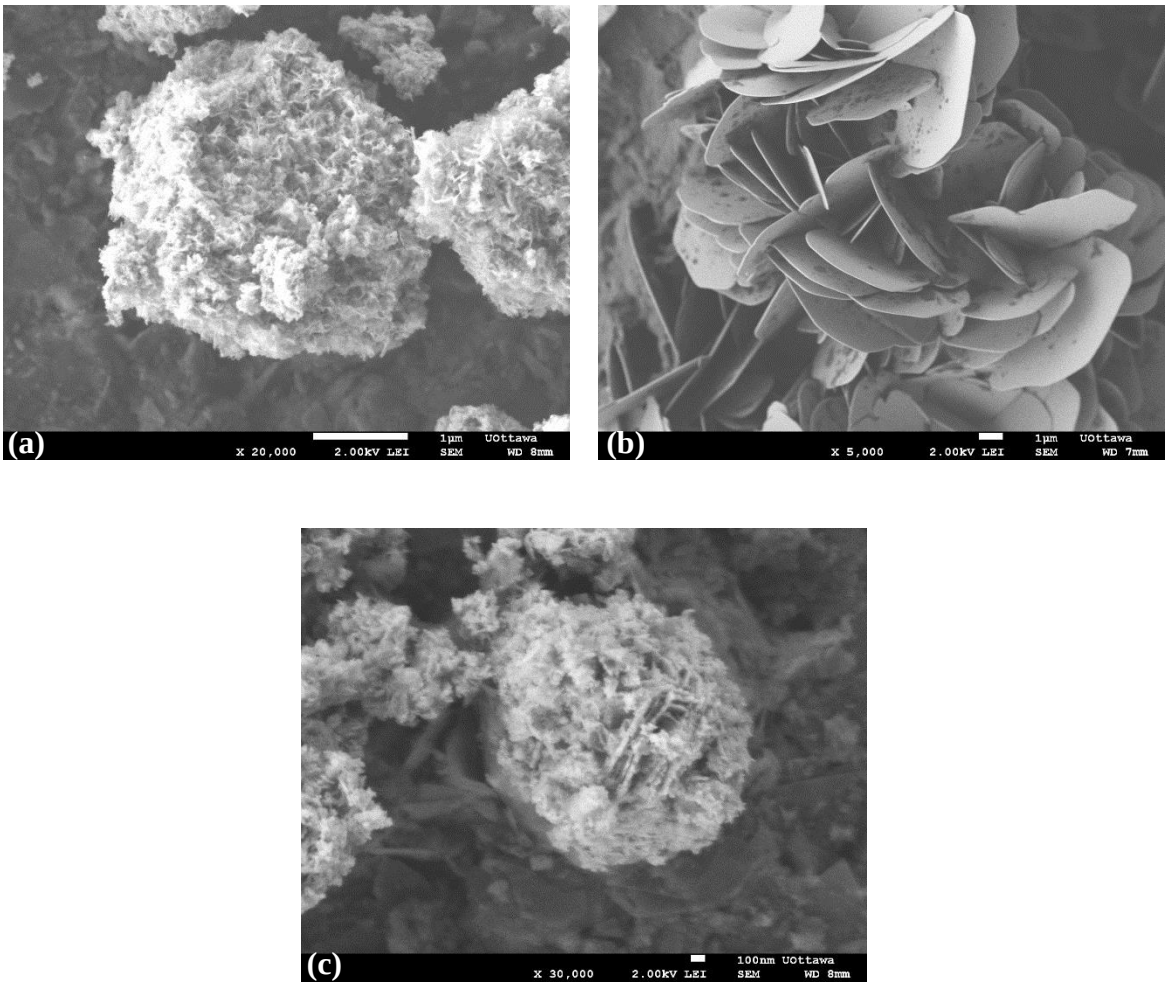

Fig. 3-8. SEM images of (a) pure Bi_2WO_6, (b) pure BiOBr and (c) BiOBr (50 at%)-Bi_2WO_6 composites.

3.3.4 Photocatalytic performance in degradation of RhB

3.3.4.1 Effect of synthesizing conditions

Photocatalytic activities of the as-prepared photocatalysts were evaluated by the degradation of RhB under visible light illumination (λ>410 nm). The degradation efficiencies for systems with photocatalysts synthesized at different reaction times and the same reaction temperature and for the same reaction time at different reaction temperatures were displayed in Fig. 3-9 and Fig. 3-10, respectively. For reaction times from 0 h to 6 h (0 h means photocatalysts

without hydrothermal process and separated from the precursor directly) at 120 ℃, the degradation efficiency improved from 50 % to 82 % within the first 10 min. This phenomenon might correspond to the increasingly better-crystal heterojunction structure which could enhance the photocatalytic degradation by improving the separation of the electron-hole pairs. From 10 min and onwards, deterioration in photocatalytic activity was probably caused by the decrease of surface defects that was introduced in section 3.3.2. As for the photocatalytic activities of photocatalysts synthesized under different reaction temperature for the same reaction time, an optimum hydrothermal temperature existed at 120 ℃ with approximately 100 % degradation efficiency in just 20 min. This could be interpreted as temperatures higher or lower than 120 ℃ hindered the establishment of the heterojunction.

Therefore, an optimum hydrothermal reaction time and temperature existed and was determined to be 6 h and 120 ℃, respectively. These results are in good correspondence with the analysis of the crystal structure of the as-prepared photocatalysts as the structure significantly influenced the reactive performance.

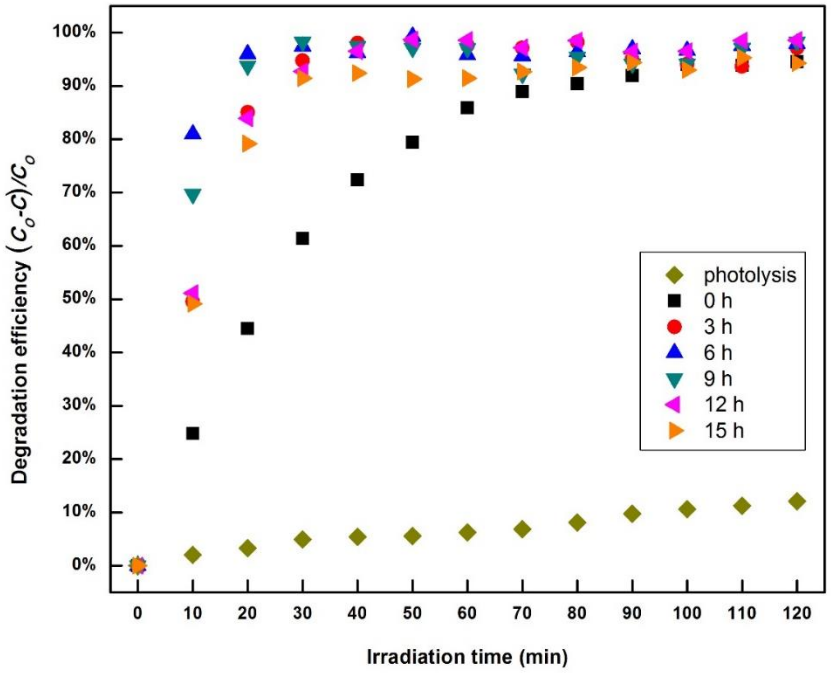

Fig. 3-9. Photocatalytic degradation efficiency as a function of time by using the photocatalysts synthesized for various reaction time under 120 °C. (Catalysts dosage: 1.0 g/L; Temperature: (20±2) °C; pH=5 and initial concentration: 10 ppm)

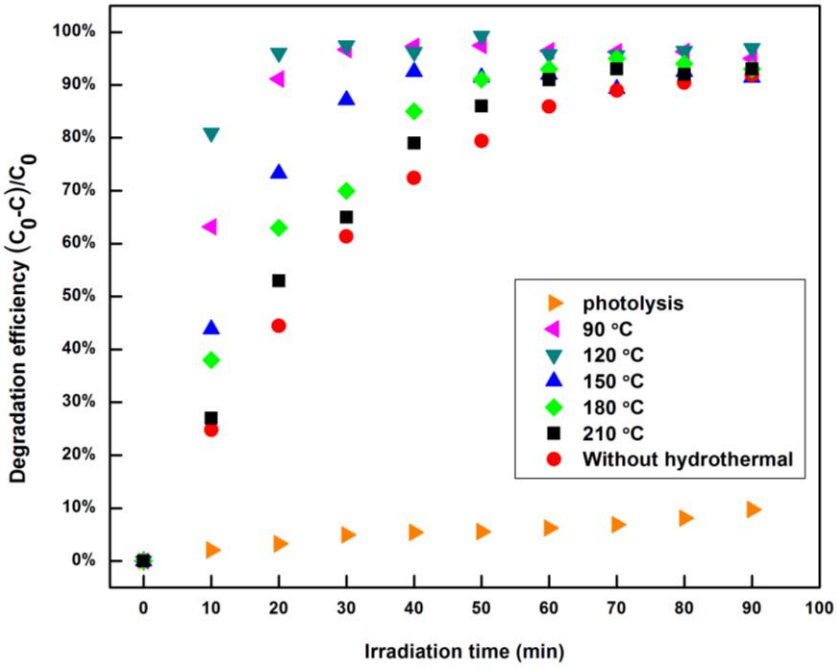

Fig. 3-10. Photocatalytic degradation efficiency as a function of time by using the photocatalysts synthesized for 6 h under various hydrothermal reaction temperature. (Catalysts dosage: 1.0 g/L; Temperature: (20±2) °C; pH=5 and initial concentration: 10 ppm)

3.3.4.2 Effect of initial concentration

Waste water from different areas usually have varying concentrations of the pollutants. Therefore, the degradation of pollutants with varying initial concentrations is a significant parameter to analyze for photocatalysts. In this work, the initial concentration of RhB was varied from 5 ppm (mg/L) to 50 ppm (mg/L) with photocatalysts synthesized under the same conditions (120 ℃ for 6 h) and the same experimental conditions such as photocatalyst dosage (1.0 g/L), pH (5) and reaction temperature (20±2 ℃). The photocatalytic degradation efficiencies in these systems were shown in Fig. 3-11. To investigate the influence of photolysis of RhB, the photolytic conversion at initial concentration of 10 ppm was measured and shown in Fig. 3-11, and was found to be negligible. It could be observed that the RhB was completely removed in 20 min in the systems with an initial concentration of 5 ppm and 10 ppm, and by increasing the initial concentration of RhB from 20 ppm to 50 ppm the degradation efficiency decreased from 60 % to 22% in 20 min. These results could be ascribed to the degradation process which involves three individual processes: adsorption of RhB, reaction of RhB with oxidative species and desorption of degraded products [31]. For a certain amount of the catalyst dosage (1.0 g/L), the adsorption and active sites were limited which resulted in increasing competition for RhB to be adsorbed and degraded with increasing concentration of the initial solution. Another reason is attributed to the reduction of the irradiation energy while passing through the solution. As expected when increasing the concentration of RhB, the color of the solution became much darker, which means much more irradiation energy would be lost before reaching the surface of the photocatalysts and it would correspondingly decrease the production efficiency of the electron-hole pairs. These two

reasons finally resulted in the phenomenon that an increase of the initial solution concentration corresponds to a decrease in the degradation efficiency.

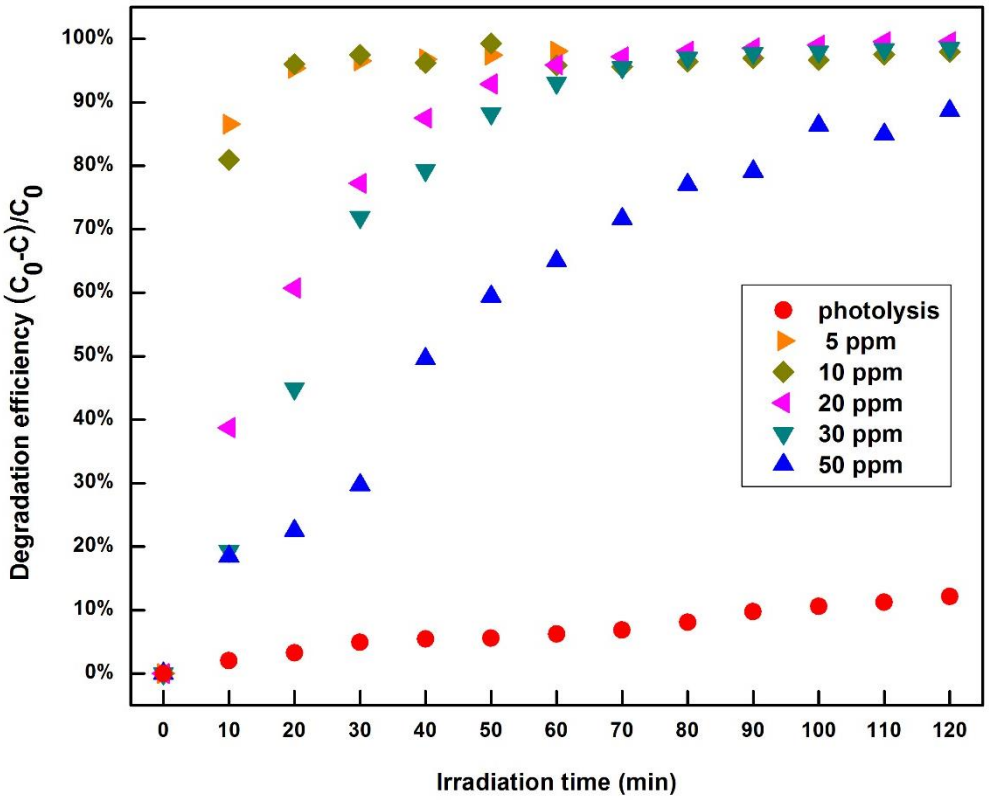

Fig. 3-11. Photocatalytic degradation efficiency as a function of time in systems with various initial concentrations of RhB solution using BiOBr (50 at%)-Bi_2WO_6 composites synthesized for 6 h under 120 °C. (Catalysts dosage: 1.0 g/L; Temperature: (20±2) °C and pH=5)

3.3.4.3 Effect of photocatalysts dosage

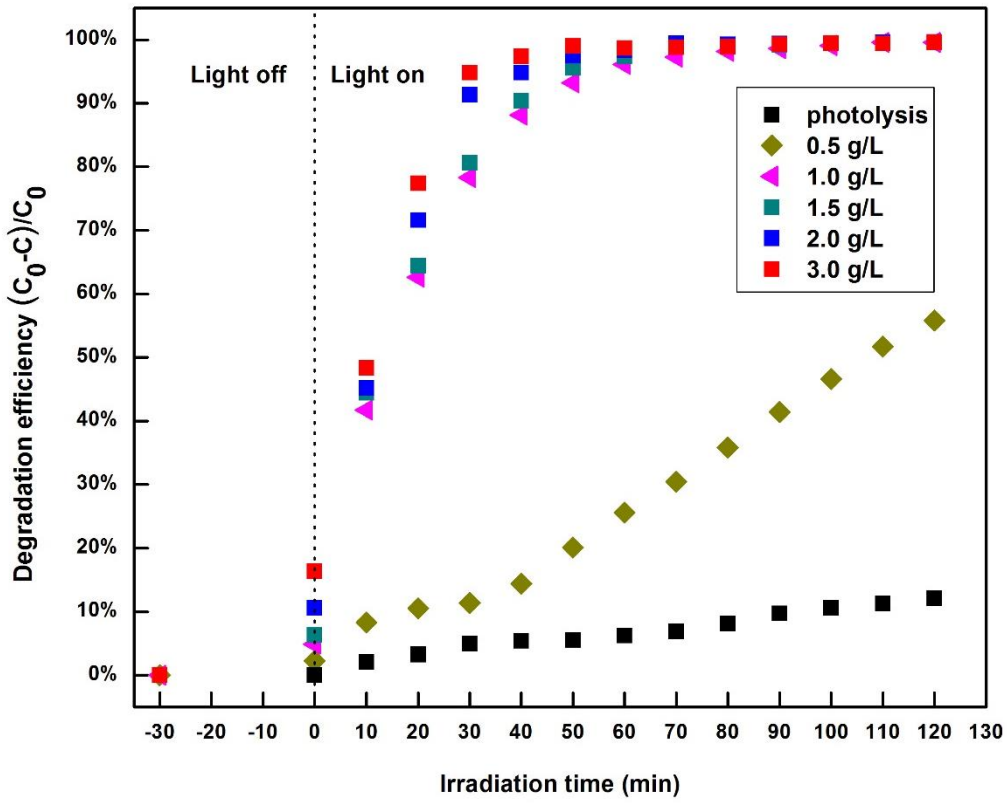

Fig. 3-12. Photocatalytic degradation efficiency as a function of time in systems with various photocatalysts dosage using BiOBr (50 at%)-Bi_2WO_6 composites synthesized for 6 h under 120 °C. (Temperature: (20±2) °C; pH=5 and initial concentration: 20 ppm)

As a relatively expensive technique, it is important to choose a suitable catalyst dosage for optimal degradation efficiencies. The dosage was varied from 0.5 g/L to 3.0 g/L (synthesized under 120 ℃ for 6 h) and tested at the initial *RhB* concentration of 20 ppm and pH of 5, as shown in Fig. 3-12. The photolytic effect of the irradiation was also measured in the system with initial concentration of 10 ppm, and found to be negligible. As for the degradation efficiencies for different systems, it surprisingly found an evident increase from about 10 % to 40 % when the catalyst dosage increased from 0.5 g/L to 1.0 g/L, and increasing the amount

of the catalysts dosage up to 3.0 g/L then resulted in a tiny increase of the degradation efficiency in 30 min as shown in Fig. 3-13.

Meanwhile, before turning on the light, the adsorption-desorption ability in systems with different catalysts dosage was also investigated, and results suggested that more of the photocatalyst in the system possessed much more active sites and were able to adsorb much more *RhB* before the photocatalytic process, which successfully explained the phenomenon that the photocatalytic activity could be enhanced by increasing the catalyst dosage. Beyond that, excessive amounts of the photocatalyst in the system would induce the increase of light scattering and decrease the irradiation penetration, thereby reducing the photocatalytic degradation efficiency [32, 33]. The integrated effects lead to the final results, which explained why intensive increase of the photocatalytic degradation efficiency has not occurred when the photocatalyst dosage was massively increased.

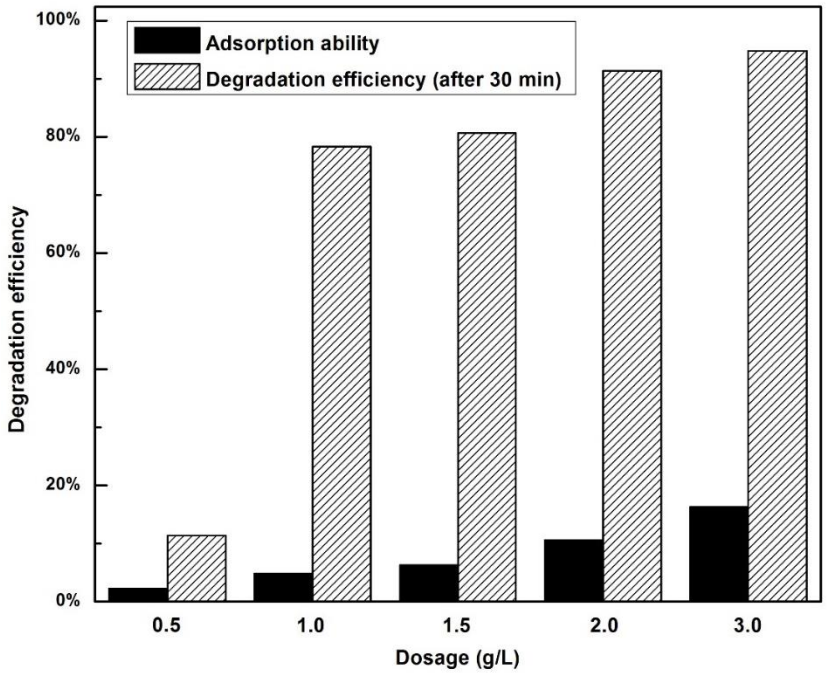

Fig. 3-13. The adsorption abilities and photocatalytic degradation efficiency (in 30 min) in systems with various photocatalysts dosage using BiOBr (50 at%)-Bi_2WO_6 composites synthesized for 6 h under 120 °C. (Temperature: (20±2) °C; pH=5 and initial concentration: 20 ppm)

3.3.4.4 Effect of pH of the *RhB* solution

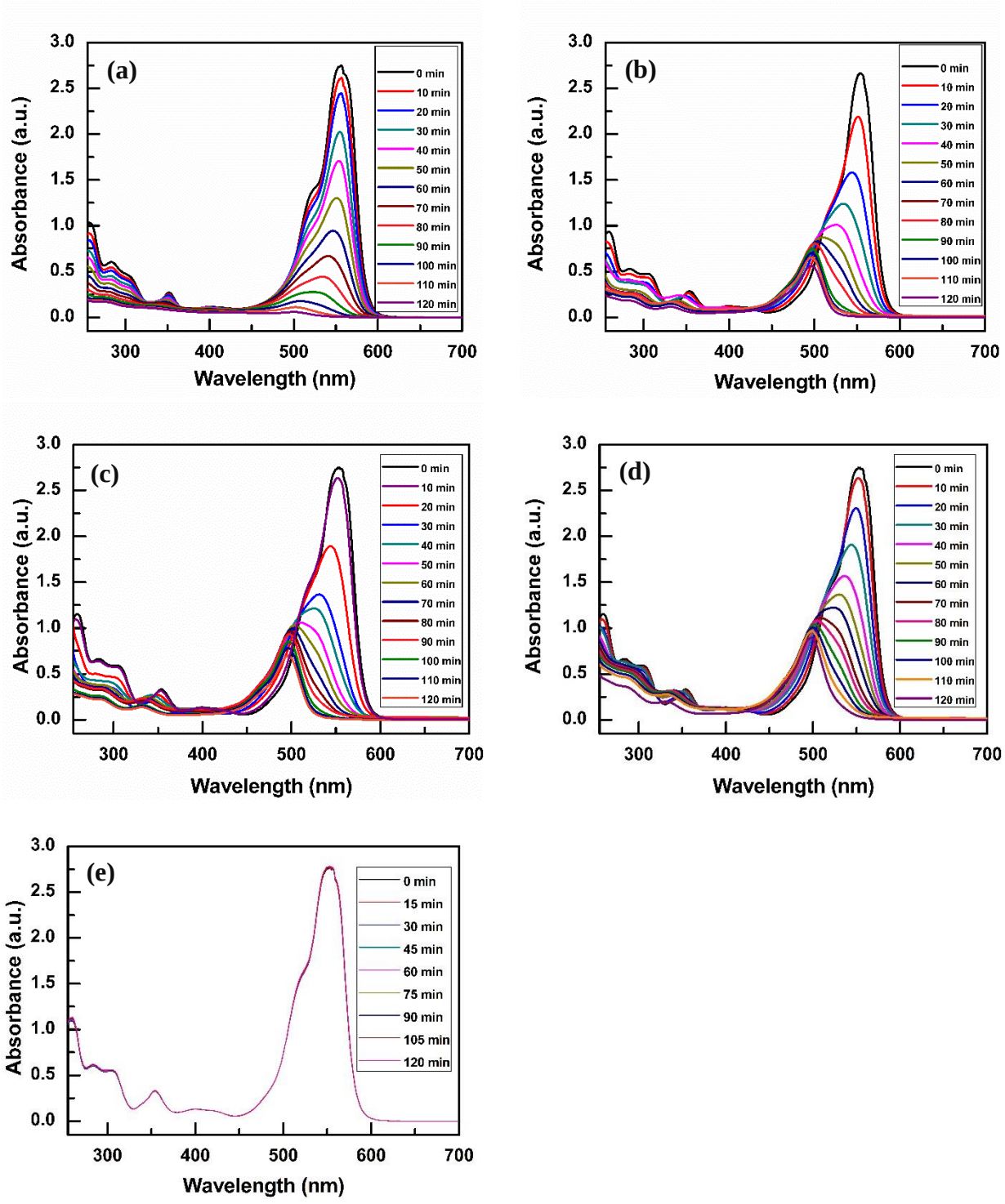

Fig. 3-14. UV-vis spectra of the samples taken during the degradation process, and the *RhB* solutions with different initial pH (a) pH=2, (b) pH=5, (c) pH=7, (d) pH=9 and (e) pH=12. (Photocatalysts: BiOBr (50 at%)-Bi_2WO_6 composites synthesized for 6 h under 120 °C; Catalysts dosage: 1.0 g/L; Temperature: (20±2) °C and initial concentration: 20 ppm)

The photodegradation of *RhB* with varying initial pH and fixed experimental conditions (initial concentration of 20ppm, catalyst dosage of 1.0 g/L, photocatalysts synthesized for 6 h under 120 ℃) was displayed by measuring the UV-vis spectra as shown in Fig. 3-14 (HCl and NaOH has been used to adjust the pH). It could be easily concluded from the results that different initial pH directly determined the mechanism of the degradation of *RhB*. By plotting the relative intensity and wavelength of the major peak at 554 nm *versus* irradiation times which were respectively shown in Fig. 3-15 and Fig. 3-16, it could be seen that when the pH of the *RhB* solution was equal to 5, 7 and 9, these degradation processes have similar mechanisms. That is, the *RhB* was step-by-step degraded into *rhodamine* by de-ethylation, observed by the blue-shift of the widely-introduced characteristic peak from 554 nm (*Rhodamine B*) to 498 nm (*Rhodamine*) [31, 34, 35]. Meanwhile, with the increase of the pH from 5 to 9, the photocatalytic degradation efficiency decreased, which is attributed to the reduced adsorption of *RhB* with increasing pH while the high adsorption at relatively lower pH promoted the degradation rate [36]. When the pH reached 12, the *RhB* hardly adsorbed on the surface of the photocatalysts, resulting in negligible degradation efficiency in 2 h. As for a pH of 2, it took longer time (about 2 h compared to 1 h for the system with initial pH equal to 7) for the blue-shift from 554 nm to 498 nm, which means it would be much more difficult for *RhB* to reach complete deethylation. This could be attributed to Bi_2WO_6 being unstable and transforming into H_2WO_4 and Bi_2O_3 in the acidic solution [36, 37]. The transformation of Bi_2WO_6 damages the BiOBr-Bi_2WO_6 heterojunction and eventually reduces the photocatalytic activity.

While adjustingthe pH influenced the adsorption of the pollutants onto the photocatalysts, the redox species were also influenced at varying pH. It could be concluded that at lower pH, the positive holes play the significant role while at neutral or alkaline circumstances, hydroxyl

radials were regarded as the major oxidative species [38-40]. The final results integrated all of these effects introduced above and it is concluded that the pH range from 5 to 9 is suitable for the as-prepared photocatalysts, and lower pH is preferable in this range.

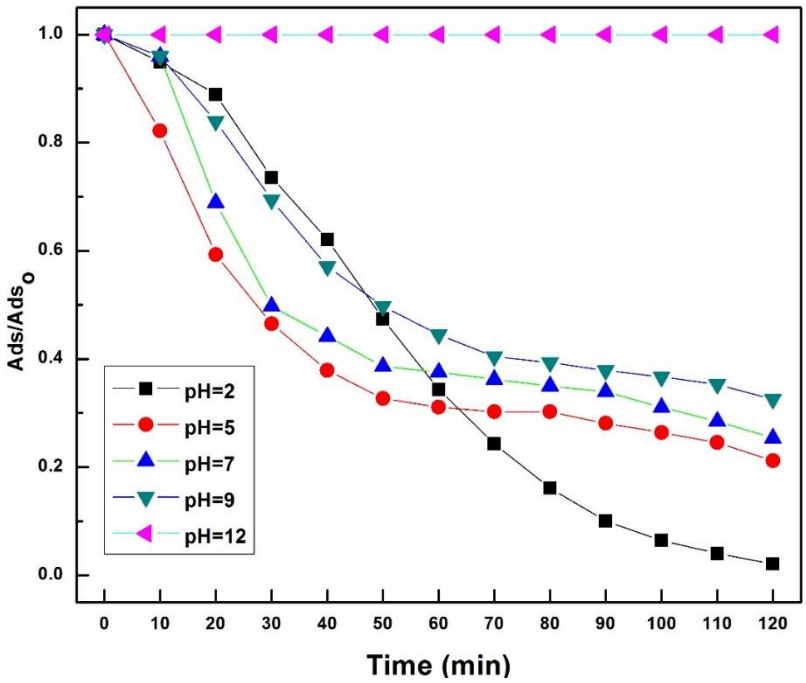

Fig. 3-15. Relative intensity of the characteristic peak at 554 nm as a function of time in systems with various initial pH of *RhB* solutions. (Photocatalysts: BiOBr (50 at%)-Bi_2WO_6 composites synthesized for 6 h under 120 °C; catalysts dosage: 1.0 g/L; Temperature: (20±2) °C and initial concentration: 20 ppm)

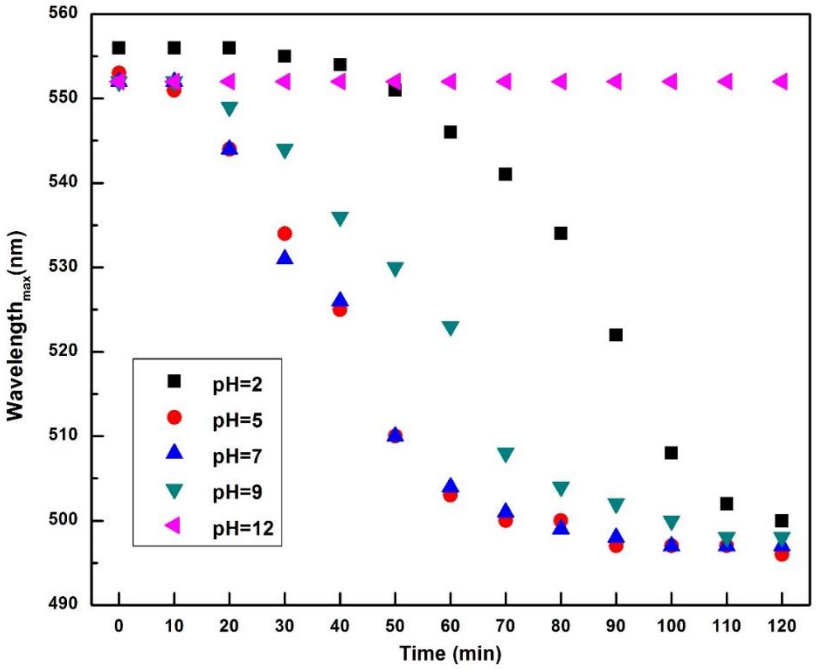

Fig. 3-16. The blue-shift of the characteristic peaks during the degradation process in systems with various initial pH of *RhB* solutions. (Photocatalysts: BiOBr (50 at%)-Bi_2WO_6 composites synthesized for 6 h under 120 °C; catalysts dosage: 1.0 g/L; Temperature: (20±2) °C and initial concentration: 20 ppm)

3.3.5 Reusability

To evaluate the reusability of the photocatalysts used in the system, consecutive photocatalytic processes for 4 runs have been measured and the results were displayed in Fig. 3-17. Between each run, photocatalysts were separated from the slurry by centrifugation. The used photocatalysts were then mixed with fresh dye water. Results show that the degradation efficiencies of *RhB* decreased from 100 % (complete degradation) to 85 % in 2 h. This proves that the as-prepared photocatalysts could be reused with relatively high photocatalytic activity. The run-by-run decrease in performance may be due to the intermediate products of degraded *RhB,* which were not completely degraded, to remain adsorbed on the surface of the photocatalysts. This would reduce the sorption ability of the photocatalysts, resulting in the decrease of the degradation efficiencies. The structure of the photocatalysts after the

degradation process for 4 runs was detected by XRD, which was shown in Fig. 3-18. All of the characteristic peaks of tetragonal BiOBr and orthorhombic Bi_2WO_6 came out in the XRD patterns of photocatalysts before and after the degradation for 4 runs, which means the main structure of the BiOBr-Bi_2WO_6 heterojunction was not destroyed and was stable enough. However, each of the peaks in the upper XRD pattern have been widened and not as sharp as that of the under XRD pattern, and it suggests the crystallinity has been reduced to some extent that exactly corresponds to the pollutants or the intermediate products being adsorbed and remaining on the photocatalysts. In conclusion, the BiOBr-Bi_2WO_6 photocatalysts synthesized by the hydrothermal method possess the stable properties and could be reused multiple times, which is a prerequisite for photocatalyst applications in practice.

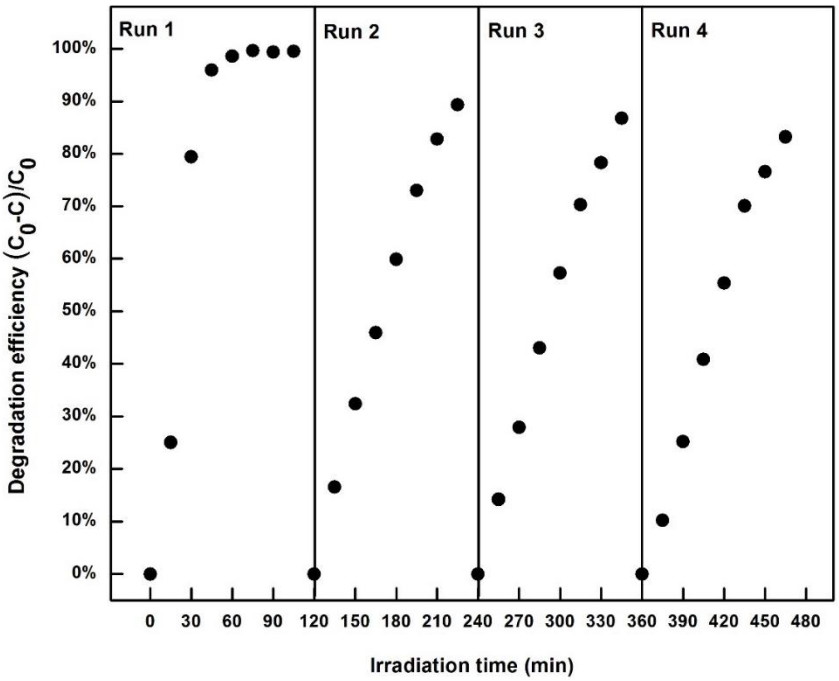

Fig. 3-17. Photocatalytic degradation efficiency as a function of time in four runs. (Photocatalysts: BiOBr (50 at%)-Bi_2WO_6 composites synthesized for 6 h under 120 °C; catalysts dosage: 1.0 g/L; temperature: (20±2) °C; pH=5 and initial concentration: 10 ppm)

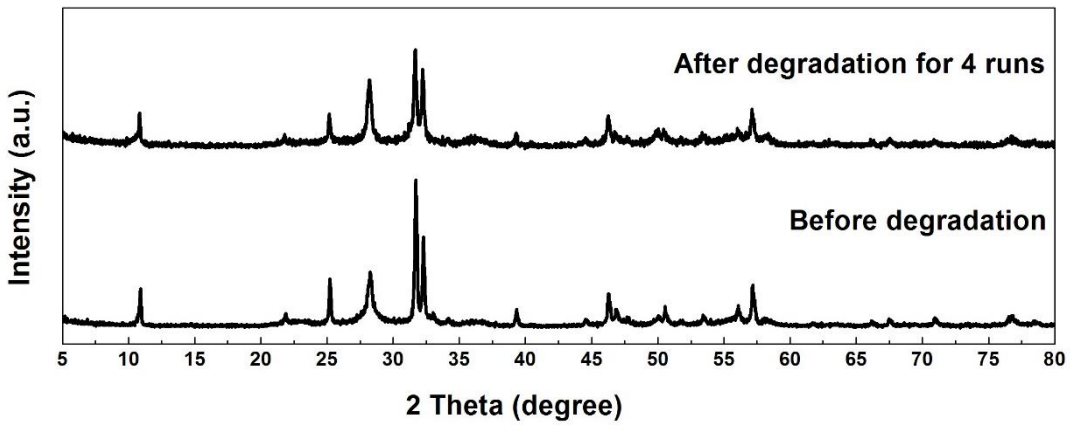

Fig. 3-18. XRD pattern of photocatalysts (BiOBr (50 at%)-Bi_2WO_6 synthesized for 6 h under 120 °C) before and after degradation process for 4 runs.

3.3.6 The mechanism of heterojunction enhancement

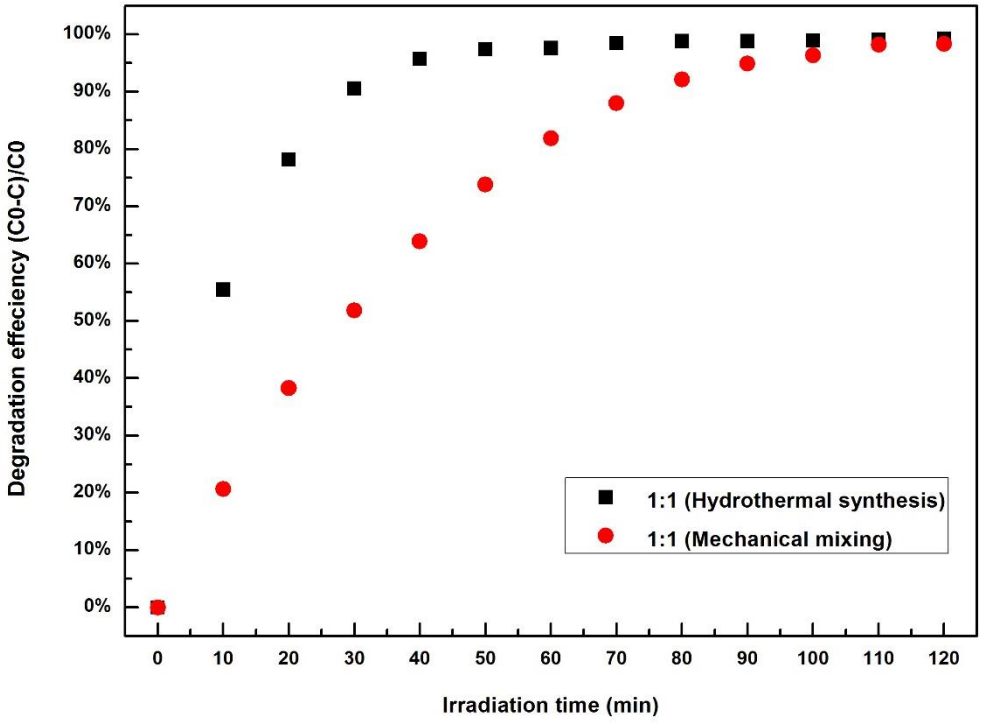

Fig. 3-19. Degradation efficiency versus irradiation time by utilizing photocatalysts hydrothermally synthesized and mechanically mixed. (Ratio of BiOBr to Bi_2WO_6: 1:1; catalysts dosage: 0.5 g/L; temperature: (20±2) °C; pH=5 and initial concentration: 10 ppm)

The degradation efficiency of the photocatalyst synthesized by the hydrothermal method under 120 ℃ for 6 h were compared to the efficiency of the photocatalyst synthesized by mechanically mixing pure BiOBr and Bi_2WO_6 by the similar hydrothermal method under the same experimental conditions, in which the fixed ratio of BiOBr and Bi_2WO_6 was equal to 1:1. The results were demonstrated in Fig. 3-19. Specifically, the degradation efficiency improved from 20% for mechanical mixing to 55% for chemical synthesis. The heterojunction photocatalyst took about 50 min to completely remove *RhB*, while it took 120 min to obtain the same degradation results from mechanical mixing. The evident enhancement probably attributed to the establishment of the BiOBr-Bi_2WO_6 heterojunction that has been introduced in other references [22, 41-43]. Similarly, the enhancement effect could simply be illustrated by the analysis of the band structure shown in Fig. 3-20. When stimulated by light energy (*hv*), electrons jump from the valence band to the conduction band, leaving behind positive holes on the valence band. In the presence of an electric field, there exists a force to drive the electrons from the conduction band of BiOBr to that of Bi_2WO_6, while holes oppositely move from the valence band of Bi_2WO_6 to that of BiOBr [27, 44]. This kind of movement effectively separates the electrons and holes so as to decrease the recombination rate of the electron-hole pairs. The accumulated electrons and holes could then individually react with adsorbed species such as oxygen or the organic pollutants.

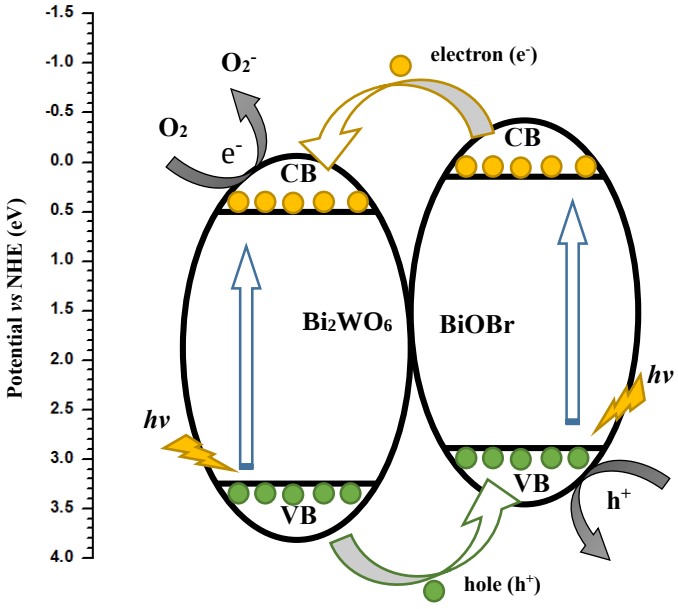

Fig. 3-20. Band structure of the BiOBr-Bi_2WO_6 heterojunction. (VB: valence band; CB: conduction band).

3.4 Conclusions

In this work, novel BiOBr-Bi_2WO_6 heterojunction photocatalysts have been synthesized by the facile hydrothermal method. The optimal synthesis conditions, especially the hydrothermal reaction temperature (120 ℃) and holding time (6 h), have been explored and discussed on the basis of evaluating its structure (XRD, SEM) and photocatalytic degradation efficiency. DRS results theoretically proved that BiOBr-Bi_2WO_6 composites have suitable band-gaps to be stimulated by visible-light irradiation. Furthermore, the influence of experimental conditions in the photocatalytic degradation process, such as the initial concentration, amount of the photocatalyst dosage and initial pH, have been studied and discussed. By recycling the photocatalysts, it proved that the BiOBr-Bi_2WO_6 composites were stable enough to be used in practice. Finally, the mechanism of the enhancement effect by establishing the heterojunction has been explained based on the band structure, and further suggested it is an effective

approach to separate the electron-hole pairs, enhancing the photocatalytic activity in the degradation of pollutants in dye water.

3.5 References:

[1] A. Fujishima, K. Honda, Electrochemical photolysis of water at a semiconductor electrode, nature, 238 (1972) 37-38.

[2] M. Ni, M.K.H. Leung, D.Y.C. Leung, K. Sumathy, A review and recent developments in photocatalytic water-splitting using for hydrogen production, Renewable and Sustainable Energy Reviews, 11 (2007) 401-425.

[3] X. Chen, S. Shen, L. Guo, S.S. Mao, Semiconductor-based photocatalytic hydrogen generation, Chem Rev, 110 (2010) 6503-6570.

[4] C. Hachem, F. Bocquillon, O. Zahraa, M. Bouchy, Decolourization of textile industry wastewater by the photocatalytic degradation process, Dyes Pigments, 49 (2001) 117-125.

[5] J.C. Crittenden, Y. Zhang, D.W. Hand, D.L. Perram, E.G. Marchand, Solar Detoxification of Fuel-Contaminated Groundwater Using Fixed-Bed Photocatalysts, Water Environ Res, 68 (1996) 270-278.

[6] M.S. Mehos, C.S. Turchi, Field testing solar photocatalytic detoxification on TCE-contaminated groundwater, Environ Prog, 12 (1993) 194-199.

[7] J.C. Yu, W. Ho, J. Yu, H. Yip, P.K. Wong, J. Zhao, Efficient Visible-Light-Induced Photocatalytic Disinfection on Sulfur-Doped Nanocrystalline Titania, Environmental Science & Technology, 39 (2005) 1175-1179.

[8] J. Lonnen, S. Kilvington, S.C. Kehoe, F. Al-Touati, K.G. McGuigan, Solar and photocatalytic disinfection of protozoan, fungal and bacterial microbes in drinking water, Water Res, 39 (2005) 877-883.

[9] P. Pichat, J. Disdier, C. Hoang-Van, D. Mas, G. Goutailler, C. Gaysse, Purification/deodorization of indoor air and gaseous effluents by TiO_2 photocatalysis, Catalysis Today, 63 (2000) 363-369.

[10] M.R. Hoffmann, S.T. Martin, W. Choi, D.W. Bahnemann, Environmental Applications of Semiconductor Photocatalysis, Chem Rev, 95 (1995) 69-96.

[11] S.G. Kumar, L.G. Devi, Review on Modified TiO_2 Photocatalysis under UV/Visible Light: Selected Results and Related Mechanisms on Interfacial Charge Carrier Transfer Dynamics, The Journal of Physical Chemistry A, 115 (2011) 13211-13241.

[12] S.C. Yan, Z.S. Li, Z.G. Zou, Photodegradation Performance of g-C_3N_4 Fabricated by Directly Heating Melamine, Langmuir, 25 (2009) 10397-10401.

[13] Q. Xiang, J. Yu, M. Jaroniec, Graphene-based semiconductor photocatalysts, Chem Soc Rev, 41 (2012) 782-796.

[14] X. Zhang, Z. Ai, F. Jia, L. Zhang, Generalized One-Pot Synthesis, Characterization, and Photocatalytic Activity of Hierarchical BiOX (X = Cl, Br, I) Nanoplate Microspheres, The Journal of Physical Chemistry C, 112 (2008) 747-753.

[15] L. Zhang, W. Wang, L. Zhou, H. Xu, Bi_2WO_6 Nano- and Microstructures: Shape Control and Associated Visible-Light-Driven Photocatalytic Activities, Small, 3 (2007) 1618-1625.

[16] H. An, Y. Du, T. Wang, C. Wang, W. Hao, J. Zhang, Photocatalytic properties of BiOX (X = Cl, Br, and I), Rare Metals, 27 (2008) 243-250.

[17] J. Cao, X. Li, H. Lin, B. Xu, S. Chen, Q. Guan, Surface acid etching of $(BiO)_2CO_3$ to construct $(BiO)_2CO_3$/BiOX (X=Cl, Br, I) heterostructure for methyl orange removal under visible light, Appl Surf Sci, 266 (2013) 294-299.

[18] G. Fu, G. Xu, S. Chen, L. Lei, M. Zhang, Ag_3PO_4/Bi_2WO_6 hierarchical heterostructures with enhanced visible light photocatalytic activity for the degradation of phenol, Catal Commun, 40 (2013) 120-124.

[19] J. Fu, Y. Tian, B. Chang, F. Xi, X. Dong, BiOBr-carbon nitride heterojunctions: synthesis, enhanced activity and photocatalytic mechanism, J Mater Chem, 22 (2012) 21159-21166.

[20] M. Hojamberdiev, K.-i. Katsumata, K. Morita, S.A. Bilmes, N. Matsushita, K. Okada, One-step hydrothermal synthesis and photocatalytic performance of $ZnWO_4/Bi_2WO_6$ composite photocatalysts for efficient degradation of acetaldehyde under UV light irradiation, Applied Catalysis A: General, 457 (2013) 12-20.

[21] L. Kong, Z. Jiang, T. Xiao, L. Lu, M.O. Jones, P.P. Edwards, Exceptional visible-light-driven photocatalytic activity over BiOBr-$ZnFe_2O_4$ heterojunctions, Chem Commun, 47 (2011) 5512-5514.

[22] H. Lin, H. Ye, X. Li, J. Cao, S. Chen, Facile anion-exchange synthesis of BiOI/BiOBr composite with enhanced photoelectrochemical and photocatalytic properties, Ceram Int, 40 (2014) 9743-9750.

[23] A. Phuruangrat, P. Dumrongrojthanath, N. Ekthammathat, S. Thongtem, T. Thongtem, Hydrothermal Synthesis, Characterization, and Visible Light-Driven Photocatalytic Properties of Bi_2WO_6 Nanoplates, J Nanomater, 2014 (2014) 7.

[24] M. Shang, W. Wang, L. Zhang, Preparation of BiOBr lamellar structure with high photocatalytic activity by CTAB as Br source and template, J Hazard Mater, 167 (2009) 803-809.

[25] D. Ma, S. Huang, W. Chen, S. Hu, F. Shi, K. Fan, Self-Assembled Three-Dimensional

Hierarchical Umbilicate Bi_2WO_6 Microspheres from Nanoplates: Controlled Synthesis, Photocatalytic Activities, and Wettability, The Journal of Physical Chemistry C, 113 (2009) 4369-4374.

[26] G. Xi, K. Xiong, Q. Zhao, R. Zhang, H. Zhang, Y. Qian, Nucleation−Dissolution−Recrystallization: A New Growth Mechanism for t-Selenium Nanotubes, Cryst Growth Des, 6 (2006) 577-582.

[27] J. Xia, J. Di, S. Yin, H. Li, H. Xu, L. Xu, H. Shu, M. He, Solvothermal synthesis and enhanced visible-light photocatalytic decontamination of bisphenol A (BPA) by g-C_3N_4/BiOBr heterojunctions, Mat Sci Semicon Proc, 24 (2014) 96-103.

[28] F. Amano, K. Nogami, B. Ohtani, Enhanced photocatalytic activity of bismuth-tungsten mixed oxides for oxidative decomposition of acetaldehyde under visible light irradiation, Catal Commun, 20 (2012) 12-16.

[29] H. Fu, S. Zhang, T. Xu, Y. Zhu, J. Chen, Photocatalytic Degradation of RhB by Fluorinated Bi_2WO_6 and Distributions of the Intermediate Products, Environmental Science & Technology, 42 (2008) 2085-2091.

[30] J. Li, Z. Guo, Y. Wang, Z. Zhu, Three-dimensional TiO_2/Bi_2WO_6 hierarchical heterostructure with enhanced visible photocatalytic activity, Micro & Nano Letters, IET, 9 (2014) 65-68.

[31] T. Wu, G. Liu, J. Zhao, H. Hidaka, N. Serpone, Photoassisted Degradation of Dye Pollutants. V. Self-Photosensitized Oxidative Transformation of Rhodamine B under Visible Light Irradiation in Aqueous TiO_2 Dispersions, The Journal of Physical Chemistry B, 102 (1998) 5845-5851.

[32] C.C. Wong, W. Chu, The direct photolysis and photocatalytic degradation of alachlor at different TiO_2 and UV sources, Chemosphere, 50 (2003) 981-987.

[33] M.A. Behnajady, B. Alizade, N. Modirshahla, Synthesis of Mg-Doped TiO_2 Nanoparticles under Different Conditions and its Photocatalytic Activity, Photochem Photobiol, 87 (2011) 1308-1314.

[34] T. Watanabe, T. Takizawa, K. Honda, Photocatalysis through excitation of adsorbates. 1. Highly efficient N-deethylation of rhodamine B adsorbed to cadmium sulfide, The Journal of Physical Chemistry, 81 (1977) 1845-1851.

[35] F. Chen, J. Zhao, H. Hidaka, Highly selective deethylation of rhodamine B: Adsorption and photooxidation pathways of the dye on the TiO_2 -SiO_2 composite photocatalyst, International Journal of Photoenergy, 5 (2003).

[36] H. Fu, C. Pan, W. Yao, Y. Zhu, Visible-Light-Induced Degradation of Rhodamine B by Nanosized Bi_2WO_6, The Journal of Physical Chemistry B, 109 (2005) 22432-22439.

[37] Y. Li, J. Liu, X. Huang, Synthesis and Visible-Light Photocatalytic Property of Bi_2WO_6 Hierarchical Octahedron-Like Structures, Nanoscale Res Lett, 3 (2008) 365-371.

[38] C. Guillard, H. Lachheb, A. Houas, M. Ksibi, E. Elaloui, J.-M. Herrmann, Influence of chemical structure of dyes, of pH and of inorganic salts on their photocatalytic degradation by TiO_2 comparison of the efficiency of powder and supported TiO_2, Journal of Photochemistry and Photobiology A: Chemistry, 158 (2003) 27-36.

[39] I. Poulios, I. Tsachpinis, Photodegradation of the textile dye Reactive Black 5 in the presence of semiconducting oxides, Journal of Chemical Technology & Biotechnology, 74 (1999) 349-357.

[40] W.Z. Tang, Z. Zhang, H. An, M.O. Quintana, D.F. Torres, TiO_2/UV Photodegradation of Azo Dyes in Aqueous Solutions, Environ Technol, 18 (1997) 1-12.

[41] S. Obregón, G. Colón, Erbium doped TiO_2–Bi_2WO_6 heterostructure with improved photocatalytic activity under sun-like irradiation, Applied Catalysis B: Environmental, 140–141 (2013) 299-305.

[42] Y. Peng, M. Yan, Q. Chen, C. Fan, H. Zhou, A. Xu, Novel one-dimensional Bi_2O_3-Bi_2WO_6 p-n hierarchical heterojunction with enhanced photocatalytic activity, Journal of Materials Chemistry A, 2 (2014) 8517-8524.

[43] M. Shang, W. Wang, L. Zhang, S. Sun, L. Wang, L. Zhou, 3D Bi_2WO_6/TiO_2 hierarchical heterostructure: Controllable synthesis and enhanced visible photocatalytic degradation performances, J Phys Chem C, 113 (2009) 14727-14731.

[44] J. Xia, J. Di, S. Yin, H. Xu, J. Zhang, Y. Xu, L. Xu, H. Li, M. Ji, Facile fabrication of the visible-light-driven Bi_2WO_6/BiOBr composite with enhanced photocatalytic activity, RSC Advances, 4 (2014) 82-90.

CHAPTER 4:

Facile Synthesis of $BiOBr/Bi_2WO_6$ Heterojunction Semiconductors with High Visible-light-driven Photocatalytic Activity*

Xiangchao Meng, Jason (Zisheng) Zhang

*Submitted to ***Journal of photochemistry and photobiology, A: Chemistry***

Abstract:

Photocatalysis is a growing area of study for a clean and renewable energy source, particularly for the degradation of solvents and the purification of water and air. Researchers have studied the combination of various semiconductors to create photocatalysts with improved activities, but little has been reported in selecting semiconductors based on their extrinsic type – namely n-type or p-type. In this study, a BiOBr (p-type)-Bi_2WO_6 (n-type) heterojunction semiconductor was synthesized by the hydrothermal method. The new materials were

characterized using X-ray diffraction (XRD), X-ray photoelectron spectroscopy (XPS), scanning electron microscopy (SEM), energy dispersive spectroscopy (EDS), and diffuse-reflection spectroscopy (DRS). Their photocatalytic activities were examined by measuring the degradation rate of *Rhodamine B* at varying concentrations of the dopants (the atomic ratio of BiOBr and Bi_2WO_6 are 1:4， 1:1， 4:1). The study shed light on the benefits of using heterojunction photocatalysts, and also on the importance of considering the semiconductor type when forming composite photocatalysts.

Keywords: BiOBr; Bi_2WO_6; Heterojunction; Photocatalysts; Rhodamine B

4.1 Introduction

Photocatalysis, one of the forceful techniques withstanding the gradually deteriorative environmental conditions, has drawn intensive investigation since 1972 [1]. Currently, two main applications of this preeminent technique are widely reviewed, namely the photocatalytic water splitting with the production of hydrogen and the photocatalytic purification or disinfection in wastewater or polluted air [2-5]. In semiconductor photocatalysis, electrons jump from the valence band to the conduction band via proper activation of UV or visible light, and each of the photo-generated electron-hole pairs directly and indirectly produce some reactive oxidative species (ROS) such as •OH, •O_2 and holes. These species are strong enough to decompose the polluted organics in the environment or sterilize most of the bacteria [6].

Most commercially used photocatalysts (*e.g.* TiO_2) still exhibit some drawbacks, including high recombination rate of the photo-generated electron-hole pairs and low photocatalytic efficiency under visible light irradiation [7]. Counter-measures have been reported incorporating the modification (*e.g.* metal deposition, doping *etc.*) of commercial photocatalysts and the exploration of synthesizing novel photocatalysts [8]. Among these methods, coupling is an effective approach to essentially improve the photocatalytic activity. Particularly, establishing a heterojunction by combining two photocatalysts provides a feasible method to decrease the recombination of photo-generated carriers and continues to drive research. By various synthesis methods, coupled systems such as TiO_2-Bi_2WO_6 [9-12], Bi_2O_3-Bi_2WO_6 [13-15], WO_3/Bi_2WO_6 [16, 17] and BiOBr-BiOI [18] composites have been prepared and applied in the degradation of waste water and purification of polluted air. It should be noteworthy that the results of experiments reported above completely indicate that heterojunction offers an excellent prospect in charge carrier separation which correspondingly

extends the life time and reduces the recombination rate of photo-generated carriers, leading to an enhanced photocatalytic performance.

As for improving visible-light response in photocatalysis, bismuth compound semiconductors have been intensively studied for the formation of various heterojunctions. Compared with the valence band (VB) of metal oxides which is commonly and simply composed of O 2p, VB of materials containing bismuth mostly consist of O 2p and Bi 6s hybrid orbitals. It has been reported that a well-dispersed Bi 6s orbital is more beneficial to increase the mobility of the photo-generated carriers and to decrease the band gap [19]. Meanwhile, a large number of bismuth compounds with varying morphology have been prepared, providing various possibilities in preparing high-efficiency catalysts.

Bismuth tungstate (Bi_2WO_6), a typical n-type semiconductor with a band gap of approximately 2.7 eV, and Bismuth oxyhalides (BiOX, X=Cl, Br, I), a typical p-type semiconductor with band gap of approximately 1.7-3.2 eV, have been synthesized by various methods and shown relatively high efficiency in photocatalytic performance [19, 20]. However, the high recombination rate of photo-generated charge carriers hinders their wide application. It has been reported that combining these two kinds of photocatalysts to form a heterojunction could effectively reduce the recombination rate [21]. Synthesizing BiOBr-Bi_2WO_6 composite using ionic liquids (ILs) is a complex method and is costly to operate. Comparatively, the hydrothermal technique has been regarded as an excellent method in synthesizing nano-particles with many advantages such as good reproducibility and high purity products [22].

Herein, novel composites consisting of BiOBr and Bi_2WO_6 with the facile one-step hydrothermal method were studied. The benefits of the heterojunction were tested by the destruction of RhB under visible-light irradiation. Experimental results evidently exhibited an

enhancement in photocatalytic performance compared to the pure Bi_2WO_6 or BiOBr. The mechanism of the enhanced photocatalytic performance was also proposed by calculating and analyzing the band structure. Meanwhile, the mechanism of the degradation process was also explored.

4.2 Experimental

4.2.1 Synthesis of $BiOBr/Bi_2WO_6$ composites

All of the reagents were purchased from Sigma-Aldrich Company in analytical purity and used as received. The $BiOBr/Bi_2WO_6$ composite photocatalysts were synthesized by the facile co-precipitation method. In a typical procedure (mole ratio of $BiOBr/Bi_2WO_6$ is 1:1), 2 g $Bi(NO_3)_3 \cdot 5H_2O$ was dissolved in 80 mL acetic acid (HAc), and was dropwise dissolved into 40 mL distilled deionized water containing 0.45 g $Na_2WO_4 \cdot 2H_2O$ and 0.16 g KBr. The mixture was magnetically stirred for 30 minutes at room temperature. After that, the suspension was transferred into 45 mL Teflon-lined stainless steel autoclaves (approximately 80% of its maximum volume) and then heated at a designated temperature (120 ℃) for a designated amount of time (12 hours). When the autoclaves naturally cooled down to the room temperature, the precipitate was separated by the centrifuge under 1500 rpm for 5 minutes three times with deionized water and ethanol to wash out any possible ionic species. The precipitate was then dried at 80 ℃ for 6 hours to obtain the $BiOBr/Bi_2WO_6$ composites. To investigate the effects of co-doping amount, The composites with different mole ratios of $BiOBr/Bi_2WO_6$ at 1:4 (20 at%) 1:1 (50 at%) and 4:1 (80 at%) were also synthesized. For comparison, pure BiOBr and Bi_2WO_6 were also prepared by the solvothermal method under the same preparation conditions mentioned above.

4.2.2 Characterization

X-ray diffraction (XRD) analysis was carried out using a Rigaku Ultima IV Diffractometer with Cu Kα radiation (λ=0.15418 nm) at 40kV and 44 mA. The surface chemical states of the photocatalysts were analyzed by the XSAM-800 X-ray Photoelectron Spectroscope (XPS).

The morphology was studied by the field-emission scanning electron microscope (FE-SEM) with JEOL JSM-7500F, equipped with an Energy Dispersive X-ray Spectroscope (EDS). The Transmission Electron Microscopy (TEM) technique was performed with JEM-2100F FETEM (JEOL). The Thermo Evolution 300 spectrophotometer was used to evaluate the Ultraviolet-visible (UV-Vis) diffuse reflectance spectra (DRS) of the photocatalysts.

4.2.3 Photocatalytic activity measurement

A slurry batch photoreactor was applied in the degradation of organic pollutants. The light source was a 300 W tungsten halide bulb (Ushio) and a cutoff (Kenko Zeta, transmittance>90%) was applied to filter out any irradiation with the wavelength below 410 nm. A 500 mL beaker with a cooling jacket was used as the container of the organic pollutants. The temperature of the reactor was controlled around (20±2) ℃ by the cooling/heating recirculating water. The apparatus was placed in a constructed reflective housing to avoid the effect of the outside light. *Rhodamine B* (RhB) was regarded as the organic pollutant and used in determining the degradation efficiency of each synthesized photocatalysts. In each degradation experiment, 200mL of aqueous solution containing RhB was added into the beaker while keeping the initial concentration at 10 mg/L (10 ppm) and then a certain amount (0.5 g/L) of the photocatalysts was mixed with the solution under constant magnetic stirring for 30 minutes in the dark prior to the photocatalytic degradation to make sure the adsorption-desorption equilibrium is reached. Then, turning on the light started the degradation process. In every 10 minutes, 1mL of the suspension was taken out and separated by the micro-centrifuge under 10000 rpm for 3 minutes. After that, the supernatant solution was measured by a UV-Vis spectrophotometer (Puxi, UV 1901) with the peak absorbance at 554 nm (Fig. 4-

1). A calibration curve was used to determine the concentration of Rhodamine B from the peak absorbance. The degradation efficiency could be calculated by the following equation:

$$\omega_{Degradation\ efficiency} = \frac{c_o - c_t}{c_o} \times 100\%$$

Where c_o is the initial concentration of *Rhodamine B* and c_t is the concentration of Rhodamine B at the specific testing time during the degradation.

The recyclability of the photocatalysts was analyzed by separating the photocatalysts after one run using the centrifuge (Hermle Z400K) and mixing the used photocatalysts with fresh dye water to start the next run. After the final run, the separated photocatalysts were dried at 80 ℃ for 6 hours and then analyzed by the XRD test. In the quenching experiments, *ethylene diamine tetraacetic acid* (EDTA) (99%, Sigma-Aldrich) was used as the holes scavenger, *isopropanol* (reagent grade, Fisher Scientific) as the •OH scavenger and N_2 bubbling for the reduction of the dissolve oxygen. They were used to analyze the roles of each species.

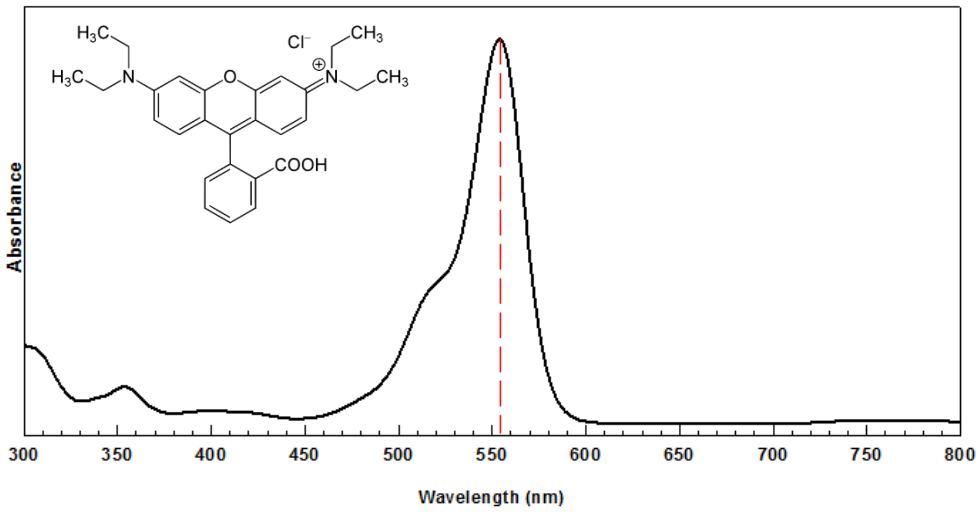

Fig. 4-1. UV-Vis spectrophotometer and the formula structure of *Rhodamine B* (RhB).

4.3 Results and discussion

4.3.1 XRD and XPS test

The XRD pattern of the as-prepared pure Bi_2WO_6, pure BiOBr and the BiOBr/Bi_2WO_6 composites at different ratios are shown in Fig. 4-2. The diffraction peaks of pure BiOBr and Bi_2WO_6 exhibit in good agreement with the tetragonal structure of BiOBr (JCPDS card # 09-0393) and the orthorhombic structure of Bi_2WO_6 (JCPDS card # 39-0256), respectively. All of the characteristic peaks are found in the BiOBr/Bi_2WO_6 composites. Especially when the BiOBr content accounts for 50 at%, the sharp peaks indicate fine crystallinity. When the BiOBr content increase to 80 at%, the characteristic peaks of Bi_2WO_6 at 28.3 ° which is the (131) plane and 32.8 ° which is the (200) plain became weaker while all of the peaks became sharper, which could be ascribed to BiOBr since the main part possesses fine crystallinity. In the 20 at% BiOBr/Bi_2WO_6 composite, the characteristic peaks of BiOBr are rarely found except for the peak at 21.9 ° which is the (002) plain and the peak at 31.7 ° which is the (102) plane which determine the existence of the BiOBr. Meanwhile, the overlap of the characteristic peaks of Bi_2WO_6 and BiOBr prove the excellent combination of these two semiconductor by the facile synthesis method.

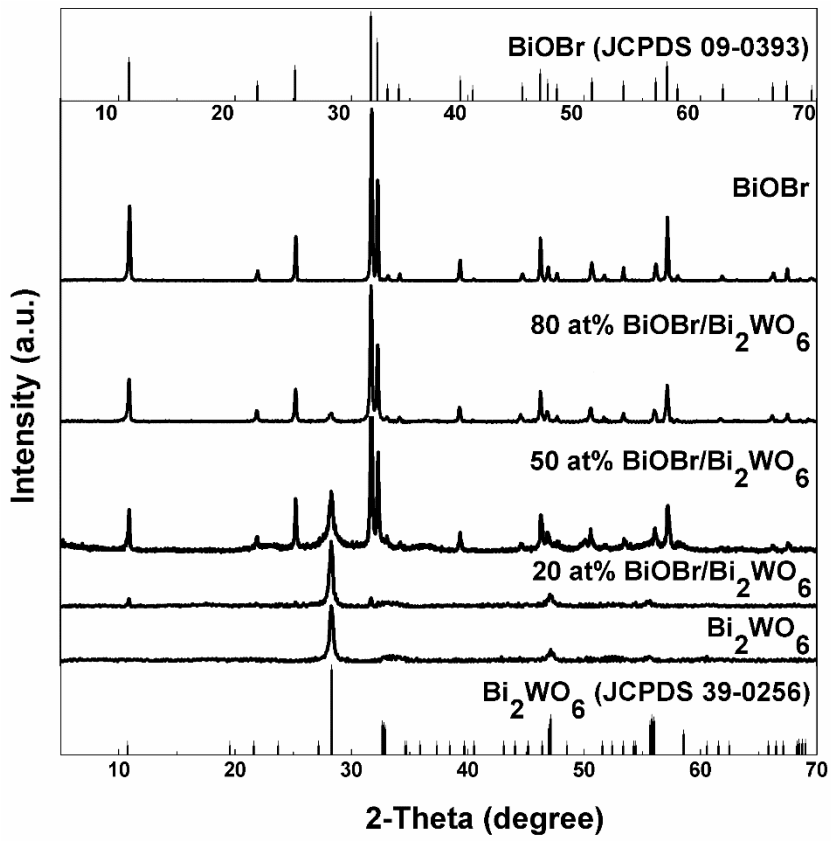

Fig. 4-2. The XRD pattern of the pure Bi_2WO_6, pure BiOBr and the composites of the BiOBr/Bi_2WO_6 with different ratios.

To investigate the chemical states of the BiOBr/Bi_2WO_6 composite, an X-ray photoelectron spectroscopy (XPS) was performed and the high resolution scan of Bi 4f, W 4f, O 1s and Br 3d orbits for the 50 at% sample are shown in Fig. 4-3. The spectra were calibrated by C 1s, the peak position of which was at 284.6 eV. For the Bi 4f XPS spectra in Fig. 4-3a, the two strong peaks centered at 164.7 eV and 159.4 eV were in good agreement with the Bi $4f_{5/2}$ and Bi $4f_{7/2}$, indicating the valence of bismuth in the BiOBr/Bi_2WO_6 composite was +2 [17, 23, 24]. It should be noted that the binding energy was not the same as the values of pure BiOBr and Bi_2WO_6 [25, 26], which could prove to be beneficial to combine these two semiconductors by this synthesis method. Similarly, the binding energy of W 4f was centered at 37.5 eV and

35.4 eV for W $4f_{5/2}$ and W $4f_{7/2}$ orbits, respectively (Fig. 4-3b), which indicates the presence of W^{6+} in the sample [27]. There were three peaks in the spectra of O 1s orbit (Fig. 4-3c), indicating that three different types of structures consist of oxygen. The highest peak at 530.4 eV attribute to the bonds of W-O and Bi-O in the 50 at% BiOBr/Bi_2WO_6 composite. In addition, the peaks at 531.6 eV and 533.0 eV were resulted from oxygen in -OH and adsorbed H_2O, respectively [28, 29]. The spectra in Fig. 4-3d show the Br in the composite in the form of Br^{-1} [23, 30]. Evidently, the XPS and XRD results determined that the hydrothermal synthesis method was feasible to prepare the heterojunction semiconductors.

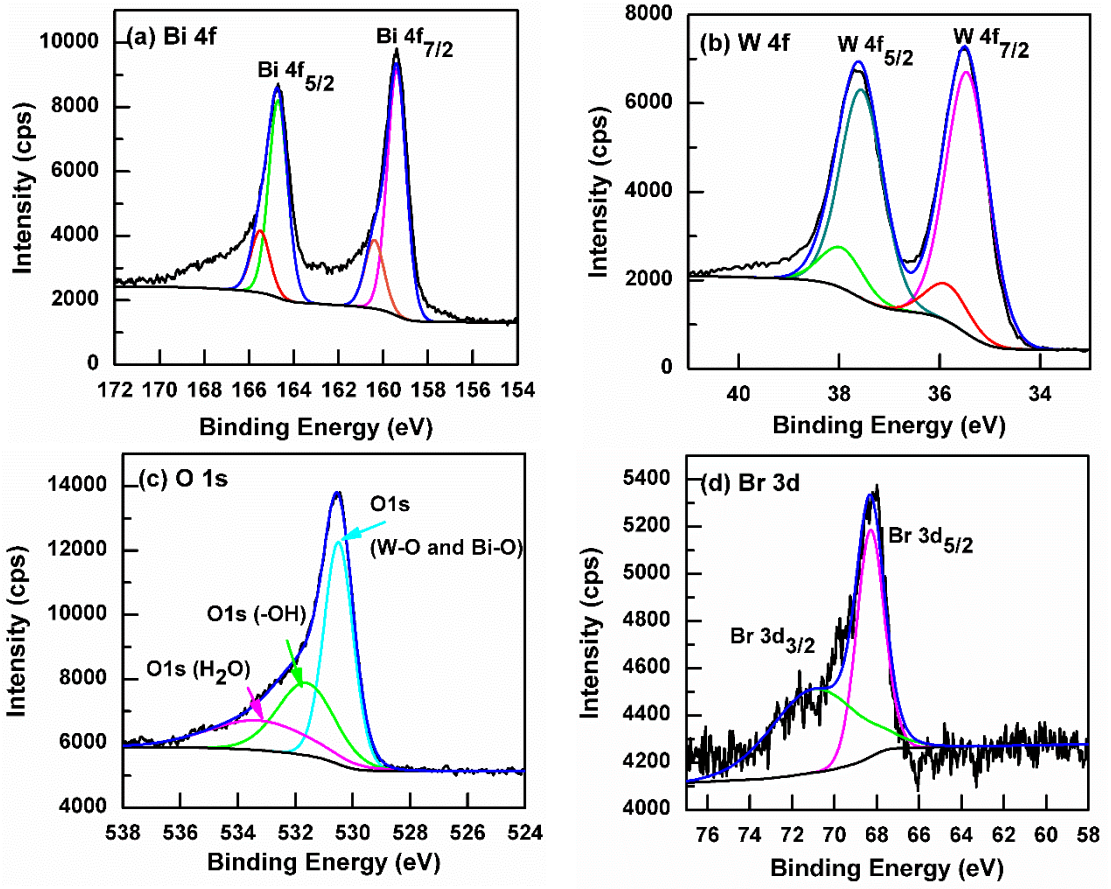

Fig. 4-3. High resolution XPS scan of (a) Bi 4f, (b) W 4f, (c) O 1s and (d) Br 3d orbits in the BiOBr (50 at%)-Bi_2WO_6 composite.

4.3.2 SEM, EDS and TEM analysis

Morphology analyses of the pure Bi_2WO_6, pure BiOBr and the composites with different ratio are shown in Fig. 4-4. The surface structure of pure Bi_2WO_6 is flake-like microspheres, sized in the range of 2-3 μm (Fig. 4-4a). Pure BiOBr produced by the hydrothermal method has a nanoplate crystal form (Fig. 4-4e). When the atomic ratio of BiOBr to Bi_2WO_6 was 1:1, the core was the hierarchical BiOBr and the flake-like Bi_2WO_6 were dispersed on its surface, the size of which was smaller than 1 μm (Fig. 4-4c). However, it should be noted that only the flake-like structure and flower-like structure were found in the BiOBr (20 at%)/Bi_2WO_6 composite (Fig. 4-4b) and BiOBr (80 at%)/Bi_2WO_6 (Fig. 4-4d) composite, respectively. The

EDS analysis on the BiOBr (50 at%)/Bi_2WO_6 composite is shown in Fig. 4-4f. It is suggested that only the elements of Bi, Br, O and W exist, which further prove that the composite consists of these two fundamental components of BiOBr and Bi_2WO_6.

The HRTEM image of the BiOBr (50 at%)-Bi_2WO_6 composite is shown in Fig. 4-5. The orderly lattice was analyzed and is shown in the figure. The clear lattice were almost at the edge, and the distance between the plane was about 0.35 nm which is in accordance with the (101) direction of BiOBr crystal according to the PDF#09-0393. The dark part in the core was due to the overlap of lattices of the BiOBr and Bi_2WO_6. As the Bi_2WO_6 was dispersed on the surface, the distance between the fringes was approximately 0.37 nm which was in good agreement with the (111) direction of Bi_2WO_6 based on the PDF#39-0256. Therefore, the HRTEM image could not only further prove that the composite consisted of these two fundamental components of BiOBr and Bi_2WO_6, but also revealed that the Bi_2WO_6 were dispersed in the core of BiOBr.

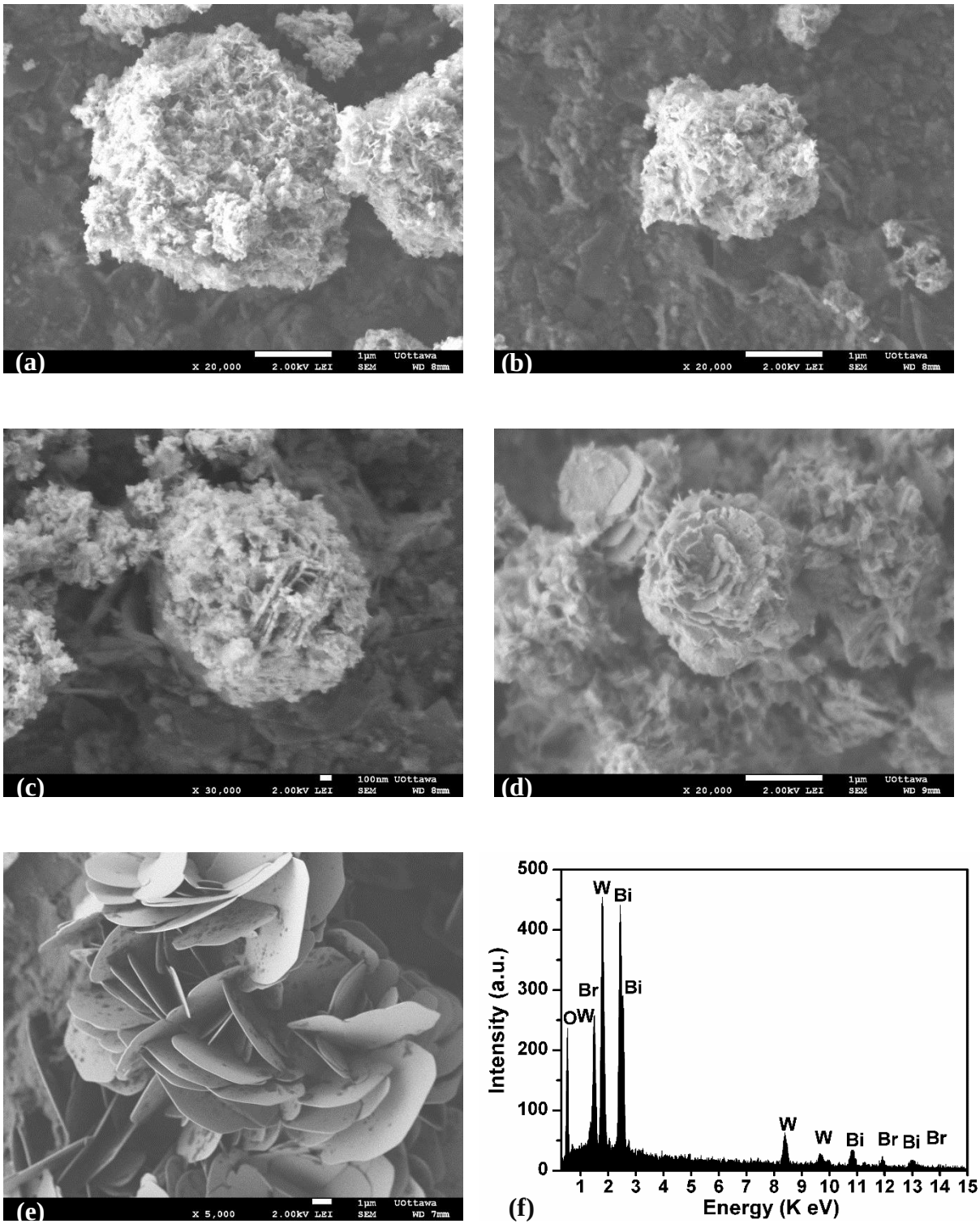

Fig. 4-4. FESEM image of (a) pure Bi_2WO_6, (b) 20 at% $BiOBr/Bi_2WO_6$ composite, (c) 50 at% $BiOBr/Bi_2WO_6$ composite, (d) 80 at% $BiOBr/Bi_2WO_6$ composite and (e) pure BiOBr; (f) EDS of 50 at% $BiOBr/Bi_2WO_6$ composite.

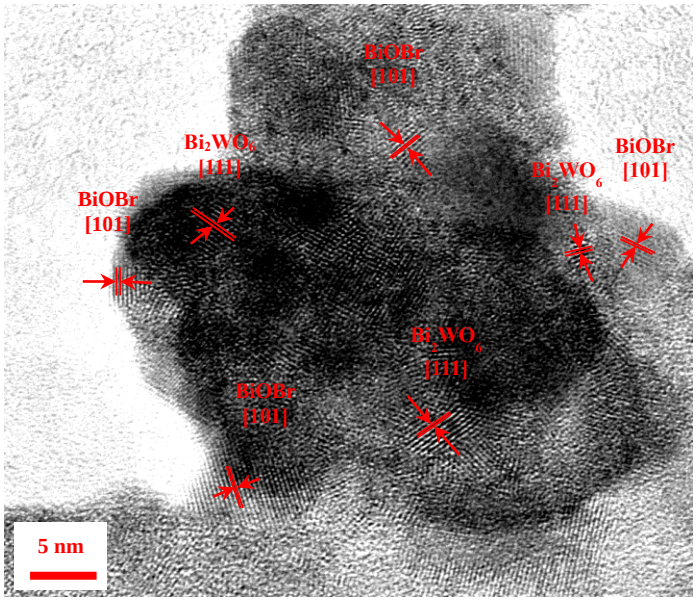

Fig. 4-5. HRTEM image of BiOBr (50 at%)-Bi_2WO_6 composite.

4.3.3 UV-Vis diffused reflectance spectra (DRS) analysis

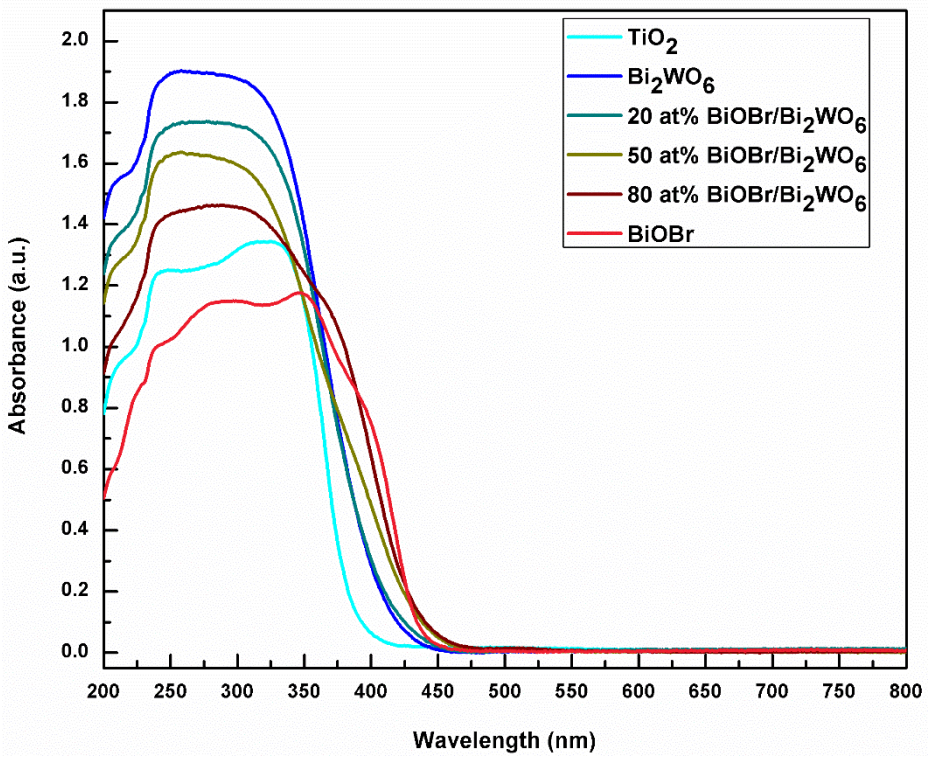

Fig. 4-6. UV-Vis diffused reflectance spectra (DRS) of the TiO_2 (anatase) and as-prepared pure BiOBr, pure Bi_2WO_6 and BiOBr-Bi_2WO_6 composite with different atomic ratio.

The optical absorbance properties were measured by the UV-Vis diffused reflectance spectroscopy and the spectra of the photocatalysts were determined as shown in Fig. 4-6. There exists a rapid increase of the absorbance when the wavelength of the irradiation was lower than a specific value (approximately 45 nm), which depends on the composition of the sample. The phenomena was due to the indirect band-gap transition. It could be concluded that with the increase of BiOBr in the composite, there was a notable red-shift in the irradiation absorbance which could be activatedd by the visible light. This is one of the primary shortcomings of the most widely used photocatalyst, TiO_2.

The bandgap (E_g) of the semiconductors could be calculated by the classical Tauc approach using the following equation:

$$\alpha E_{photon} = K(E_{photon} - E_g)^{\frac{n}{2}}$$

where $E_{photon} = h\nu$; α, K, E_g, n, h and ν represent the absorption coefficient, constant for semiconductor (usually equal to 1), bandgap energy, constant for semiconductor depending on the type of the band gap (direct transition: n=1; indirect transition: n=4), Planck constant and irradiation frequency, respectively [12]. Herein, for BiOBr, the value of n was 4 for its indirect band-gap transition (Appendix A.4) [31]. However, it is still controversial for Bi_2WO_6. Some researchers reported that n is 4 [32, 33], and some studies have confirmed its n is 1 [34, 35]. In this study, the band gap of Bi_2WO_6 attribute to the indirect type, so the n was 4. By plotting $(\alpha E_{photon})^{1/2}$-$E_{photon}$ shown in Fig. 4-7 and Table 4-1, all of the band gaps of these as-prepared BiOBr/Bi_2WO_6 were in the range of 2.61-2.79 eV, indicating that the photocatalysts could be activated by visible light (wavelengths higher than 400nm). Meanwhile, with the combination of the BiOBr, the values of band gaps in each composite slightly and irregularly

decreased due to BiOBr possessing a narrower band gap than Bi_2WO_6 [21]. The special thin nano-sheet structure of BiOBr is suitable for the quantum effect resulting in the blue-shift, which was why BiOBr had a relatively wide band gap. The BiOBr (50 at%)-Bi_2WO_6 composite with the narrowest band gap is probably due to the effect of sensitization to one another. These results, to some extent, prove that these as-prepared BiOBr/Bi_2WO_6 with well-established heterojunction have suitable band gaps for effective use in the degradation of organic pollutants under visible light.

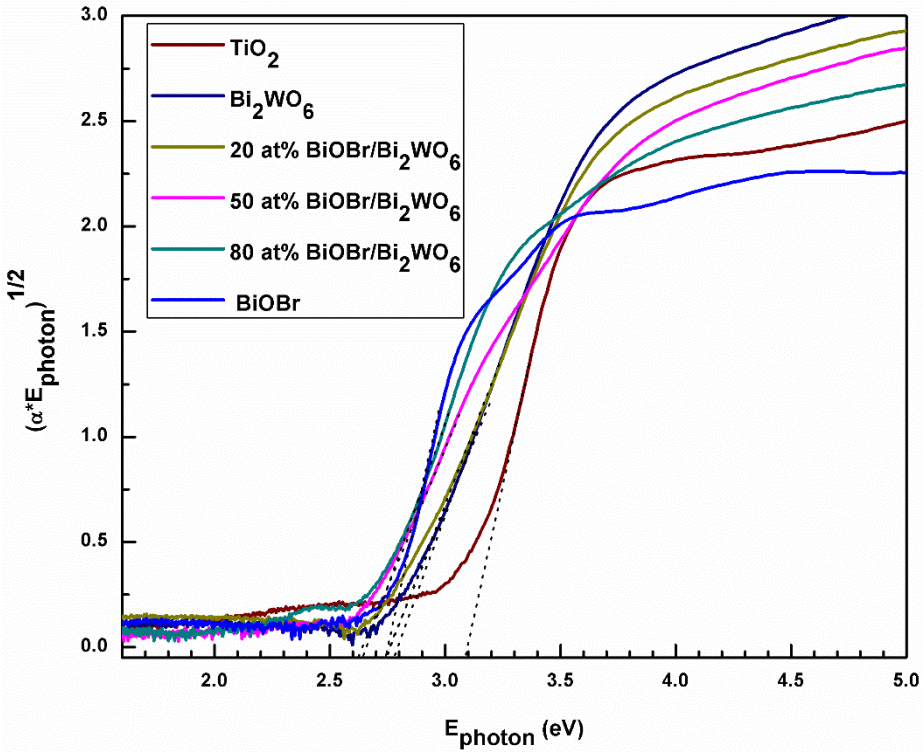

Fig. 4-7. $(\alpha E_{photon})^{1/2}$-$E_{photon}$ curves of TiO_2 (anatase) and as-prepared composites.

Table 4-1. Band gaps of TiO_2 and as-prepared samples

	TiO_2	Bi_2WO_6	20at% BiOBr/Bi_2WO_6	50at% BiOBr/Bi_2WO_6	80 at% BiOBr/Bi_2WO_6	BiOBr
E_g/eV	3.1	2.79	2.75	2.61	2.63	2.74

4.3.4 Photocatalytic degradation of RhB

4.3.4.1 The effect of the atomic ratio of BiOBr in the composites

The photocatalytic activity of the as-prepared composites was observed by degrading *Rhodamine B* (RhB). All of the screening test results were plotted as shown in Fig. 4-8. Initially, the adsorption-desorption property of the photocatalysts was tested in the dark with a 0.5 g/L BiOBr (50 at%)-Bi_2WO_6 composite. It was noted that the adsorption-desorption balance was attained in 10 minutes. Correspondingly, it was rational to have a 30 min pretreatment before the photocatalytic degradation process. For another screening test, photolysis was performed by turning on the light without any photocatalysts. The removal efficiency after 2 hours was just around 10%. As for the comparison of the bismuth composite with TiO_2, an apparent improvement was observed in the photocatalytic degradation for the bismuth photocatalysts over TiO_2 under visible light irradiation. To be more specific for the bismuth photocatalysts, the pure Bi_2WO_6 showed the lowest degradation efficiency with 81% after 2 hours. For the combination of BiOBr and Bi_2WO_6 such as the BiOBr (20 at%)-Bi_2WO_6 composites, the degradation efficiency showed improvements to some extent. However, when the atomic ratio of BiOBr in the composites was 50%, 90% of RhB decomposed in the first 30 minutes, and after 1 hour almost all of the dye water was purified. The sharp improvement of the degradation efficiency was probably due to the well-establishment of the heterojunction, which directly influences the separation of the hole-electron pairs and indirectly increases the efficiency. Comparing the pure BiOBr with the BiOBr (50 at%)-Bi_2WO_6 composite in the

degradation of RhB, the composite showed an increase in the degradation efficiency by 47.2% after 10 minutes.

To understand the kinetics of the RhB degradation, the Pseudo-first-order model ($ln\frac{c_o}{c} = kt$) was applied for low RhB concentrations, where *k* is the reaction constant and *t* is the irradiation time. By plotting $ln(c_o/c)$ with irradiation time (*t*) as shown in Fig. 4-9, the observed linear relationship proved that the Pseudo-first-order was suitable for this degradation process. The calculated results of the reaction constants shown in Table 4-2 indicated that the heterojunction effect suppressed the recombination of the hole-electron pairs to a large extent, especially for the BiOBr (50 at%)-Bi_2WO_6 composite. When the atomic ratio is lower than 50%, fewer heterojunctions are formed which lead to the relatively lower reaction rate. However, when the atomic ratio increased to 80%, even though more heterojunctions formed and the recombination rate of the electron-hole pairs sharply decreased, the lower surface area resulted in less chemical reaction sites and lower degradation efficiency. Similar results were reported in [36]. Overall, the optimal atomic ratio of BiOBr in the composite with high photocatalytic activity was 50%.

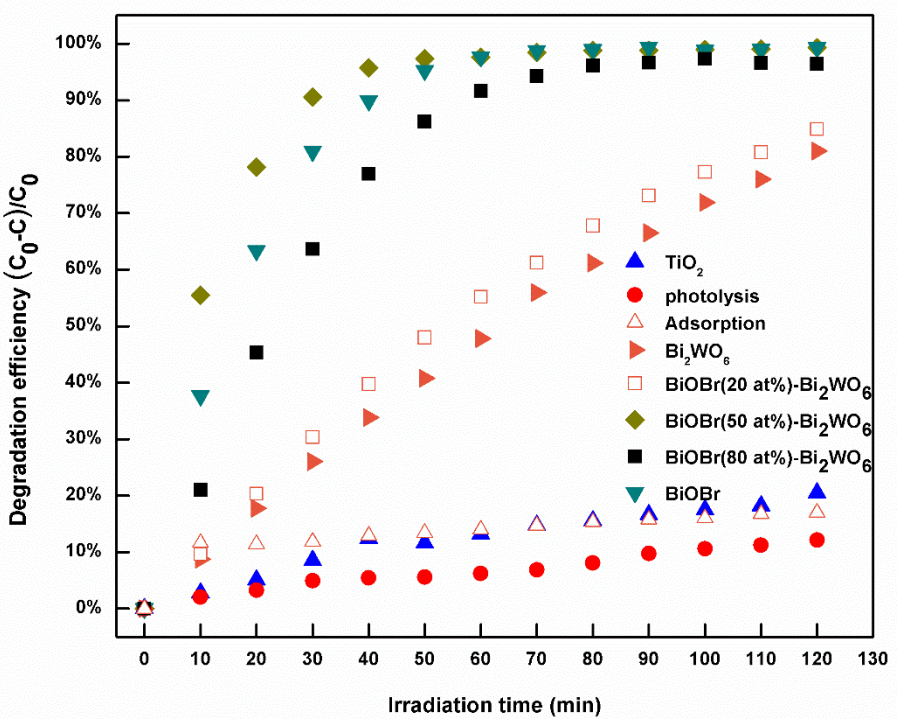

Fig. 4-8. Photocatalytic degradation efficiency as a function of time under various conditions. (catalysts dosage: 0.5 g/L; Temperature: (20±2) °C; pH=4.7 and initial concentration: 10 ppm)

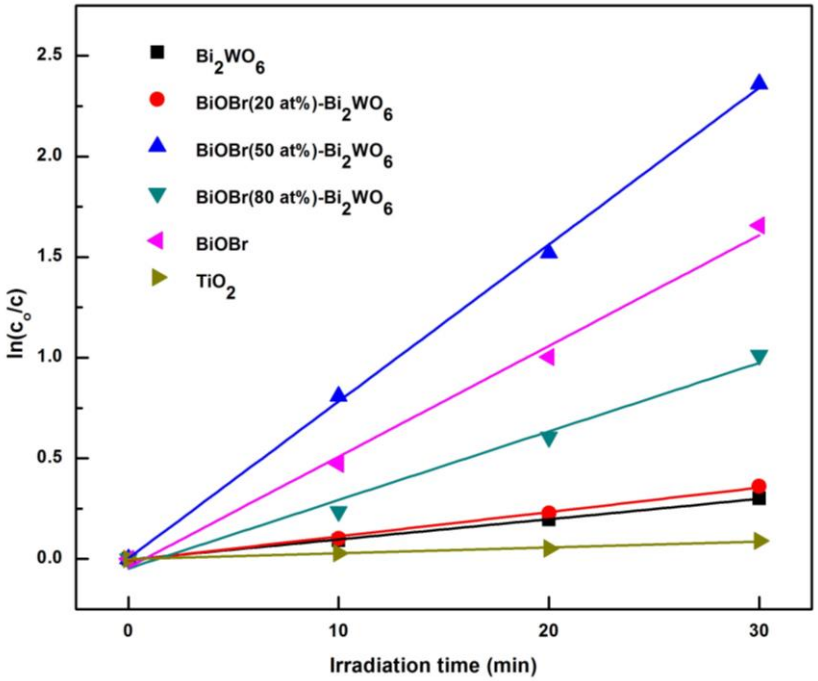

Fig. 4-9. Photocatalytic kinetics for each process. (catalysts dosage: 0.5 g/L; Temperature: (20±2) °C; pH=4.7 and initial concentration: 10 ppm)

Table 4-2. Pseudo-first order reaction rate constant for various processes respectively

	TiO_2	Bi_2WO_6	20at% $BiOBr/Bi_2WO_6$	50at% $BiOBr/Bi_2WO_6$	80 at% $BiOBr/Bi_2WO_6$	BiOBr
Pseudo-first order:						
$k(10^{-2}min^{-1})$	0.292	1.009	1.210	7.796	3.405	5.503
R^2	0.9863	0.9982	0.9942	0.9986	0.9802	0.9916

4.3.4.2 The mechanism of the degradation process

It was reported that the degradation process of RhB was divided into two competitive processes, namely the N-de-ethylation process and the destruction of conjugated structure [33, 37]. The intermediate products of N-de-ethylation include *N, N, N'-Triethyl-Rhodamine* (TER), *N, N'-Diethyl-Rhodamine* (DER), *N-Ethyl-Rhodamine* (ER) and *Rhodamine* (molecular formulas in Appendix A.3). The wavelength of the peaks are 539 nm, 522nm, 510nm and 498 nm, respectively [37, 38], which indicates that this process could lead to the blue-shift of the wavelength. In this study, the UV-Vis spectra of the degraded RhB solution after each specific irradiation time were tested (Fig. 4-10). The wavelength of the major absorbance peak and the relative intensity of the absorbance as a function of the irradiation time were also plotted (Fig. 4-11). Apparently, the blue-shift of the peak wavelength occurred in the UV-Vis spectra, which indicates that de-ethylation initially dominates the degradation process (Scheme 1). After 40 minutes, the peak wavelength was stable at 498 nm with a decrease in intensity due to the destruction of the aromatic ring [38, 39]. The inset in Fig. 4-10 shows that the solution underwent a series of color changes from red to orange, to light yellow and finally to a colorless solution. This was ascribed to the initial degradation of RhB being dominated by de-ethylation; followed by the degradation process shifting to the destruction of the conjugated structure once the ethyl compound was completely decomposed.

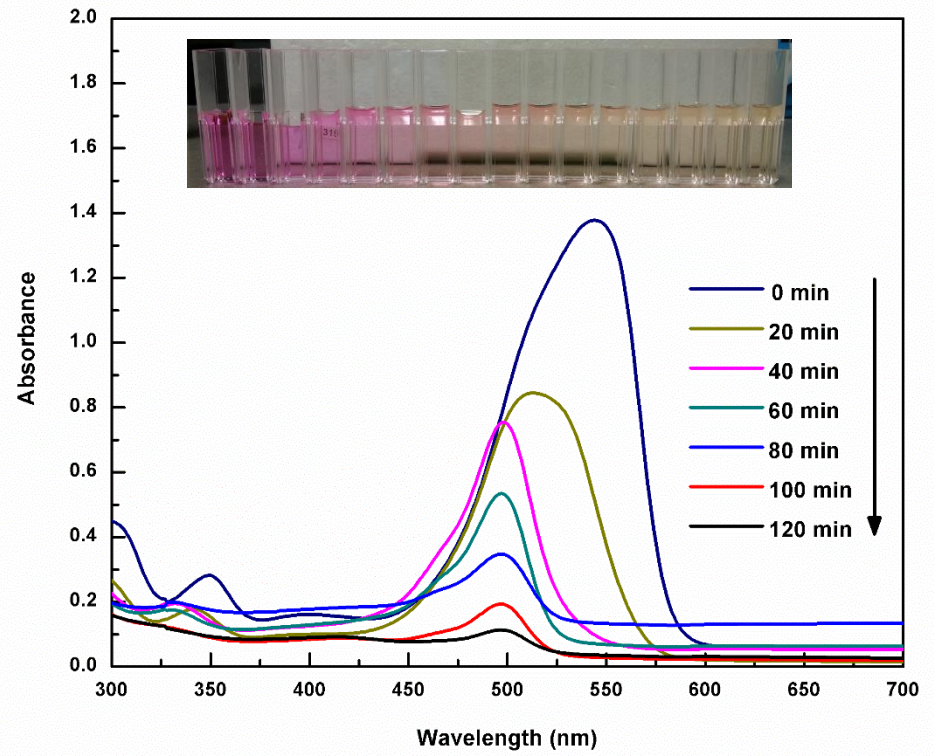

Fig. 4-10. UV-Vis spectra of RhB as a function of irradiation time. (BiOBr (50 at%)-Bi_2WO_6 composite; Catalysts dosage: 0.5 g/L; Temperature: (20±2) °C; pH=4.7 and initial concentration: 10 ppm)

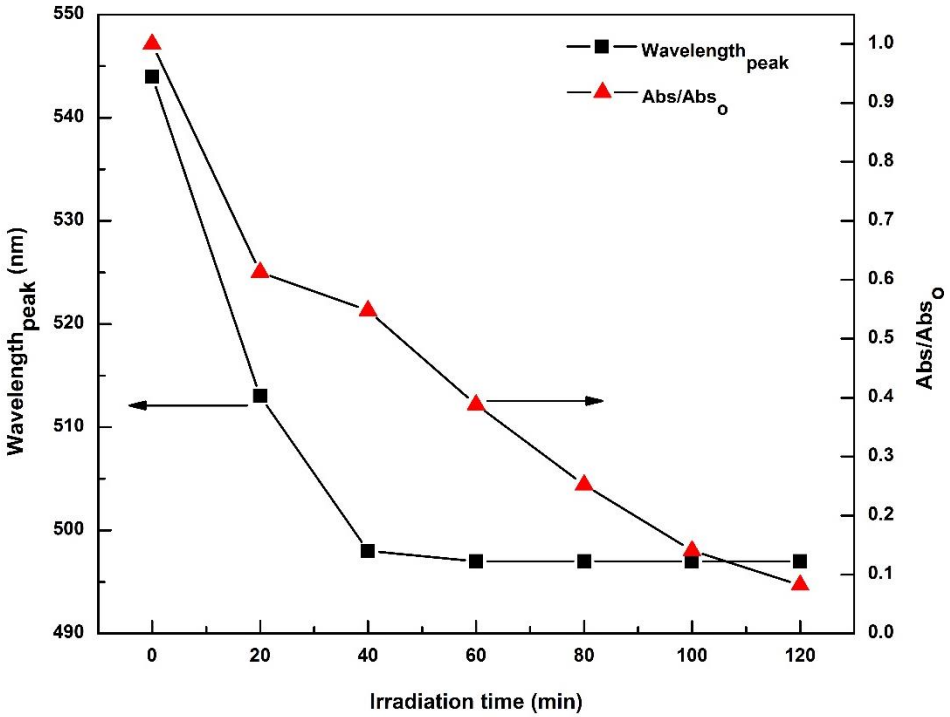

Fig. 4-11. The wavelength of the major absorbance peak and the relative absorbance intensity under each specific irradiation time.

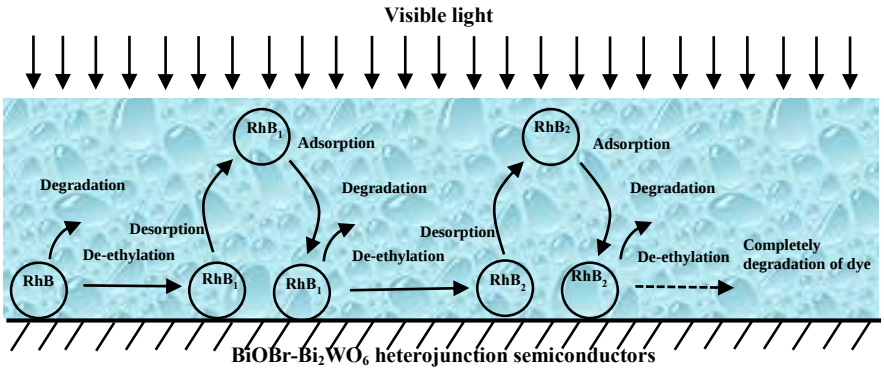

Fig. 4-12. Model of the degradation process of *Rhodamine B* on the BiOBr-Bi_2WO_6 composite

4.3.4.3 The enhancement of heterojunction

To prove the feasibility of the hydrothermal synthesis method in the enhancement of the photocatalytic activity, another screening test was performed by mechanically mixing the as-prepared BiOBr and Bi_2WO_6 together with the catalysts' dosage at 0.5 g/L and the atomic ratio of BiOBr at 50%. The degradation efficiency with the irradiation time was plotted as shown in Fig. 4-13. In the first 10 min, the degradation efficiencies were 20.7% and 50.5% for the photocatalysts synthesized by hydrothermal method and mechanical mixing method, respectively. The degradation efficiency of photocatalysts by mechanical mixing was just between the pure BiOBr and Bi_2WO_6, indicating that the photocatalytic effect of the physical mixture was simply the superposition of each component. The apparent enhancement of the composite synthesized by hydrothermal method was probably due to the well-establishment of the heterojunction, which effectively suppressed the recombination of the electron-hole pairs leading to a massive production rate of the oxidants. The particular mechanism of the heterojunction effect was schemed as shown in Fig. 4-18.

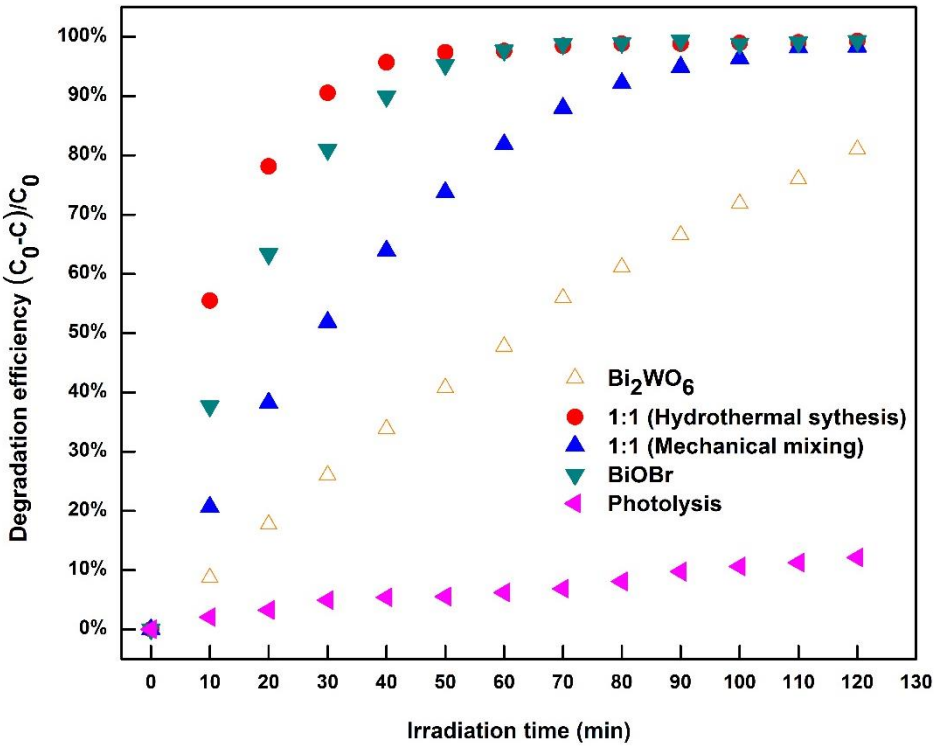

Fig. 4-13. Comparison of hydrothermal synthesis method and physical mechanical mixing method in the degradation of RhB. (Catalysts dosage: 0.5 g/L; Temperature: (20±2) °C; pH=4.7 and c_o= 10 ppm)

4.3.5 Reusability

Reusability was tested as a significant parameter in the evaluation of the BiOBr (50 at%)-Bi_2WO_6 composite with a dosage of 1g/L (RhB solution). Both the adsorptive and photocatalytic performance of the photocatalysts in each run were tested and experimental results were observed as shown in Fig. 4-14. After 30 min in the dark to attain the adsorption-desorption balance, the adsorbed quantity by the photocatalysts in each run decreased. This was because there are some RhB, or the species of RhB after partial degradation, adsorbed on the photocatalysts without being completely degraded in the prior run. This decreased the surface area of the photocatalyst which was crucial in the adsorption-desorption process. As for the synergetic effect of adsorption and photocatalysis, the degradation efficiency in the

first run reached 99.5% after 90 minutes. Afterwards, the degradation efficiencies decreased in every successive run, and 83.2% of the RhB was decomposed in the fourth run.

After the four runs, the photocatalyst was separated by centrifuge and then dried in the oven before the XRD test was performed. The results are shown in Fig. 4-15. Comparing the XRD pattern of the photocatalysts before and after the degradation process, it could be noted that the similar peak shapes that represent almost all of the characterization peaks of BiOBr and Bi_2WO_6 appeared based on the JCPDS card. This indicated that the structure of the composite was not destroyed and correspondingly proved the strong stability of the as-prepared photocatalysts in the purification of wastewater. Additionally, the widening peaks and the decrease of the peak intensity such as in (1,0,2) and in (1,1,0) could be interpreted as molecular RhB or the species of RhB degraded being adsorbed into the structure of the composite, decreasing its degree of crystallization of the structure.

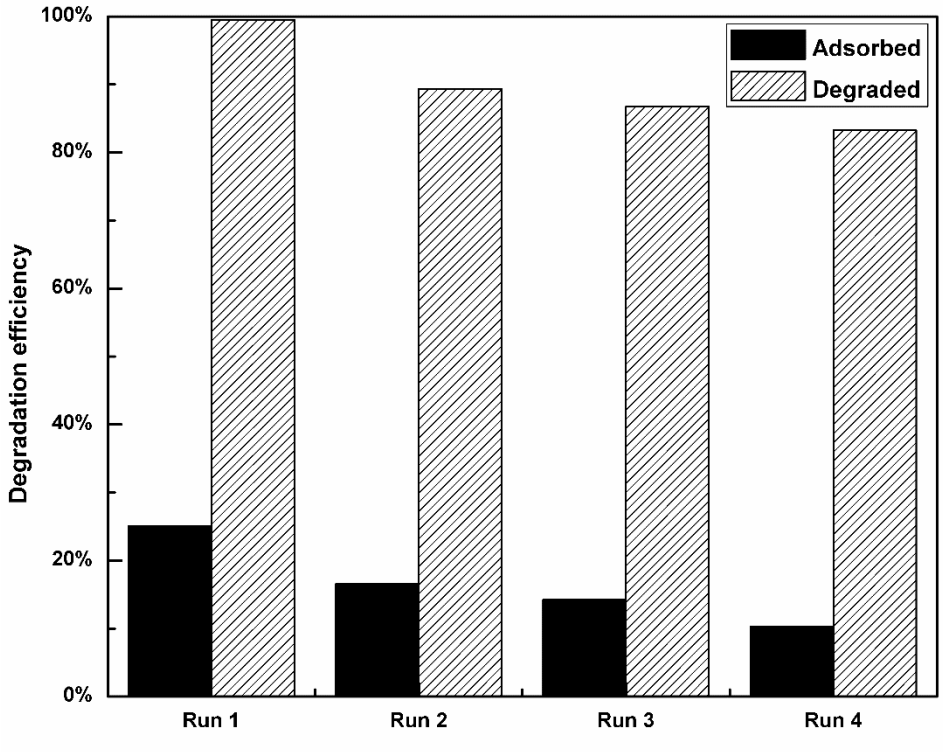

Fig. 4-14. Reusability of the BiOBr (50 at%)-Bi_2WO_6 composite performed in the degradation of RhB. (Catalysts dosage: 1.0 g/L; Temperature: (20±2) °C; pH=4.7 and c_o= 10 ppm)

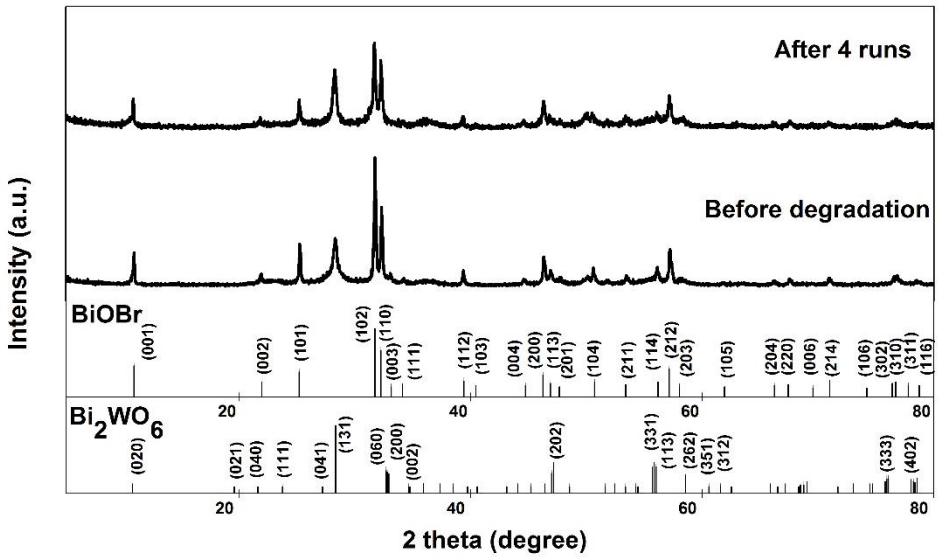

Fig. 4-15. XRD pattern of the BiOBr (50 at%)-Bi_2WO_6 before the degradation process and after 4 runs.

4.3.6 Roles of species

The photocatalytic degradation of RhB was due to the oxidative process, producing extremely powerful reactive oxidants including •OH, $•O_2$ and holes [40]. Aiming to acknowledge the specific effect of each species, the scavengers of these oxidative species were introduced in [41]. In this paper, the quenching experiment was performed by adding the EDTA to remove the holes, isopropanol to suppress the hydroxyl radicals and N_2 bubbling to decrease the dissolved oxygen so as to suppress the production of $•O_2$ during the degradation process of RhB [31, 42, 43]. The results of each quenching degradation experiments were plotted as shown in Fig. 4-16. Apparently, when scavengers were added in the solution, the degradation efficiency would decrease to some extent, which indicated that all the scavengers played an inhibiting effect in the degradation process by influencing the production of the oxidative species. Meanwhile, the different degrees of the effect of quenching were probably due to the various roles of each oxidative species in the degradation of the organics in the wastewater. To better explore the roles of each species, a kinetic analysis was performed by plotting the $ln(c_0/c)$ *vs.* irradiation time t as shown in Fig. 4-17 and the calculated slope of the line was summarized as shown in Table 4-3. The rate constant and the quenching effect shown in Table 4-3 suggest that the photo-generated holes play a dominant role in the photocatalytic degradation of organics. The holes could either react with H_2O to produce hydroxyl radicals which could completely decompose the pollutants (*Eq. 2* & *Eq. 4*) or directly oxidize the pollutants (*Eq. 3*) [40]. Correspondingly, when the hydroxyl radical were suppressed by isopropanol, the holes could also degrade the pollutant to some extent. Furthermore, the photo-generated electrons were able to react with the adsorbed dissolved oxygen to produce the superoxide radicals in Eq. 5 which could also degrade some pollutants. The relatively lower

quenching effect when the electrons were suppressed might be caused by the weaker oxidative properties of superoxide radicals compared with that of holes [44, 45]. These results indicate that the photo-generated holes play a predominant role in the photocatalytic degradation of the pollutants in the BiOBr-Bi_2WO_6 system (similar results have also been reported in [31] [25, 46]).

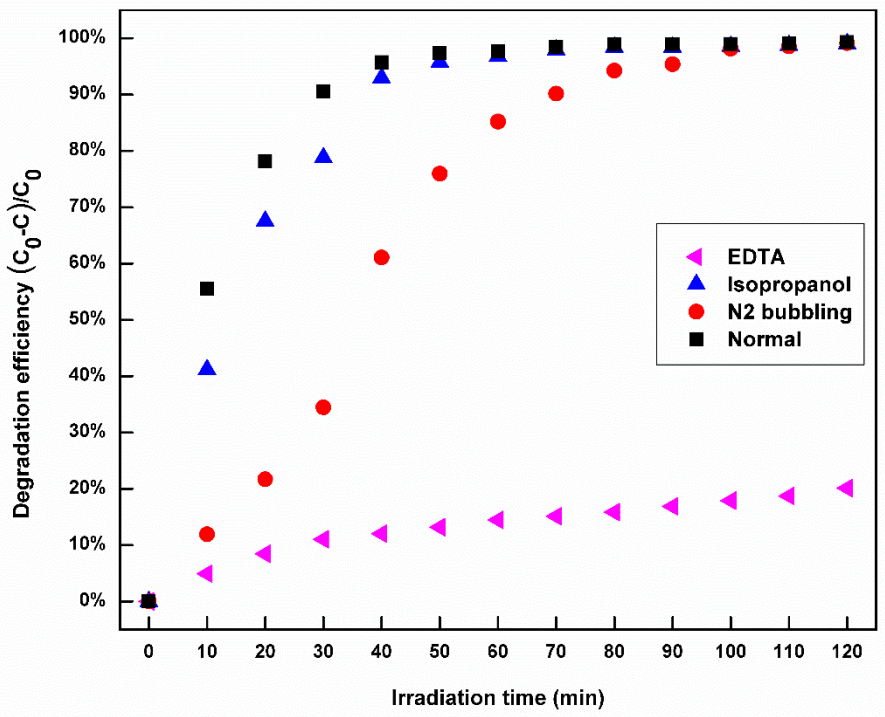

Fig. 4-16. The degradation efficiencies in the presence of different scavenges for BiOBr (50 at%)-Bi_2WO_6 composite. (Catalysts dosage: 0.5 g/L; Temperature: (20±2) °C; pH=4.7 and c_0= 10 ppm)

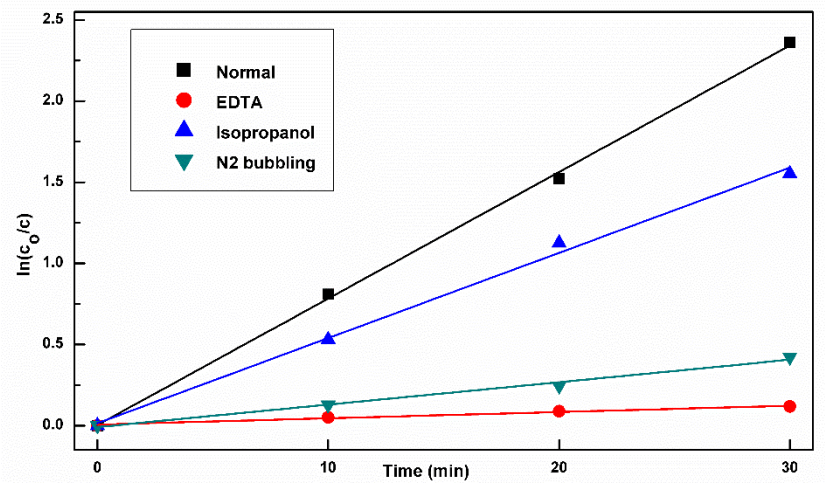

Fig. 4-17. Kinetic analysis comparison of processes with or without scavenges.

Table 4-3. The quenching effect of different scavenges in the degradation of RhB

Scavenge	Species suppressed	k (10^{-2} min^{-1})	R^2 (%)	$(k_{normal}-k_{scavenge})/k_{normal}$ (%)
Normal	--	7.80	99.9	0
EDTA	Holes (h^+)	0.39	97.6	95
Isopropanol	Hydroxyl radicals (•OH)	5.25	99.4	32.7
N_2 bubbling	Superoxide radicals (•O_2)	1.39	98.6	82.2

$$Photocatalysts + h\nu \longrightarrow h^+_{VB} + e^-_{CB} \quad \textit{(Eq. 1)}$$

$$H_2O + h^+_{VB} \longrightarrow \bullet OH + H^+ \quad \textit{(Eq. 2)}$$

$$h^+ + Pollutant \longrightarrow Pollutant^+ \quad \textit{(Eq. 3)}$$

$$\bullet OH + Pollutant \longrightarrow CO_2 + H_2O \quad \textit{(Eq. 4)}$$

$$O_2 + e^-_{CB} \longrightarrow \bullet O_2^- \quad \textit{(Eq. 5)}$$

4.3.7 The proposed mechanism

To further acknowledge the photocatalytic degradation ability of the BiOBr-Bi_2WO_6 composite, analysis of its band structure (valence band and conduction band) was essential.

Based on the band gap calculation results shown in Table 4-1, the band gaps of Bi_2WO_6 and BiOBr were 2.79 and 2.74, respectively. The flat-band potentials are calculated using the Mulliken electronegative theory for atoms: $E_{CB} = X_{Photocatalyst} - E^e - \frac{1}{2}E_g$, where E_{CB} is the bottom position of the conduction band, $X_{Photocatalyst}$ is the electronegativity of the semiconductor, E^e is the energy of free electrons on the hydrogen scale (≈4.5 eV) and E_g is the band gap of the photocatalyst[47, 48]. Based on this equation, the bottom potential of conduction band for Bi_2WO_6 and BiOBr were calculated to be 0.56 eV and 0.296 eV, respectively. Correspondingly, the top potential of the valence band could be calculated via $E_{VB} = E_{CB} + E_g$. Therefore, the E_{VB} of Bi_2WO_6 and BiOBr were approximately 3.35 eV and 3.036 eV, respectively. Based on these results, the band structure of the BiOBr-Bi_2WO_6 system was determined as depicted in Fig. 4-17. As previously reported, Bi_2WO_6 and BiOBr are typically an n-type and a p-type semiconductor, respectively [20, 49]. The synergetic effect of closely contacted p-n heterojunction was confirmed as an effective way to improve the photocatalytic efficiency by decreasing the recombination rate of the photo-generated electron-hole pairs [31, 50]. When photocatalysts are activated by visible light, electrons are produced on the conduction band and positive carriers are produced on the valence band. During this phenomena, the p-n heterojunction creates an electric field which pushes electrons accumulated on the conduction band of BiOBr (p-type) to the conduction band of Bi_2WO_6, while the holes on the valence band of Bi_2WO_6 (n-type) migrate in the opposite direction towards the valence band of BiOBr. This kind of migration could efficiently separate the electrons and holes and indirectly increase the photocatalytic efficiencies. The experimental results in Fig. 4-12 further indicate that a close contact of the p-type and n-type semiconductors was established.

The mechanism of the photocatalytic oxidative degradation of the organics for the BiOBr-Bi_2WO_6 system, depicted in Fig. 4-17, could be divided into two main process: (a) photocatalytic degradation process and (b) photosensitization. As it was reported in [51], the redox potential of RhB is -1.42 eV *vs.* NHE and experimental results demonstrate the maximum absorption peak at 554 nm in the wavelength range of visible light. Therefore, both the BiOBr-Bi_2WO_6 composite (photocatalyst) and the RhB can be activated under visible light to produce electrons. The electrons react with dissolved oxygen to produce $\bullet O_2^-$, an oxidative species which could break down the RhB. The redox potential of the valence bands of Bi_2WO_6 and BiOBr were located at 3.35 eV and 3.036 eV, respectively. This indicates that the photo-generated holes possess far more oxidative properties than that of general oxidants such as H_2O_2 (+1.77 eV), O_3 (+2.07 eV) and $\bullet OH/OH^-$ (+1.99 eV) [52]. Additionally, the standard redox potential of $Bi_2O_4/BiO+$ (Bi^V/Bi^{III}) is +1.59 eV which is more negative than that of $\bullet OH/OH^-$ (+1.99 eV) [46, 52]. This suggests that the production of •OH was impossible. As a result, •OH had little influence on the oxidative process and holes were treated as the main oxidative species in the degradation process of RhB for the BiOBr-Bi_2WO_6 system. The corresponding experimental results were analyzed in section 3.6 (Fig. 4-15， Fig. 4-16 and Table 4-3).

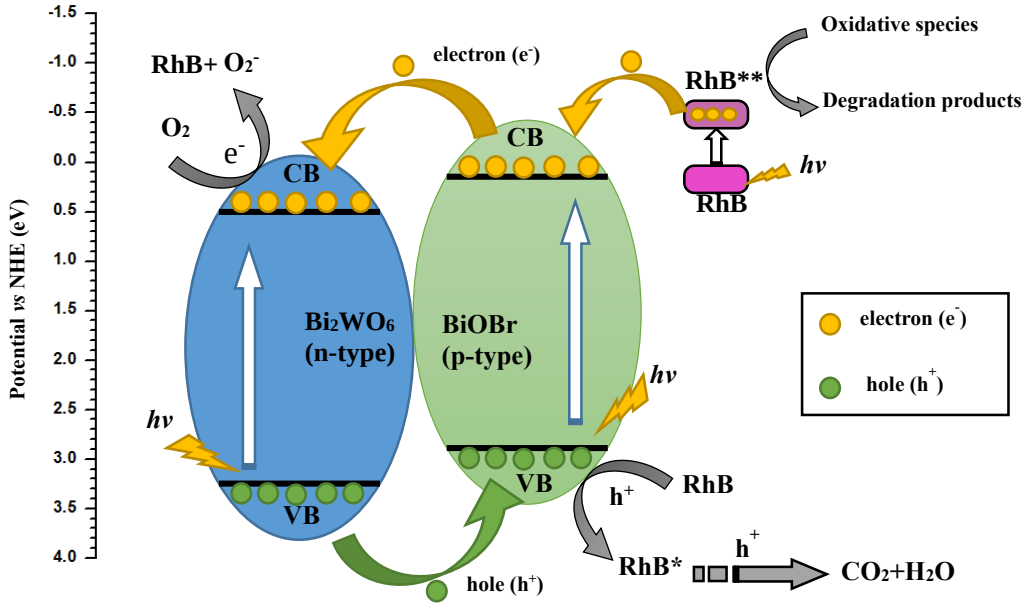

Fig. 4-18. Schematic band structure of the BiOBr-Bi_2WO_6 system and the proposed mechanism of the photocatalytic degradation process of RhB under visible-light irradiation.

4.4 Conclusions

In this work, BiOBr-Bi_2WO_6 heterojunctions were synthesized by the facile hydrothermal method with various BiOBr loading amounts, and were successfully applied in the purification of dye water (RhB) under visible light. The characterization of composites were obtained by XRD, SEM, TEM, XPS and DRS techniques. The BiOBr (50 at%)-Bi_2WO_6 composite with an "egg-shell" structure were prone to possess the highest photocatalytic degradation efficiency. Lower or higher loading of BiOBr hindered the photocatalytic performance to some extent. The analysis of DRS results demonstrated that the as-prepared photocatalysts could easily be activated under visible light and these two photocatalysts were suitable to establish the heterojunction which was confirmed by the apparent enhancement in the degradation process. In summary of the proposed mechanism for BiOBr-Bi_2WO_6, holes with high oxidative properties played a predominant role in the degradation of RhB as it was not possible to produce any •OH. This research provided a feasible way to increase the degradation efficiency by establishing a heterojunction to solve the photocatalytic challenges such as low photo-efficiencies under visible light and high recombination of the photo-generated electron-hole pairs. However, photosensitization effects of the chosen dye organic (RhB) significantly influenced the degradation process. Future work could focus on the degradation of other dye organics or some colorless organics such as Phenol to explore the photocatalytic activity of the BiOBr-Bi_2WO_6 system.

4.5 References

[1] A. Fujishima, K. Honda, Electrochemical photolysis of water at a semiconductor electrode, nature, 238 (1972) 37-38.

[2] L. Zhang, W. Wang, S. Sun, D. Jiang, E. Gao, Selective transport of electron and hole among {0 0 1} and {1 1 0} facets of BiOCl for pure water splitting, Applied Catalysis B: Environmental, 162 (2015) 470-474.

[3] M.R. Hoffmann, S.T. Martin, W. Choi, D.W. Bahnemann, Environmental Applications of Semiconductor Photocatalysis, Chem Rev, 95 (1995) 69-96.

[4] M. Ni, M.K.H. Leung, D.Y.C. Leung, K. Sumathy, A review and recent developments in photocatalytic water-splitting using for hydrogen production, Renewable and Sustainable Energy Reviews, 11 (2007) 401-425.

[5] S. Malato, P. Fernández-Ibáñez, M.I. Maldonado, J. Blanco, W. Gernjak, Decontamination and disinfection of water by solar photocatalysis: Recent overview and trends, Catalysis Today, 147 (2009) 1-59.

[6] R. Portela, M.D. Hernández-Alonso, Environmental Applications of Photocatalysis, Design of Advanced Photocatalytic Materials for Energy and Environmental Applications, Springer2013, pp. 35-66.

[7] R. Thiruvenkatachari, S. Vigneswaran, I.S. Moon, A review on UV/TiO_2 photocatalytic oxidation process (Journal Review), Korean J Chem Eng, 25 (2008) 64-72.

[8] H. Park, Y. Park, W. Kim, W. Choi, Surface modification of TiO_2 photocatalyst for environmental applications, Journal of Photochemistry and Photobiology C: Photochemistry

Reviews, 15 (2013) 1-20.

[9] M. Shang, W. Wang, L. Zhang, S. Sun, L. Wang, L. Zhou, 3D Bi_2WO_6/TiO_2 Hierarchical Heterostructure: Controllable Synthesis and Enhanced Visible Photocatalytic Degradation Performances, The Journal of Physical Chemistry C, 113 (2009) 14727-14731.

[10] S. Obregón, G. Colón, Erbium doped TiO_2–Bi_2WO_6 heterostructure with improved photocatalytic activity under sun-like irradiation, Applied Catalysis B: Environmental, 140–141 (2013) 299-305.

[11] Q.C. Xu, D.V. Wellia, Y.H. Ng, R. Amal, T.T.Y. Tan, Synthesis of porous and visible-light absorbing Bi_2WO_6/TiO_2 heterojunction films with improved photoelectrochemical and photocatalytic performances, J Phys Chem C, 115 (2011) 7419-7428.

[12] J. Li, Z. Guo, Y. Wang, Z. Zhu, Three-dimensional TiO_2/Bi_2WO_6 hierarchical heterostructure with enhanced visible photocatalytic activity, Micro & Nano Letters, IET, 9 (2014) 65-68.

[13] Y. Hao, F. Li, F. Chen, M. Chai, R. Liu, X. Wang, In situ one-step combustion synthesis of Bi_2O_3/Bi_2WO_6 heterojunctions with notable visible light photocatalytic activities, Mater Lett, 124 (2014) 1-3.

[14] Y. Peng, M. Yan, Q. Chen, C. Fan, H. Zhou, A. Xu, Novel one-dimensional Bi_2O_3-Bi_2WO_6 p-n hierarchical heterojunction with enhanced photocatalytic activity, Journal of Materials Chemistry A, 2 (2014) 8517-8524.

[15] M. Gui, W. Zhang, Q. Su, C. Chen, Preparation and visible light photocatalytic activity of Bi_2O_3/Bi_2WO_6 heterojunction photocatalysts, J Solid State Chem, 184 (2011) 1977-1982.

[16] M. Gui, W. Zhang, Y. Chang, Y. Yu, One-step hydrothermal preparation strategy for

nanostructured WO_3/Bi_2WO_6 heterojunction with high visible light photocatalytic activity, Chemical Engineering Journal, 197 (2012) 283-288.

[17] G. He, G. He, A. Li, X. Li, X. Wang, Y. Fang, Y. Xu, Synthesis and visible light photocatalytic behavior of WO_3 (core)/Bi_2WO_6 (shell), Journal of Molecular Catalysis A: Chemical, 385 (2014) 106-111.

[18] L. Lin, M. Huang, L. Long, Z. Sun, W. Zheng, D. Chen, Fabrication of a three-dimensional BiOBr/BiOI photocatalyst with enhanced visible light photocatalytic performance, Ceram Int, 40 (2014).

[19] H. An, Y. Du, T. Wang, C. Wang, W. Hao, J. Zhang, Photocatalytic properties of BiOX (X = Cl, Br, and I), Rare Metals, 27 (2008) 243-250.

[20] Y. Tian, G. Hua, W. Xu, N. Li, M. Fang, L. Zhang, Bismuth tungstate nano/microstructures: Controllable morphologies, growth mechanism and photocatalytic properties, Journal of Alloys and Compounds, 509 (2011) 724-730.

[21] J. Xia, J. Di, S. Yin, H. Xu, J. Zhang, Y. Xu, L. Xu, H. Li, M. Ji, Facile fabrication of the visible-light-driven Bi_2WO_6/BiOBr composite with enhanced photocatalytic activity, RSC Advances, 4 (2014) 82-90.

[22] S. Chaiwichian, B. Inceesungvorn, K. Wetchakun, S. Phanichphant, W. Kangwansupamonkon, N. Wetchakun, Highly efficient visible-light-induced photocatalytic activity of $Bi_2WO_6/BiVO_4$ heterojunction photocatalysts, Mater Res Bull, 54 (2014) 28-33.

[23] L. Kong, Z. Jiang, H.H. Lai, R.J. Nicholls, T. Xiao, M.O. Jones, P.P. Edwards, Unusual reactivity of visible-light-responsive AgBr–BiOBr heterojunction photocatalysts, Journal of Catalysis, 293 (2012) 116-125.

[24] M. Ge, Y. Li, L. Liu, Z. Zhou, W. Chen, Bi_2O_3−Bi_2WO_6 Composite Microspheres: Hydrothermal Synthesis and Photocatalytic Performances, The Journal of Physical Chemistry C, 115 (2011) 5220-5225.

[25] H. Lin, H. Ye, X. Li, J. Cao, S. Chen, Facile anion-exchange synthesis of BiOI/BiOBr composite with enhanced photoelectrochemical and photocatalytic properties, Ceram Int, 40 (2014) 9743-9750.

[26] Y. Fu, C. Chang, P. Chen, X. Chu, L. Zhu, Enhanced photocatalytic performance of boron doped Bi_2WO_6 nanosheets under simulated solar light irradiation, J Hazard Mater, 254–255 (2013) 185-192.

[27] G. He, C. Liang, Y. Ou, D. Liu, Y. Fang, Y. Xu, Preparation of novel Sb_2O_3/WO_3 photocatalysts and their activities under visible light irradiation, Mater Res Bull, 48 (2013) 2244-2249.

[28] J. Wielant, T. Hauffman, O. Blajiev, R. Hausbrand, H. Terryn, Influence of the Iron Oxide Acid−Base Properties on the Chemisorption of Model Epoxy Compounds Studied by XPS, The Journal of Physical Chemistry C, 111 (2007) 13177-13184.

[29] J. Torres, C.C. Perry, S.J. Bransfield, D.H. Fairbrother, Low-Temperature Oxidation of Nitrided Iron Surfaces, The Journal of Physical Chemistry B, 107 (2003) 5558-5567.

[30] K. Li, W. Lee, C. Lu, Y. Dai, S. Chou, H. Chen, H. Lin, C. Chen, Synthesis of BiOBr, Bi_3O_4Br, and $Bi_{12}O_{17}Br_2$ by controlled hydrothermal method and their photocatalytic properties, J Taiwan Inst Chem E, 45 (2014) 2688-2697.

[31] J. Xia, J. Di, S. Yin, H. Li, H. Xu, L. Xu, H. Shu, M. He, Solvothermal synthesis and enhanced visible-light photocatalytic decontamination of bisphenol A (BPA) by g-

C_3N_4/BiOBr heterojunctions, Mat Sci Semicon Proc, 24 (2014) 96-103.

[32] F. Amano, K. Nogami, B. Ohtani, Enhanced photocatalytic activity of bismuth-tungsten mixed oxides for oxidative decomposition of acetaldehyde under visible light irradiation, Catal Commun, 20 (2012) 12-16.

[33] H. Fu, S. Zhang, T. Xu, Y. Zhu, J. Chen, Photocatalytic Degradation of RhB by Fluorinated Bi_2WO_6 and Distributions of the Intermediate Products, Environmental Science & Technology, 42 (2008) 2085-2091.

[34] C. Bhattacharya, H.C. Lee, A.J. Bard, Rapid Screening by Scanning Electrochemical Microscopy (SECM) of Dopants for Bi_2WO_6 Improved Photocatalytic Water Oxidation with Zn Doping, The Journal of Physical Chemistry C, 117 (2013) 9633-9640.

[35] G. Zhao, S. Liu, Q. Lu, F. Xu, H. Sun, Fabrication of electrospun Bi_2WO_6 microbelts with enhanced visible photocatalytic degradation activity, Journal of Alloys and Compounds, 578 (2013) 12-16.

[36] Z. Liu, H. Ran, B. Wu, P. Feng, Y. Zhu, Synthesis and characterization of BiOI/BiOBr heterostructure films with enhanced visible light photocatalytic activity, Colloids and Surfaces A: Physicochemical and Engineering Aspects, 452 (2014) 109-114.

[37] T. Watanabe, T. Takizawa, K. Honda, Photocatalysis through excitation of adsorbates. 1. Highly efficient N-deethylation of rhodamine B adsorbed to cadmium sulfide, The Journal of Physical Chemistry, 81 (1977) 1845-1851.

[38] T. Wu, G. Liu, J. Zhao, H. Hidaka, N. Serpone, Photoassisted Degradation of Dye Pollutants. V. Self-Photosensitized Oxidative Transformation of Rhodamine B under Visible Light Irradiation in Aqueous TiO_2 Dispersions, The Journal of Physical Chemistry B, 102

(1998) 5845-5851.

[39] P. Lei, C. Chen, J. Yang, W. Ma, J. Zhao, L. Zang, Degradation of Dye Pollutants by Immobilized Polyoxometalate with H2O2 under Visible-Light Irradiation, Environmental Science & Technology, 39 (2005) 8466-8474.

[40] S. Kwon, M. Fan, A.T. Cooper, H. Yang, Photocatalytic applications of micro-and nano-TiO_2 in environmental engineering, Crit Rev Env Sci Tec, 38 (2008) 197-226.

[41] G. Li, K.H. Wong, X. Zhang, C. Hu, J.C. Yu, R.C.Y. Chan, P.K. Wong, Degradation of Acid Orange 7 using magnetic AgBr under visible light: The roles of oxidizing species, Chemosphere, 76 (2009) 1185-1191.

[42] J. Gamage McEvoy, W. Cui, Z. Zhang, Synthesis and characterization of Ag/AgCl–activated carbon composites for enhanced visible light photocatalysis, Applied Catalysis B: Environmental, 144 (2014) 702-712.

[43] J. Fu, Y. Tian, B. Chang, F. Xi, X. Dong, BiOBr-carbon nitride heterojunctions: synthesis, enhanced activity and photocatalytic mechanism, J Mater Chem, 22 (2012) 21159-21166.

[44] Y. Xu, D. Zhong, J. Jia, K. Li, J. Li, X. Quan, Dual slant-placed electrodes thin-film photocatalytic reactor: Enhanced dye degradation efficiency by self-generated electric field, Chemical Engineering Journal, 225 (2013) 138-143.

[45] Y.L. Xu, J.X. Li, D.J. Zhong, J.P. Jia, Dual electrodes degradation of Amaranth using a thin-film photocatalytic reactor with dual slant-placed electrodes, Journal of Environmental Science and Health, Part A, 48 (2013) 1700-1706.

[46] H. Fu, C. Pan, W. Yao, Y. Zhu, Visible-Light-Induced Degradation of Rhodamine B by Nanosized Bi_2WO_6, The Journal of Physical Chemistry B, 109 (2005) 22432-22439.

[47] A.H. Nethercot, Prediction of Fermi Energies and Photoelectric Thresholds Based on Electronegativity Concepts, Phys Rev Lett, 33 (1974) 1088-1091.

[48] M.A. Butler, D.S. Ginley, Prediction of Flatband Potentials at Semiconductor - Electrolyte Interfaces from Atomic Electronegativities, J Electrochem Soc, 125 (1978) 228-232.

[49] L. Kong, Z. Jiang, T. Xiao, L. Lu, M.O. Jones, P.P. Edwards, Exceptional visible-light-driven photocatalytic activity over BiOBr-$ZnFe_2O_4$ heterojunctions, Chem Commun, 47 (2011) 5512-5514.

[50] A. Matilainen, M. Sillanpää, Removal of natural organic matter from drinking water by advanced oxidation processes, Chemosphere, 80 (2010) 351-365.

[51] W. Zhang, Y. Sun, F. Dong, W. Zhang, S. Duan, Q. Zhang, Facile synthesis of organic-inorganic layered nanojunctions of g-C_3N_4/$(BiO)_2CO_3$ as efficient visible light photocatalyst, Dalton T, 43 (2014) 12026-12036.

[52] Z. Jiang, F. Yang, G. Yang, L. Kong, M.O. Jones, T. Xiao, P.P. Edwards, The hydrothermal synthesis of BiOBr flakes for visible-light-responsive photocatalytic degradation of methyl orange, Journal of Photochemistry and Photobiology A: Chemistry, 212 (2010) 8-13.

Section Ⅲ:

Conclusions

CHAPTER 5:

PROJECT CONCLUSIONS AND FUTURE WORK

5.1 Project conclusions

In this project, the BiOBr-Bi_2WO_6 heterojunction semiconductors had been synthesized by facile hydrothermal method. The well-crystal structure of the as-prepared photocatalysts were characterized by XRD. The morphologies, tested by SEM and TEM, varied for the composites synthesized at different experimental conditions, such as nanoplates of pure BiOBr, flake-like structure of BiOBr-Bi_2WO_6 composites *etc*. The optical properties of the semiconductors were performed by the DRS analysis, for example, the band gap of the BiOBr (50 at%)-Bi_2WO_6 was about 2.61 eV which was suitable to be activated by visible-light irradiation.

The photocatalytic activities were evaluated by degrading *Rhodamine B* (*RhB*). Results show that it achieved the highest photocatalytic degradation efficiency at the hydrothermal temperature of 120 ℃ and the reaction duration of 6 hours. The influences of experimental conditions in the degradation process, including the initial concentration, pH of the dye water and the amount of catalysts dosage, have also been explored. Furthermore, the mechanism of decomposition of RhB was discussed by analyzing the UV-Vis spectra of the samples taken

during the process at various times, which could be divided into two separate processes: the de-ethylation and destruction of the aromatic ring. The complete mineralization of the organics further prove the high activity of the photocatalysts synthesized in this work. In the tests for the reusability of the photocatalysts, it confirmed the structure of the photocatalysts was stable enough to be reused and kept at high photocatalytic activity all through.

The mechanism of degradation process and the enhancement of heterojunction structure were explored by the quenching effect of scavengers and the band structure. Results demonstrated that holes played the most important role in the degradation process, and the oppositely interfacial transfer of the electrons and holes enhance the separation efficiency of charges and correspondingly improve the photocatalytic activity in degradation of organics.

In conclusion, the synthesis method of BiOBr-Bi_2WO_6 heterojunction semiconductors was facile, and the as-prepared photocatalysts possessed an appropriate crystal-structure, was stable and reusable, and had highly beneficial visible-light-induced photocatalytic properties.

5.2 Recommendations of future work

- Bismuth composites used in the area of photocatalysis are very costly. Further exploration of inexpensive photocatalysts with high visible-light-driven activity are still needed. Meanwhile, another possible approach is adjusting the synthesis conditions or exploring some novel methods to prepare special structures which can improve the photocatalytic activity.
- The photocatalytic reactor applied in this work was slurry, which is not economical for the industrial application because a separation process of the photocatalysts from the suspension is needed. It would be essential to further develop the type of reactor used;

one possibility is the immobilization of the photocatalysts on the support to establish an immobilized photocatalytic reactor.

- The dye water was simulated by using RhB, a simplex component. However, the real dye water is much more complex, so the degradation experiments by using real dye water from the factory should be explored.

All in all, BiOBr-Bi_2WO_6 heterojunction semiconductors could potentially be implemented for practical utilization if all of the abovementioned recommendations have been remedied in the coming future.

Section Ⅳ:

Appendix

A.1 Relationship between the absorption intensity and concentration

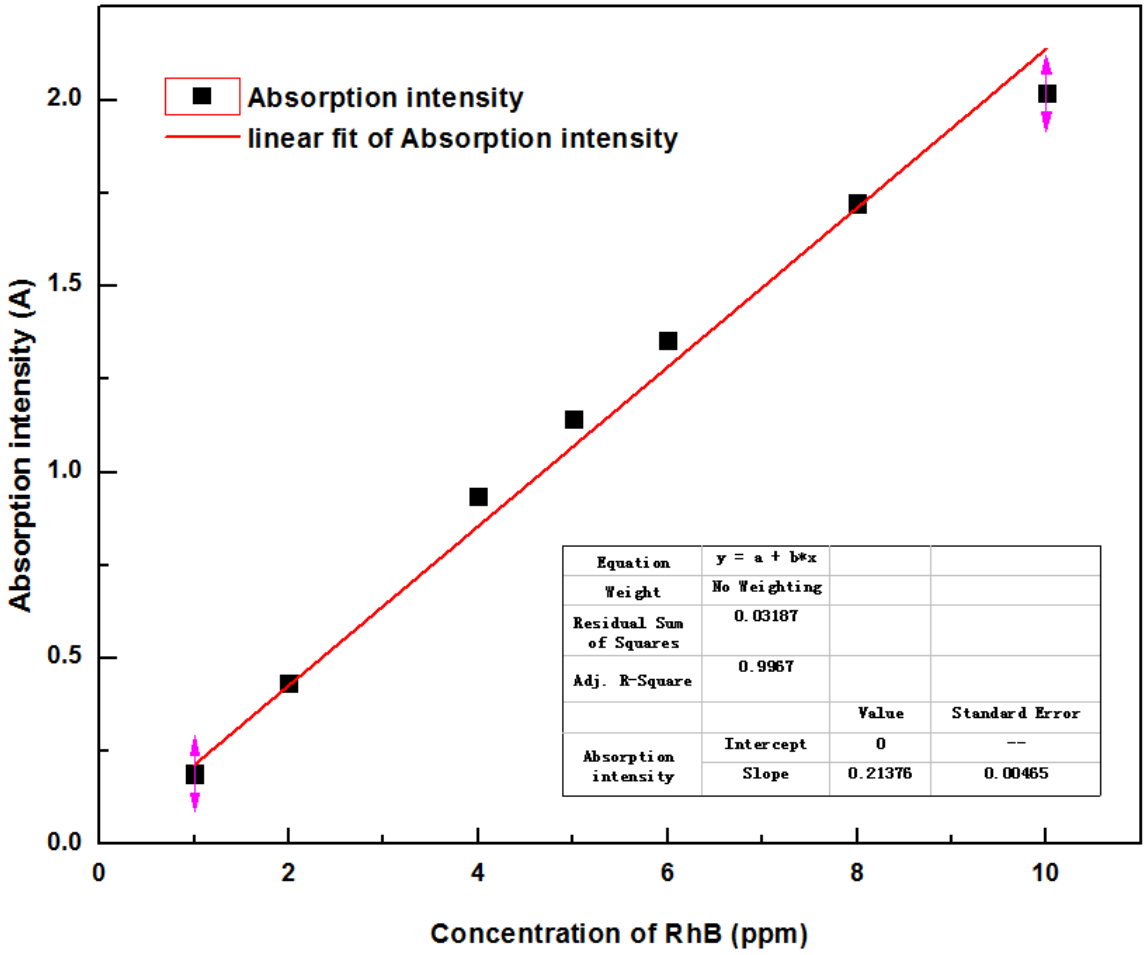

Fig. A- 1. Relationship between the absorption intensity and the concentration of RhB.

By plotting the absorption intensity *vs* the concentration of RhB, a linear relationship exists with fulfilling the following formula:

$$A=0.2138\times c \quad (R^2=0.9967)$$

So:

$$\omega_{Degradation\ efficiency} = \frac{c_o - c_t}{c_o} \times 100\% = \frac{\frac{A_0}{0.2138} - \frac{A_t}{0.2138}}{\frac{A_0}{0.2138}} \times 100\% = \frac{A_o - A_t}{A_o} \times 100\%$$

Where c_0, c_t, A_0 and A_t mean the initial concentration of RhB, the concentration of RhB in the samples taken at a specific time, the absorption intensity of initial solution and the absorption intensity of the sample taken at a specific time. From the above relationship, it proves that detection of the concentration of RhB solution by measuring the absorption intensity is valid.

A.2 Properties of the bulb

Following figure shows the spectra of meatal halide lamp and the terrestrial solar (Fig. A-2).

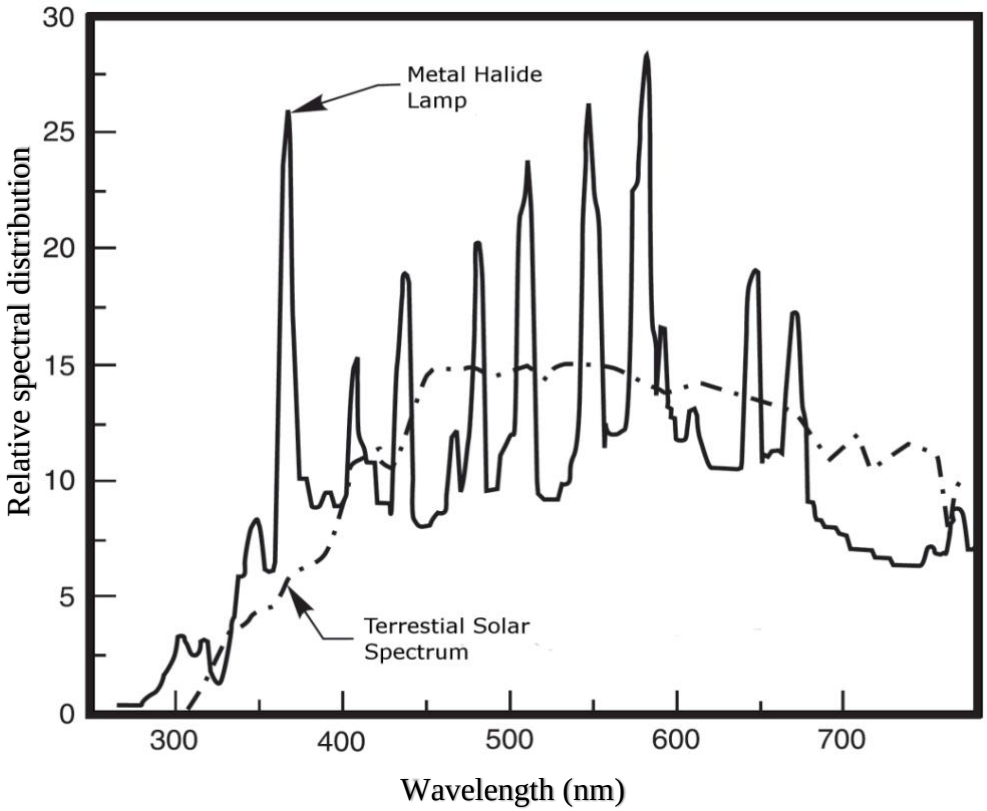

Fig. A- 2. Spectral distribution of the metal halide lamp and the terrestrial solar.

A.3 Molecular formulas of the dye

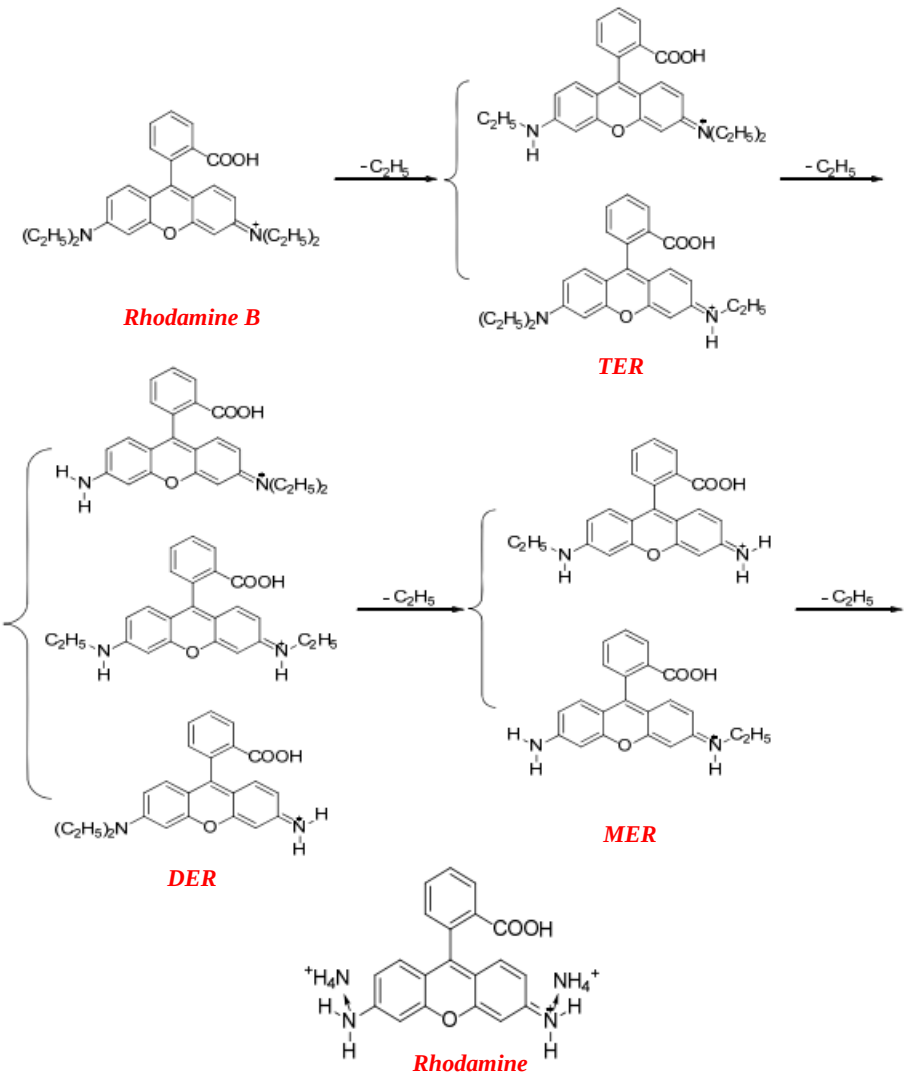

A.4 Direct and indirect semiconductor

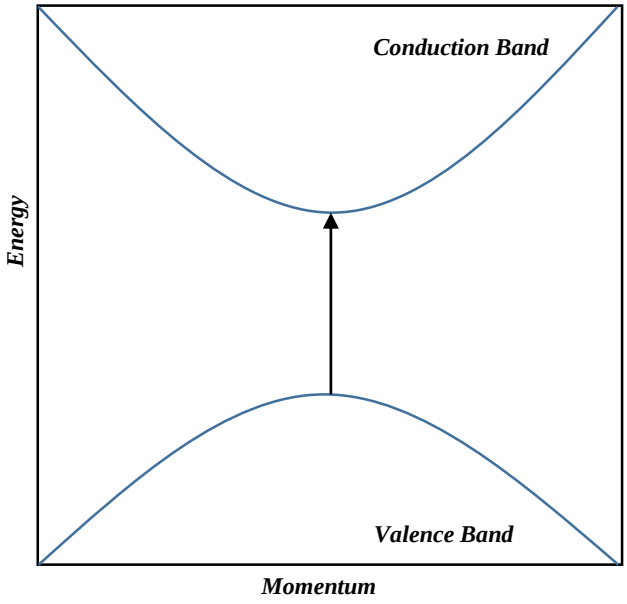

Direct Band gap semiconductor

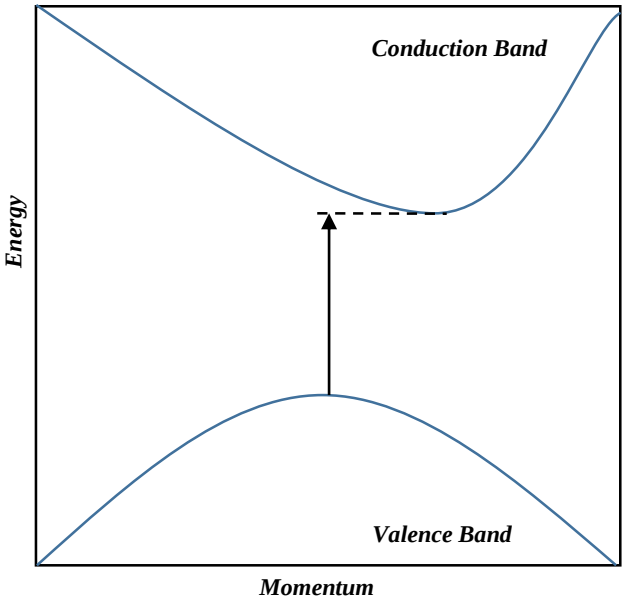

Indirect Band gap semiconductor

A.5 Scholarly contributions

Journal Article (submitted):

[1] Xiangchao Meng, Z. Jason Zhang, "Synergetic Photoelectrocatalytic Reactor for Environmental Remediation: a Review" (Journal of photochemistry and photobiology, C: Photochemistry reviews);

[2] Xiangchao Meng, Z. Jason Zhang, "Facile Synthesis of $BiOBr/Bi_2WO_6$ Heterojunction Semiconductors with high visible-light-driven photocatalytic activity" (Journal of photochemistry and photobiology, A: Chemistry);

[3] Xiangchao Meng, Z. Jason Zhang, "Synthesis, Analysis and Testing of $BiOBr\text{-}Bi_2WO_6$ Photocatalytic Heterojunction Semiconductors" (International journal of photoenergy).

[4] Xiangchao Meng, Lingyun Jiang, Weiwen Wang, Z. Jason Zhang, “Synthesis, Test and Analysis of BiOBr/ZnO p-n Heterojunction Semiconductors” (International journal of photoenergy)

Conference presentations:

[1] Xiangchao Meng*, Fahad Chowdhury, Jason Zhang, “Synthesis and Analysis of Heterojunction Semiconductors for Photocatalysis”, 64th Canadian Chemical Engineering Conference, Niagara Falls, Canada, 19th -22nd, Oct., 2014.

*Presenting author